AN INELASTIC ELECTRON TUNNELING SPECTROSCOPIC INVESTIGATION OF INORGANIC AND ORGANOMETALLIC MOLYBDENUM COMPLEXES ADSORBED ON ALUMINUM OXIDE SURFACES

Thesis by

Gregory Joseph Gajda

In Partial Fulfillment of the Requirements

for the Degree of

Doctor of Philosophy

California Institute of Technology

Pasadena, California

1986

(Submitted December 10, 1985)

Acknowledgments

I would like to express my appreciation to my advisors, Professors Bob Grubbs and Henry Weinberg, for their advice and encouragement, and to past and present members of their research groups for invaluable assistance. I would also like to thank the members of the electrical and instrument shops in Chemical Engineering. Their ability to convert line drawings into working equipment was almost miraculous. I would like to thank Kathy Lewis for her patience in typing the numerous drafts which every research paper went through. And I would like to express my appreciation to the National Science Foundation for its financial support of my work.

I would especially like to thank my family for their support and to them I respectfully dedicate this thesis.

Abstract

The design, construction and operation of an integrated glove box-based tunnel junction fabrication system are described. This versatile, all stainless steel, ultrahigh vacuum compatible system provides both vapor and liquid phase adsorption capabilities with a wide variety of molecules. The differences between adsorption from the liquid phase under an inert atmosphere and in the laboratory atmosphere are illustrated by spectra from junctions prepared with ethanolamine (2-amino-ethanol). A rapid (~ 10 s) and accurate (~ 1%) constant modulation current tunnel junction spectrometer displays the obtained spectrum on a storage oscilloscope. The design of these electronics is discussed, and the ability to rapidly optimize the lock-in detector phase setting simplifies the measurement of inelastic electron tunneling spectra. The use of a numerical first derivative routine to remove the linear background slope in tunneling spectra is described, and its ability to determine peak positions in the processed spectra is discussed.

Molybdenum hexacarbonyl adsorbs reversibly on hydroxylated alumina surfaces at 22°C to form a carboxylic acid-type adspecies. An estimate of the heat of adsorption energy, 15 ± 3 kcal/mole, is derived from the desorption kinetics. Heating the alumina surface to 140 ± 2°C during adsorption produces thick (> 500 Å) molybdenum films. Heating the surface to 100°C during adsorption produces decomposition products which consist of molybdenum oxides and subcarbonyls, depending on the decomposition parameters (time and post-heating sequence). The decomposition products show no reaction with 2 Torr of ethylene at 100°C even after one hour.

At 22°C, molybdenum oxytetrachloride adsorbs and reacts with the surface hydroxyl groups on the alumina to form a dioxo-bridged molybdenum dichloro

complex, which desorbs slowly at 295 K. Heating during the adsorption produces poorly reproducible molybdenum suboxide compounds. At 22°C molybdenum dioxodichloride adsorbs from the vapor phase and reacts with surface hydroxyl groups on the alumina to form a molybdenum oxide which reacts readily with background water vapor. Heating the surface during exposure produces a partially polymerized oxide which still reacts with background water vapor. Heating the exposed surfaces in vacuum dehydrates the oxide and increases the extent of oligomerization. The oxides show no reaction with 2 Torr of ethylene at 100°C after 30 minutes, or with acetic acid at 10^{-1} Torr after five minutes at 22°C. Exposure to 5 x 10^{-2} Torr of 4-t-butylpyridine for 100 s at 22°C results in complete desorption of the oxide.

Table of Contents

Chapter One.

Introduction

The study of inorganic and organometallic molybdenum complexes represents an extension of inelastic electron tunneling spectroscopy to new substrate surfaces. The study of adsorbates to determine their structure and reactivity (primarily thermal decomposition) dominates the applications of tunneling spectroscopy. This study extends this work by exploring the suitability of several molybdenum complexes for the formation of practical surface layers capable of satisfying the demanding requirements of the insulating layer of a tunnel junction. In addition to studying the properties of the individual adsorbed complexes, the observation of a suitable molybdenum oxide surface formed by decomposition of molybdenum dioxydichloride indicates the potential for expansion in the types of oxide surfaces available to tunneling studies.

The construction of a glove box based high vacuum fabrication system, along with a near-real time tunnel junction measurement system, has significantly increased the range of adsorbates available for use in tunneling spectroscopy. This work represents several exploratory steps in the effort to expand the versatility and applicability of inelastic electron tunneling spectroscopy.

In the twenty years since its discovery by Jaklevic and Lambe **(1)**, inelastic electron tunneling has developed into a mature, surface-sensitive, vibrational spectroscopy. This moderate resolution, high sensitivity technique combines the relatively simple fabrication technology of metal-insulator-metal tunnel diodes with a straightforward interpretation of the inelastic tunneling channels, based on energy conservation principles. Although applicable to a wide range of metals and insulators, rigorous practical considerations have limited widespread use to only two systems: Al-Al_2O_3-Pb and Mg-MgO-Pb. Furthermore, most studies have emphasized the adsorption of Bronsted acids, such as acetic acid or phenol, due to the ease of junction fabrication using these compounds. A recent compilation of tunneling spectra by Walmsley and Tomlin **(2)** provides a

concise overview of the adsorbate/substrate systems studied to date. In addition, numerous reviews of the theory, practice and application of tunneling spectroscopy are available **(3-12)**.

The end of the initial exploratory phase in the use of tunneling spectroscopy has led to the development of new techniques to overcome the identified limitations on the types of insulators and adsorbates that can be used successfully. Recently work on the formation of insulators based on aluminum fluoride **(13)** and aluminum sulfates **(14)**, prepared by adding CF_4 or SO_2 to the glow discharge, respectively, suggests a method for overcoming the poor tunneling characteristics associated with many metal oxides formed by thermal or glow discharge oxidation of the base metal electrode. We have attempted to expand the class of usable metal oxide insulators by adsorption and hydrolysis of metal oxyhalides; in particular, molybdenum oxytetrachloride and molybdenum dioxodichloride. Another approach has been the development of glove box-based junction fabrication systems, such as the system described by Hipps and Mazur **(15)** and our fabrication system, discussed in Chapter Two, which allow a wide range of adsorbates to be investigated. These systems allow both liquid phase and vapor phase adsorption of air- or water-sensitive molecules on the insulator surface. Finally, the development of tunneling systems that do not rely on the fixed, metal-insulator-metal junction geometry hold the promise of removing one of the major limitations involved in tunneling: the inability to use a single tunnel junction in a series of temperature-programmed (or sequential reagent application) experiments. These techniques, 'squeezable' electron tunnel junctions **(16)** and the scanning tunneling microscope **(17)**, are only at the very beginning of their development.

One major advantage of the standard aluminum-aluminum oxide-lead tunnel junction is ease of fabrication. A basic fabrication system consists of a holder

for the glass substrates, resistively heated evaporation sources for the aluminum and lead, a mask and shutter assembly to define the metal electrode pattern, and a glow discharge electrode to produce an oxygen/water plasma to oxidize the aluminum electrode and form the aluminum oxide insulator. Such a system, however, is limited to vapor phase adsorption or requires liquid phase adsorption to be done in contact with the laboratory atmosphere. A significant improvement in adsorbate application results if the liquid phase exposure can be performed in an inert atmosphere.

The design and use of a glove box based fabrication system is the subject of Chapter Two. This system provides the capability of using vapor phase adsorption when the reactant is sufficiently volatile, as well as an inert atmosphere for liquid phase adsorption when handling the compound in solution is more convenient. The level of water vapor in the glove box, about 1 ppm (or $\sim 10^{-3}$ Torr), is quite low compared to the laboratory atmosphere (about 1% or 10,000 ppm), yet quite high compared to the level attained in the high vacuum fabrication system ($< 5 \times 10^{-8}$ Torr). Thus, although hexane solutions of ethylaluminumdichloride can be handled easily and safely in the glove box, the water content is too high for tunnel junction fabrication. This topic is discussed further in Chapter Seven.

The level of water vapor in the glove box is sufficiently low to provide evidence of different degrees of water condensation on the aluminum oxide surface. When ethanolamine (2-aminoethanol) is adsorbed on the alumina surface via vapor phase exposure, an aluminum-amine Lewis acid/Lewis base complex is formed between an aluminum site and the 2-aminoethoxide surface species formed by loss of the alcohol proton **(18)**. A similar species is formed by the adsorption of ethanolamine from the liquid phase (1% w/v in hexane) in the glove box. In contrast, adsorption from the same solution while the aluminum

oxide surface is exposed to laboratory air produces a surface species similar to that observed in aqueous ethanolamine solutions **(19)**. This suggests the formation of a surface hydroxyl-amine complex as described in Chapter Two.

The glove box based fabrication system allows the use of moderately reactive chemicals while minimizing the interferences from atmospheric water or oxygen during liquid phase adsorption. However, the intrinsic reactivity of the aluminum oxide surface must be considered when choosing a suitable solvent. The use of hexane or toluene has proven satisfactory, while acetone, diethylether and methanol all produce significant hydrocarbon contamination of the tunnel junctions. The use of oxygen or nitrogen containing solvents is likely to result in unsatisfactory tunneling spectra due to contamination.

The actual measurement of tunneling spectra has primarily involved the use of constant modulation current, second harmonic lock-in detection devices. These systems have the advantage of simplicity and relatively wide impedance range (~ 20-2000 ohms). The use of a lock-in amplifier adds one undefined variable to the measuring circuit: the lock-in phase setting. Traditionally, the phase angle was set by obtaining the maximum signal at a fixed bias voltage (250 mV in the present system). By modifying the computer controlled system to allow near real time (~ 10 s) viewing of the spectra, an overall optimization of the phase angle is possible. This is discussed in detail in Chapter Three.

The use of a relatively large time constant on the lock-in amplifier (100 ms), provides a reasonable compromise between the signal-to-noise ratio and the instrumental broadening of the peaks in the spectrum. This allows the changes produced by varying the phase angle to be observed in sufficient detail and at relatively short intervals to provide a visual feedback mechanism for setting the phase angle. Although some degree of subjectivity in selecting the optimum

spectrum remains, the technique allows for the rapid screening of tunnel junctions to find the best signal-to-noise and linear background characteristics.

The presentation of tunneling data has resulted in some problems due to the upward sloping background in the spectra. The determination of relative peak heights or peak positions is more difficult when the background is not flat, in contrast to vibrational spectroscopies. A method for removing this background is the subject of Chapter Four. By using the simple calculation of the average slope of the data, an accurate estimate of the background slope is obtained. This average is calculated by using an eleven point, cubic, least-squares convolution described by Savitzky and Golay **(20)**. In addition to producing a flat background, the computer routine employs a peak locating algorithm based on a routine developed by Templeton **(21)**. The routine is capable of locating peak positions to ± 1 cm^{-1} with a high degree of reproducibility between different spectra of the same compound.

The study of the reactions of molybdenum hexacarbonyl is the topic of Chapter Five. The hexacarbonyl adsorbs reversibly to form a molybdenum carboxylic acid species. This represents the initial chemisorption step in the adsorption and decomposition of molybdenum hexacarbonyl on alumina — a reaction investigated extensively in high surface area systems **(22)**. Unfortunately, the next stable molecule formed on the surface under the junction preparation conditions is the molybdenum oxide. This prevented the study of any intermediates in the decomposition reactions and any correlation with the numerous surface species postulated to occur on the basis of the high surface area alumina studies.

One of the more interesting reactions catalyzed by the decomposed molybdenum hexacarbonyl on alumina is the metathesis reaction. Considerable experi-

mental evidence **(23)**, as well as ab initio calculations **(24)**, support the proposal of an oxomolybdenum carbene as the active catalyst. An attempt was made to activate the molybdenum oxide with ethylene, but no evidence of carbene formation was obtained.

The difficulties encountered in the study of the hexacarbonyl adsorption indicate one of the most serious limitations in current tunneling spectroscopy: the inability to repeatedly measure a single junction as a function of time (or temperature, or reagent addition). In this case, the problem was overcome by preparing a series of junctions with increasing delay times between the end of the exposure to molybdenum hexacarbonyl and the start of the lead evaporation. The data would be more concise, of course, if a single system could have been repetitively cycled (immersing in liquid helium for measurement, then heated to 300 K for five minutes) to show the gradual desorption of the hexacarbonyl. This limitation represents the most promising (and most difficult) area for research on extending the applications of tunneling. Current efforts in other research groups are centered on new tunneling configurations which eliminate the 'one-shot' approach of present tunnel junctions.

The interactions of molybdenum oxychlorides with the hydroxylated alumina surface are the subject of Chapter Six. The primary interaction is hydrolysis, although the two different halides exhibit very different results. The molybdenum oxytetrachloride appears to dimerize on the surface, and then desorb, leaving a partially dehydrated surface. The molybdenum dioxodichloride hydrolyzes to form a molybdenum oxide which is quite reactive with residual water vapor in the fabrication chamber. It readily reacts with water vapor and even forms hydroxides.

Heating the molybdenum oxytetrachloride during adsorption produces a

molybdenum oxide with very poor electrical characteristics, which make it undesirable for use as a tunneling substrate. In contrast, the oxide formed by hydrolysis of molybdenum dioxodichloride is quite suitable as a tunneling substrate. Heating during adsorption produces a more highly polymerized oxide, while post-heating in vacuum causes desorption of water.

This new substrate was subjected to initial tests of its acid/base properties. The strong reaction with water suggests that the oxide is acting as a strong Lewis acid. The hydroxylated aluminum oxide, by contrast, reacts as a weak Lewis acid or even a weak Bronsted base (with Bronsted acids such as acetic acid). A moderate exposure (10^{-1} Torr for 300 s) of acetic acid produces acetate-like surface species, although the bonding is probably more covalent than ionic, on aluminum oxide. A similar exposure on the molybdenum oxide produces no identifiable surface complex.

A large exposure of 4-t-butylpyridine (10^{-1} Torr for 1000 s) produces some dehydroxylation of the surface, but no stable adsorbate, on aluminum oxide. A much smaller exposure (5×10^{-2} Torr for 100 s) causes the complete desorption of the molybdenum oxide layer, and produces a highly dehydroxylated aluminum oxide surface. This extreme reactivity with Lewis bases indicates the desirability of new tunneling substrates to explore reactions that do not readily occur on alumina. Molybdenum oxide is itself a good oxidation catalyst **(25)**, and further experiments on this surface appear promising. The method of formation, hydrolysis of metal halides, is reasonably general, so additional metal oxide surfaces can be investigated for their utility as tunneling substrates and reaction systems.

A brief series of experiments involving an impure molybdenum hexacarbonyl and a second series involving ethylaluminumdichloride comprise the discussion

of Chapter Seven. The impure hexacarbonyl readily reacts with the alumina surface to form a complex molybdenum oxide species which appears to incorporate a carboxylate and possibly a hydride functionality. One hypothesis for the identity of the impurity and its surface reaction product is presented. The results of the aluminum alkylchloride experiments were negative, indicating that some compounds are still too reactive for use in present fabrication systems.

The basic aim of this research has been not only to study the surface reactions of inorganic and organometallic complexes, but also to expand the range of substrates and adsorbates accessible to tunneling spectroscopy. This has been accomplished by the design and construction of a versatile, state-of-the-art glove box based fabrication system, improvements in the measurement of tunneling spectra and the investigation of new metal oxide substrates. This research also indicates the complexity and difficulty of studying weakly adsorbed species, and the considerable differences in reaction products that closely related compounds (the oxychlorides) can exhibit. The present research trend in tunneling spectroscopy, which is strongly oriented toward expanding the applications and applicability of tunneling, indicates that inelastic electron tunneling is still a vital and viable element in the array of surface vibrational spectroscopies.

References

1. R. C. Jaklevic and J. Lambe, Phys. Rev. Letters **17**, 1139 (1966).
2. D. G. Walmsley and J. L. Tomlin, Prog. Surface Sci. **18**, 247 (1985).
3. P. K. Hansma, Phys. Rep. C **30**, 146 (1977).
4. W. H. Weinberg, Ann. Rev. Phys. Chem. **29**, 115 (1978).
5. *Inelastic Electron Tunneling Spectroscopy*, T. Wolfram, Ed., Springer, Berlin (1978).
6. P. K. Hansma and J. R. Kirtley, Acc. Chem. Res. **71**, 440 (1978).
7. H. W. White and T. Wolfram, Methods Exp. Phys. A, **16**, 149 (1980).
8. H. W. White, L. M. Godwin and R. Elliatioglu, J. Adhes. **13**, 177 (1981).
9. S. Ewert, Appl. Phys. A, **26**, 63 (1981).
10. *Tunneling Spectroscopy*, P. K. Hansma, Ed., Plenum, New York (1982).
11. W. H. Weinberg, Vibrational Spectra and Structure, **11**, 1 (1982).
12. S. K. Khanna and J. Lambe, Science **220**, 1345 (1983).
13. S. Gauthier, S. De Cheveigne, G. Salace, J. Klein and M. Belin, Surface Sci. **155**, 31 (1985).
14. M. Suzuki, U. Mazur and K. Hipps, Surface Sci. **161**, 156 (1985).
15. K. W. Hipps and U. Mazur, Rev. Sci. Instrum. **55**, 1120 (1984).
16. J. Moreland, S. Alexander, M. Cox, R. Sonnenfeld and P. K. Hansma, Appl. Phys. Lett. **43**, 387 (1983).
17. G. Binnig, N. Garcia and H. Rohrer, Phys. Rev. B **32**, 1336 (1985).
18. R. J. Turner, N. M. D. Brown and D. G. Walmsley, Vacuum **31**, 603 (1981).

19. S. A. S. Ghazanfar, J. T. Edsall and D. V. Myers, J. Am. Chem. Soc. **86**, 559 (1964).

20. A. Savitzky and M. J. E. Golay, Anal. Chem., **36**, 1627 (1964).

21. M. K. Templeton, PhD Thesis, California Institute of Technology, 1984.

22. T. L. Brown, J. Mol. Catal. **12**, 41 (1981).

23. R. H. Grubbs, in *Comprehensive Organometallic Chemistry*, G. Wilkinson, Ed., Pergamon, Oxford (1982), Ch. 54..

24. A. K. Rappe and W. A. Goddard III, J. Am. Chem. Soc. **102**, 5144 (1980).

25. See, for example, *Fourth Int. Conference: The Chemistry and Uses of Molybdenum*, Climax, Ann Arbor (1982).

Chapter Two.

A Glove-Box Based Fabrication System for Inelastic Electron Tunneling Junctions

I. Introduction

Inelastic electron tunneling spectroscopy is a highly sensitive, moderately high resolution vibrational spectroscopy which can be used to probe the structure and bonding of adsorbates on thin films of metal oxides of low surface area. The theory and practice of tunneling spectroscopy, as well as numerous examples of its use, have been reviewed extensively **(1-10)**. One significant limitation on the types of adsorbates that have been studied heretofore has been due to the necessity of either vapor phase adsorption or 'open air' liquid phase adsorption. A large class of compounds may be either too toxic or too air sensitive to be used in an open system, and/or not sufficiently reactive or too low in vapor pressure to be adsorbed from the vapor phase.

An approach to circumvent these problems is to combine the standard high (or an ultrahigh) vacuum fabrication system with a controlled-atmosphere glove box. One such system, which provides a diffusion pumped bell jar fabrication system with a working pressure of 2×10^{-8} Torr, has been described recently by Hipps and Mazur **(11)**. Their fabrication system is mounted into the base of the inert-atmosphere section of their glove box and uses a specially designed solvent removal system to prevent contamination of the atmosphere purification catalyst used in the glove box. Our system, on the other hand, is an all stainless steel, UHV-compatible, turbomolecularly pumped fabrication system which is mounted to the base of the vacuum chamber side of the glove box. The rationale for this design is the following: (1) solvent contamination is prevented by pumping away all solvent after the junction preparation; (2) standard vacline syringe techniques can be used for the junction preparation; and (3) the fabrication system may be repaired or otherwise modified without any possibility of contaminating the glove box atmosphere. Although the two systems differ in detail and design philosophy, the basic goal of both is the same, namely the

preparation of tunnel junctions employing adsorption from the liquid phase in an inert atmosphere.

A versatile and convenient glove box-based tunnel junction fabrication system is described here that can successfully handle both extremely reactive and toxic compounds and allow their use in the synthesis of tunnel junctions. Any compound which can be successfully handled with standard vac-line techniques **(12)**, can be used in this system.

II. Description of the Glove Box Fabrication System

The fabrication system consists of two major components, an ultrahigh vacuum system and a glove box, which are combined to produce an extremely versatile system. An external view of the glove box fabrication system is shown in Fig. 1. The ultrahigh vacuum chamber and its associated pumping system is mounted on the lower right. This ultrahigh vacuum chamber can be used independently for experiments involving vapor phase adsorption or liquid phase adsorption of air-stable compounds. The ultrahigh vacuum chamber is operated in conjunction with the glove box for experiments involving solutions of air- or water-sensitive compounds.

A. Ultrahigh Vacuum Chamber

An external view of the ultrahigh vacuum chamber is shown in Fig. 2. The flask mounted on the mini-manifold is covered to minimize reactions induced by fluorescent lighting. The ultrahigh vacuum chamber is a 10.5" diameter stainless steel cylinder 12" in length with a stainless steel lid. The vacuum is achieved with a 270 l/s Balzers TPU270 turbomolecular pump (turbopump) that is backed by a 195 l/min direct-drive Precision DD-195 mechanical pump. This combination provides a base pressure of 2×10^{-9} Torr after a modest bakeout below 100°C. The seal to the lid of the vacuum chamber is provided by two Viton

O-rings separated by a differentially pumped channel. At a system pressure of 2 x 10^{-9} Torr, varying the pressure in the differentially pumped channel from 760 Torr to 10^{-3} Torr produces no change in pressure within the vacuum chamber, indicating that leakage through the O-rings is not limiting this base pressure.

The vacuum chamber is connected to the turbopump with a Huntington Mechanical Labs (HML) GVA-400 4" ID gate valve. This valve allows the chamber to be isolated from the pump during the glow discharge oxidation of the metallic substrate to form the thin metal oxide barrier, the adsorbate exposure, or the chamber opening phases of the fabrication cycle.

The vacuum chamber is equipped with a Varian 844 nude ionization gauge for monitoring the pressure below approximately 10^{-5} Torr. A Varian 531 thermocouple gauge is available to monitor the pressure between approximately 10^{2} and 10^{-3} Torr during the initial phases of the pumpdown. Both gauges must be turned off prior to exposures of reactive species to avoid decomposition on the hot filaments.

The tunnel junctions that we fabricated with this system consisted of an aluminum lower electrode, a thin film aluminum oxide upon which the molecules are adsorbed, and a lead upper electrode. The metal electrodes are formed by evaporation of high purity metal through pattern-forming masks, while the oxide is synthesized via oxidation of the aluminum electrode by a glow discharge in high purity oxygen, with admixed water vapor. Two resistively heated metal evaporation sources for deposition of the upper (lead) and lower (aluminum) electrodes have been provided. The interior view of the vacuum system, shown in Fig. 3, displays the shielded evaporation sources. The molybdenum boat for the lead evaporation is visible through the left shield, while the tungsten filament for the aluminum evaporation is visible on the right. The

aluminum is evaporated from a stranded tungsten wire (R. C. Mathis F4-3X-030W) that supports small U-shaped pieces of Balzers 99.999% aluminum (approximately 3/4" in length and 1/8" in diameter). The lead is evaporated from a molybdenum boat (R. C. Mathis S8A-Mo) using Balzers 99.995% lead shot. The power for the metal evaporation is provided by a Cooke Vacuum FPS 1-40 12 V/100 A power supply, connected by #2 gauge copper wire to two HML EF-251 medium current feedthroughs each of which is rated for 150 A. The connections on the vacuum side are 1/4" x 1" cross section OFHC copper bars with Corning Macor insulator blocks for support. The metal evaporation sources are shielded to minimize stray deposition, with slit geometries adjusted to compensate for the size of the source (approximately 3" in length x 1/2" in width for the aluminum, and approximately 1/2" diameter for the lead).

The oxidation of the aluminum strips (typical thickness of 800 Å) to form the aluminum oxide tunneling barrier (~15-20 Å thickness) is accomplished via a 1100 V, 12 mA glow discharge in a 1000:1 oxygen:water vapor mixture at a total pressure of 60-80 microns. The glow discharge electrode is a T-shaped aluminum assembly which is connected directly to a HML EF-151 medium voltage feedthrough rated for 12 kV. The electrode assembly is shown on the left side in Fig. 3. A pyrex tube 4" in length x 1/2" ID with a wall thickness of 1/16" forms an insulator to prevent a discharge with the feedthrough mount or the vacuum chamber wall. The ground electrode is a rectangular stainless steel shield which blocks line-of-sight to the evaporation sources, but does not block the line-of-sight to the junctions. The discharge electrode is located approximately eight inches from the junctions to provide a uniform oxidation rate. The discharge is supported by a Fluke 415B high voltage power supply rated at 3100 V/25 mA. The vacuum chamber is connected directly to the supply ground to avoid floating the chamber at high voltage. The high voltage lead is connected to a 2500

ohm resistor in series with the aluminum electrode. The voltage drop across this resistor is measured with a Simpson 260 analog volt meter which is floating with respect to ground. The voltage drop provides a direct measurement of the glow discharge current.

The final module inside the vacuum chamber is the mask/shutter assembly, shown in Fig. 4(A), which also contains the slide holder and the crystal frequency monitor, shown in Fig. 4(B). The crystal frequency monitor, is a Sloan 000488 system using Sloan 103950 5 MHz silver coated quartz crystals. When a 5 V potential is applied to the monitor from an external Analog Devices 903 power supply, the crystal oscillates at a frequency near 5 MHz. As mass is deposited onto the crystal during metal evaporation, the frequency of oscillation is decreased. This provides a sensitive measurement of the metal film thickness. The oscillation frequency is measured with a Data Precision 5240 frequency counter with 0.1 Hz maximum resolution. The counter is normally used, however, at 1 Hz resolution (1 second time constant) which provides approximately 1 Å resolution for the aluminum evaporation and 0.4 Å resolution for the lead evaporation. Details of the measurement procedure and resolution calculations are given by Evans **(13)**. The crystal monitor is mounted slightly lower than the glass slides (closer to the evaporation sources) to compensate for its greater distance from the central axis of the vacuum chamber.

The slide holder, shown in Fig. 5, is mounted on the mask/shutter assembly using static friction to hold it in place and provides for mounting four 1" x 1/2" x 0.065" Corning 9053 glass slides upon which the metal electrodes are evaporated. This holder consists of three parts. The base metal plate has been machined to a thickness of 0.065", which provides both a clearance of 0.005" for the 0.070" slots milled into the support rails and sufficient friction to prevent slipping when the slide holder is inserted into the mask/shutter assembly. An

intermediate metal sheet has been slotted and bent to function as a spring to provide sufficient friction to hold the slides in place against the top piece. The top piece has been machined into U-shaped openings with a flange of 0.003" thickness by 0.010" in width, left along the inside edges of the U. This flange forms the top of the section and has been sized to hold the glass slides with 0.005" of clearance. The assembly is screwed together and functions like the slide holder on a microscope. The system is equipped to allow heating of the junctions via the resistance heating technique of Bowser and Weinberg **(14)**. The connections to the slides are made through five #26 AWG teflon insulated copper wires connected to a Macor quick-connect fitting of local design. The quick-connect leads to a HML IF-150 eight-pin feedthrough (which also carries the crystal monitor connections). Four wires provide switch-selectable heating of individual junctions, while the fifth provides a common ground. The power is supplied by an HP 6201B 20 V/1.5 A unit which is connected in series with a one ohm precision resistor. By measuring the voltage drop across this resistor, the current flow through the aluminum strip can be calculated. A measurement of the voltage drop across the aluminum strip divided by the current yields the dynamic resistance, which is used to calculate the temperature of the substrate of which the latter is equal to the temperature of the thin aluminum oxide film. The quick-connect allows the connections along the slide holder to be removed easily inside the glove box for liquid phase adsorption.

The mask/shutter assembly houses the mask set and the shutter which provide the patterns for the metal evaporation. The masks contain four I-shaped patterns for the aluminum evaporation and four three-bar patterns for the lead. These patterns correspond to the configuration described by Bowser **(15)**. The mask/shutter assembly also provides an open area for use during the glow discharge or adsorption phases of the experiment. The shutter regulates the

exposure of the slides to the metal vapor and allows the evaporation to stabilize before the slides are exposed. The pressure during evaporation is $\leq 2 \times 10^{-6}$ Torr. The masks and shutter are moved by a rack-and-pinion technique with the rack attached to the back of the mask or shutter carrier and the pinions mounted on HML VF-106 rotary feedthroughs. The limits of travel are determined by the length of the slots in the side rails. The slot for the shutter is visible in Fig. 4(B), as is the rack-and-pinion. The corresponding rack-and-pinion for the mask is not visible in this view.

Connected to the vacuum chamber are a 'mini-manifold' and a standard all-metal gas manifold. The mini-manifold consists of a female VCR fitting connected to a 1/4" OD stainless steel tube that is welded to a 2-3/4" conflat flange. This permits a direct, short path-length connection of glass flasks (fitted with glass-to-metal seals and matching VCR couplings) containing sufficiently volatile (vapor pressure $\geq 10^{-3}$ Torr) compounds. The mini-manifold can also be used with small amounts of expensive materials such as isotopically labeled compounds.

The main manifold uses a Whitey SS-4BMW precision metering valve to regulate the flow rate of the oxygen/water vapor mixture during the glow discharge. Flow through this valve is conductance limited for pressures below one Torr on the manifold side of the valve. The main manifold consists of 1/4" OD stainless steel tubing and Swagelok fittings. It provides three 3/8" ID Ultratorr connections for flasks containing very volatile compounds (i.e. vapor pressure at room temperature $\gtrsim 1$ Torr) or gases, and five 1/4" Ultratorr connections for connection to gas cylinders. One of the 3/8" connections is used exclusively for the supply of water vapor for the glow discharge. The water is Alfa ultrapure grade lot 021584 (purity 99.99%). Two of the 1/4" connections are also dedicated: one connects to the inert gas supply, (99.99% pure argon gas) from the glove box

purification system, while the second connects to the oxygen supply for the glow discharge. The oxygen is Matheson research purity (99.98%).

The main manifold also is equipped with a Matheson 63-5601 760 to 0 Torr absolute pressure gauge and a Varian 531 thermocouple gauge for monitoring pressure. The manifold is pumped by a Precision DD-195 195 ℓ/min direct-drive mechanical pump. The base pressure in the manifold is less than 10 microns. The manifold is wrapped with heating tape, which allows a bakeout at temperatures in excess of 100°C. It is connected to the vacuum system through a Whitey SS-4BMW precision metering valve, which allows accurate pressure control during the glow discharge.

B. Glove Box

The glove box, of local design and construction, is a modified version of a standard glove box. It consists of two chambers: an atmospheric pressure inert gas box, and an evacuable entrance chamber to which the ultrahigh vacuum fabrication system is mounted. The two chambers are connected by a standard pass-through port.

The inert gas chamber is equipped with a Vacuum Atmosphere HE-63P Pedatrol pressure control unit, which is supplied with high purity (99.99%) argon gas and a Precision DD-195 195 ℓ/min vacuum pump; a 120 V, 15 A 3-wire electrical connector; and the inert atmosphere purification system. The inert atmosphere box can be used as a standard glove box for the preparation of air or water sensitive materials. Experience has shown, however, that it is more convenient to prepare solutions on a vac-line, and the inert atmosphere box is used primarily for transferring solid chemicals to Schlenk-flasks and the storage of materials prior to use in the synthesis of the tunnel junctions.

The purification system consists of an Air Cadet 7530-40 900 ml/min pressure pump which circulates the atmosphere in the inert gas box, a cylinder containing one l of "Catalyst R3-11" (Chemical Dynamics) oxygen removing catalyst, and a cylinder containing one l of Linde 4A molecular sieve dehydrating agent. The R3-11 catalyst is activated with hydrogen at 160°C for 12 hours. In use, the R3-11 catalyst is operated at 120°C. This catalyst is sufficient to remove residual oxygen from at least ten size 1A cylinders of 99.95% argon before regeneration (about 300 moles of argon or 0.2 moles of oxygen).

The entrance chamber to the vacuum box has been designed specifically for the purpose of attaching the ultrahigh vacuum fabrication system. Rather than the standard cylindrical chamber, a rectangular chamber has been constructed. The flat surfaces allow the attachment of the ultrahigh vacuum chamber through an O-ring mount to the floor of the entrance chamber. In addition, windows (1" thick Plexiglas) are provided on the top and front to allow viewing of the liquid phase adsorption, and covered gloves are provided on the front panel to manipulate the junctions. The covered gloves, visible on the vacuum box in Fig. 1, are connected to a pressure equalization line to prevent the gloves from exploding due to trapped air during pumpdown of the vacuum box. The pressure equalization line is closed and the covers opened during use. Obviously, the gloves can be used only when the vacuum box has been pressurized up to one atm with inert gas from the purification system. Finally, the larger entrance port facilitates frequent maintenance of the ultrahigh vacuum system, e.g. aluminum and lead replacement.

The entrance chamber is pumped by a Precision DD-195 195 l/min mechanical pump which is capable of reducing the chamber pressure to below 100 microns in approximately 25 minutes. A pump-purge-pump-purge cycle produces acceptably low levels (approximately 5-10 ppm) of residual oxygen and

water. By allowing sufficient time (approximately 30 minutes) for the residual 5-10 ppm of oxygen and water to be removed from the box by the purification system, a base condition of approximately one ppm oxygen and one ppm water is obtained.

For adsorption from solution onto the oxide surface of a tunnel junction, the materials to be used are placed in the entrance chamber, and the pass-through port is closed. After the adsorption, the materials are immediately returned to the storage chamber. This minimizes the concentration of any solvent vapors that might contaminate the main box, and any such contamination is removed quickly by the purification system. There has been no evidence either of solvent contamination on junctions prepared in this system or of contamination of materials stored in this system. The volume of solution that is used ($\lesssim 5\ \mu l$) is sufficiently small that static evaporation (as opposed, for example, to sample spinning) has proved satisfactory.

III. Results and Discussion

To demonstrate the advantages of liquid phase adsorption on aluminum oxide employing this system, tunnel junctions exposed to m-cresol (3-methylphenol) were synthesized from both the vapor and liquid phases. Spectra were obtained with the electronic system described previously **(16)**, and background subtraction was employed for peak position determination **(17)**. A previous spectrum of m-cresol, adsorbed from the vapor phase onto aluminum oxide, has been obtained by inelastic electron tunneling spectroscopy, but the vibrational frequencies were not determined **(18)**. The tunneling spectrum we obtained after a 100 Torr-s exposure (10^{-1} Torr for 1000 s) is shown in Fig. 6(A). Only weak modes consistent with molecular adsorption are present. The differences in the surface concentration of m-cresol between our system and

that of Walmsley et al. **(18)** may be due to variations in the nature of the aluminum oxide surface (e.g. extent of hydroxyl coverage) which result from differences in oxide preparation conditions (e.g. glow discharge voltage and current, and electrode location). The tunneling spectrum obtained after an exposure of 5 μl of a 1% weight/volume (w/v) solution (~0.1 M) of m-cresol in hexane (approximately 3 x 10^{17} molecules of m-cresol) is shown in Fig. 6(B), and it is quite similar to that obtained by Walmsley et al. **(18)**. This tunneling spectrum was processed to remove the background, and the resulting spectrum is shown in Fig. 6(C). The reaction of m-cresol with the aluminum oxide surface results in the cleavage of the OH bond to form water, which desorbs, and aluminum 3-methylphenoxide.

The vibrational spectra of m-cresol as a pure liquid and dissolved in various solvents have been measured and analyzed by Varsanyi (dissolved in CCl_4, CS_2 and n-hexane) **(19)**, Lagrange et al. (dissolved in CCl_4, CS_2 and n-hexane) **(20)**, Herz (pure liquid) **(21)**, and Biswas (pure liquid) **(22)**. The assignments for the vibrational **(19)** and tunneling spectra are presented in Table 1, together with the peak values observed in the tunneling spectrum for m-cresol chemisorbed on aluminum oxide from the liquid phase. The mode numbering is based on the normal modes of the unsubstituted benzene molecule **(19)**, and the mode descriptions have been modified to account for the substitution. The vibrational spectrum of adsorbed m-cresol (in its phenoxide form) matches the vibrational structure of the solvated m-cresol quite well. This implies that the aluminum 'salt' of m-cresol is quite similar to the protonated species. A similar effect was noted in a study of phenol and the o-, m- and p-hydroxy phenols adsorbed on Al_2O_3 employing tunneling spectroscopy **(23)**. Only the ν(C-H) and $\delta(CH_3)$ modes show significant downshifts (1-2%), probably due to the presence of the lead overlayer. The effects of the lead overlayer on tunneling spectra are dicussed by

Kroecker and Hansma **(24)**.

The glove box fabrication system also provides a dry (water vapor approximately one ppm vs. 1% in normal air), inert atmosphere for the preparation of junctions with atmosphere-sensitive compounds. As an example, junctions were prepared with 1% w/v (~0.2 M) solutions of ethanolamine (2-aminoethanol) in hexane, both in the inert atmosphere glove box and in the laboratory atmosphere. The results are shown in Fig. 7(A) (inert atmosphere) and 7(B) (laboratory atmosphere). The junctions prepared in the inert atmosphere produce spectra with differences in the intensities and the frequencies of the carbon-hydrogen stretching modes. The frequencies are summarized in Table 2. Turner et al. **(25)** have prepared tunnel junctions by adsorbing ethanolamine from the vapor phase, and Ghazanfar et al. **(26)** have obtained Raman spectra from pure liquid ethanolamine and ethanolamine dissolved in water. Data from these references are also included in Table 2.

A comparison of the vibrational frequencies observed after liquid adsorption in the inert atmosphere (Fig. 7A) and the vapor phase adsorption indicates a strong correspondence between the two systems. Turner et al. **(25)** propose a bidentate surface species to fit their data. Our data are consistent with an oxygen, nitrogen bound bidentate structure, such as

(I)

The laboratory atmosphere system (Fig. 7B) shows several similarities with aque-

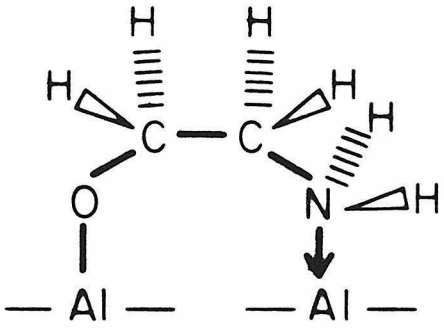

(I)

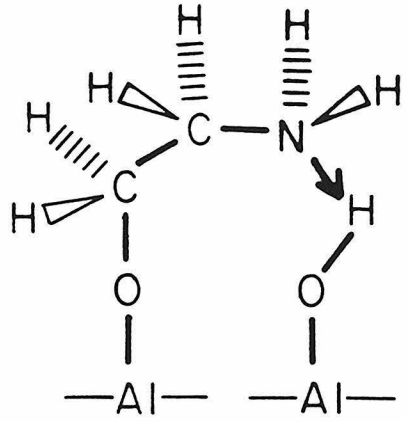

(II)

ous ethanolamine **(26)**. In particular, the ν_s(CH), ν_a(CH) and $\delta(NH_2)$ vibrational modes of the two systems are very similar, but differ from the inert atmosphere system by 20 to 30 cm^{-1}. This correspondence between the laboratory atmosphere system and the aqueous system suggests hydroxyl group interactions, i.e.

(II)

These data serve to illustrate the effects that preparation conditions can exert on the structure of the adsorbed molecule, and to demonstrate the utility of the glove box system in the preparation of air or water sensitive systems.

Acknowledgment

This work was supported by the National Science Foundation under Grant No. DMR-8500789.

References

1. P. K. Hansma, Phys. Rep. C **30**, 146 (1977).
2. W. H. Weinberg, Ann. Rev. Phys. Chem. **29**, 115 (1978).
3. *Inelastic Electron Tunneling Spectroscopy*, T. Wolfram, Ed. (Springer, Berlin) 1978.
4. P. K. Hansma and J. R. Kirtley, Acc. Chem. Res. **11**, 440 (1978).
5. H. W. White and T. Wolfram, Methods Exp. Phys. A **16**, 149 (1980).
6. S. Ewert, Appl. Phys. A **26**, 63 (1981).
7. H. W. White, L. M. Godwin and R. Elliatioglu, J. Adhes. **13**, 177 (1981).
8. *Tunneling Spectroscopy*, P. K. Hansma, Ed. (Plenum, New York) 1982.
9. W. H. Weinberg, Vibrational Spectra and Structure **11**, 1 (1982).
10. S. K. Khanna and J. Lambe, Science **220**, 1345 (1983).
11. K. W. Hipps and U. Mazur, Rev. Sci. Instrum. **55**, 1120 (1984).
12. D. F. Shriver, *The Manipulation of Air-Sensitive Compounds* (McGraw-Hill, New York) 1969.
13. H. E. Evans. PhD thesis, California Institute of Technology, 1980.
14. W. M. Bowser and W. H. Weinberg, Rev. Sci. Instrum. **47**, 583 (1976).
15. W. M. Bowser, PhD thesis, California Institute of Technology, 1980.
16. G. J. Gajda and W. H. Weinberg, Rev. Sci. Instrum. **56**, 700 (1985).
17. G. J. Gajda and W. H. Weinberg, J. Vacuum Sci. Technol. A **3**, 2208 (1985).
18. D. G. Walmsley, W. E. Timms and N. M. D. Brown, Solid State Commun. **20**, 627 (1976).

19. G. Varsanyi, *Assignments for Vibrational Spectra of Seven Hundred Benzene Derivatives* (Wiley, New York) 1974.

20. C. Garrigou-Lagrange, M. Chehata and J. Lascombe, J. Chim. Phys. **63**, 552 (1966).

21. E. Herz, Monatsh. Chem. **74**, 160 (1941).

22. D. C. Biswas, Ind. J. Phys. **29**, 257 (1955).

23. W. H. Weinberg, W. M. Bowser and B. F. Lewis, Jpn. J. Appl. Phys., Supp. 2, Pt. 2, 863 (1974).

24. R. M. Kroecker and P. K. Hansma, Catal. Rev. Sci. Eng. **23**, 553 (1981).

25. R. J. Turner, N. M. D. Brown and D. G. Walmsley, Vacuum **31**, 603 (1981).

26. S. A. S. Ghazanfar, J. T. Edsall and D. V. Myers, J. Am. Chem. Soc. **86**, 559 (1964).

Table 1. Vibrational Frequencies in cm^{-1} and their Assignments for m-Cresol

Mode (19)	IR/Raman Herz (21)	Biswas (22)	Lagrange (20)	Varsanyi (19)	Adsorbed on Al_2O_3 (this work)	Assignment (19)
1	734	734	734	734		ν_s ring
2	3047	3052		3052	3015	ν_s(C-H)
3	1281	1276	1281	1281	1284	ν_a ring
4			686	686	697	γ(C-H)
5		956	959	959	945[a]	γ_a ring
6a	540	543	537	537	521	ν_a ring
6b	518	518	517	517	521	ν_a ring
7a				2995-3050[b]	2941	ν_a(C-H)
7b			928	928	860-945[c]	ν_a ring
8a	1592	1593	1590	1590	1587	β_s(C-H)
8b	1616	1616	1613	1613	1617	β_a(C-H)
9a	303	305		307	307	β_s subst.
9b	1161	1166	1150	1150	1152	δ_a ring
10a	243	245		239	<240[d]	γ_a subst.
10b	215	216		214		γ_a subst.
11		779	776	776	780	γ_s ring
12	1000	1002	1000	1000	1008	ν_s ring
13	1267	1276	1267	1226	1265	ν_a ring
14			1305	1370	1302	β_a(C-H)
15				290-495[b]	338	β_a subst.
16a	564	569		564	571	γ_a(C-H)
16b		450	442	442	445	γ_s(C-H)
17a			925	928	860-945[c]	γ ring
17b		848	854	854	860	γ_a ring
18a			1080	1080	1076	δ_a ring
18b	1086	1085	1086		1090	δ_s ring
19a	1474	1460	1460	1460	1463	β_s(C-H)
19b	1474		1490	1490	1486	β_a(C-H)
20a				3000-3060[b]	2960[e]	ν_a(C-H)
20b				3040-3120[b]	3050[e]	ν_a(C-H)
$\nu(CH_3)$	2922	2920		2920	2893	$\nu(CH_3)$
$\delta_s(CH_3)$	1378	1383	1377	1377	1357	$\delta_s(CH_3)$
$\delta_a^+(CH_3)$	1435		1436	1436	1421	$\delta_a(CH_3)$
$\delta_a^-(CH_3)$			1039	1039	1030	$\delta_a(CH_3)$
β(OH)			1186	1186	1178[f]	β(OH)

Abbreviations: ν = stretching mode, δ = deformation mode, β = in-plane bending mode of a ring substituent, γ = out-of-plane bending mode, s = symmetric, and a = asymmetric.

[a]This mode is primarily the ν(Al-O) in the tunneling spectrum. [b]Only a range

was given in Ref. 19. [c]Range indicated since two intense peaks overlap in this region. [d]Peak occurs below 240 cm^{-1}; only the high frequency (>240 cm^{-1}) part appears in the spectrum. [e]Peaks not well resolved. [f]The presence of this mode in the tunneling spectrum suggests that the 1178 cm^{-1} peak may not be a pure β(OH) local mode.

Table 2. Vibrational Frequencies in cm^{-1} and their Assignments for Ethanolamine

Adsorption on Alumina from Vapor Phase **(25)**		Adsorption on Alumina from Hexane Solution in Inert Atmosphere	Ethanolamine **(26)**[a]		Adsorption on Alumina from Hexane Solution in Laboratory Atmosphere
Assignment	Frequency	(this work)	Pure Liquid	Aqueous Solution	(this work)
Al phonon	284	296			295
ν_s(C-C-O/N)	889				
ν(Al-O)	940	944			941
ν(CN,CO)	1051	1051			1062
ν_a(C-C-O/N)	1192	1194w			1194
CH_2 torsion	1262	1266	1251	1264	1279
CH_2 torsion	1303	1298			
CH_2 rock	1383	1379			1395
CH_2 scissors	1454	1455	1458	1463	1470
$\delta(NH_2)$	1575	1567	1597	1599	1605
ν(AlH)?		1850vbr			1850vbr
ν(CH)?	2734	2731			2751
ν(CH)	2835	2844			
ν_s(CH)	2865	2864	2865	2886	2890
ν_a(CH)	2916	~2920sh	2924	2946	2955
$\nu_s(NH_2)$	3269	3263[b]			3300-
$\nu_a(NH_2)$	3319	3336[b]			3500vbr
ν[(Al)OH]	3650	3640			3650

Abbreviations: sh = shoulder, w = weak, vbr = very broad.

[a]Only vibrational modes which exhibit shifts of more than 10 cm^{-1}, the $\delta(NH_2)$ mode and the CH_2 scissoring mode are included in this list. [b]Peaks poorly resolved from a very broad mode.

Figure Captions

Figure 1. General view of the glove box based fabrication system.

Figure 2. View of the ultrahigh vacuum fabrication chamber showing a flask mounted on the "mini-manifold".

Figure 3. View of the glow discharge subsystem (left) and the metal evaporation sources. The molybdenum boat for the lead (left box) and tungsten filament for the aluminum (right box) are visible through the shielding boxes.

Figure 4. (A) View of the mask/shutter assembly with the slide holder in place. The shutter (left) and mask holder (right), with masks for aluminum and lead patterns, are both shown in the open position. (B) Close-up view of the crystal monitor (top), quick connect (bottom left) and monitor lead connector (bottom right).

Figure 5. The slide holder with completed junctions and heating leads soldered in place. The male half of the quick-connect is at the top.

Figure 6. (A) Tunneling spectrum of m-cresol adsorbed from the vapor phase [500 scans, lock-in amplifier time constant, τ = 10 ms, V_{mod} = 1.7 mV rms]. (B) Tunneling spectrum of m-cresol adsorbed from the liquid phase 1% w/v (~0.1 M) m-cresol in hexane [1000 scans, τ = 3 ms, V_{mod} = 1.7 mV rms]. (C) Spectrum B with the background removed.

Figure 7. (A) Tunneling spectrum of 1% w/v (~0.2 M) ethanolamine adsorbed from hexane solution in the glove box with the background removed [1000 scans, τ = 1 ms, V_{mod} = 1.7 mV rms]. (B) Tunneling spectrum of 1% w/v (~0.2 M) ethanolamine adsorbed from hexane solution in the laboratory atmosphere with the background removed [4000

scans, τ = 1 ms, V_{mod} = 1.7 mV rms].

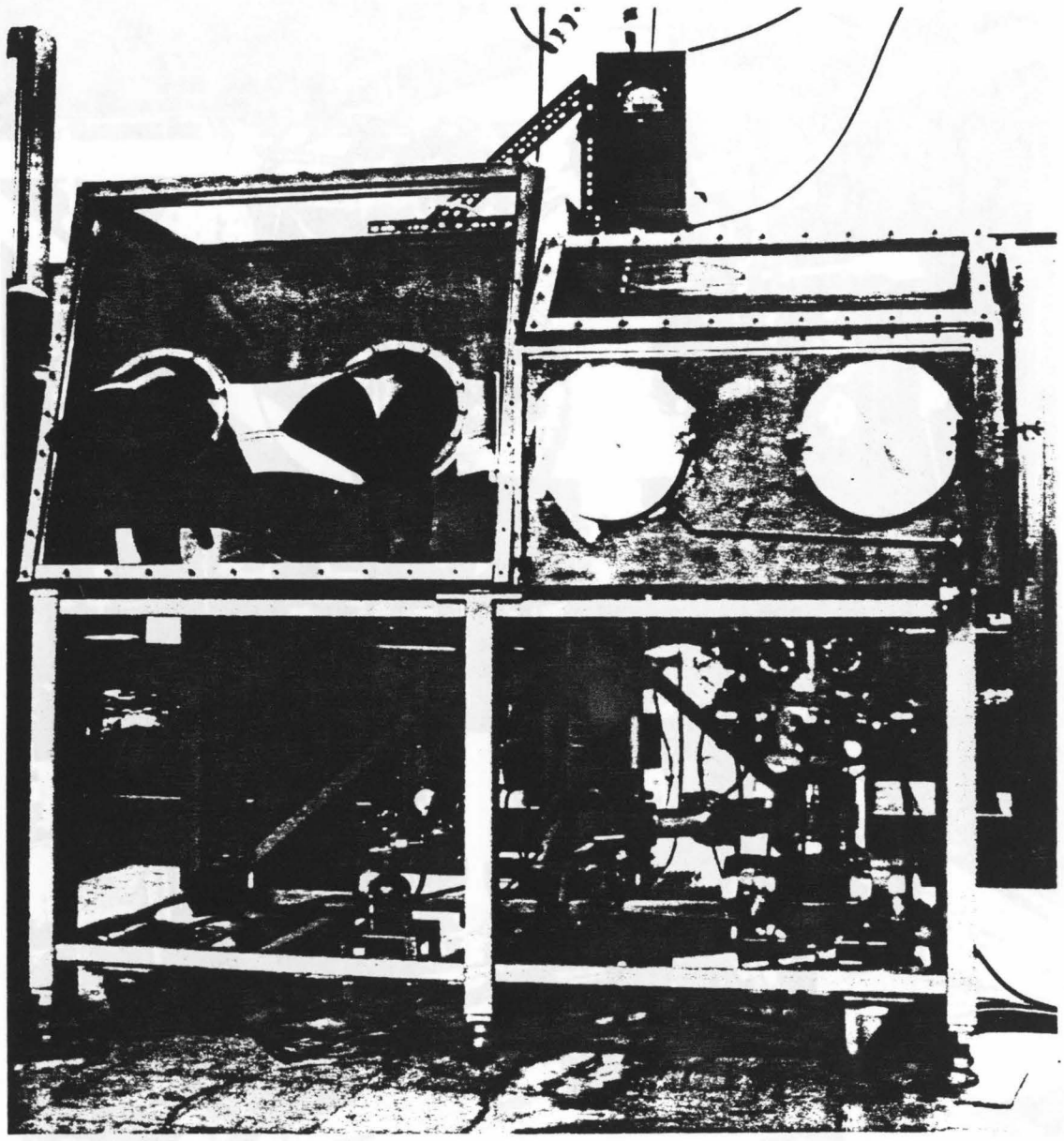

Fig. 1

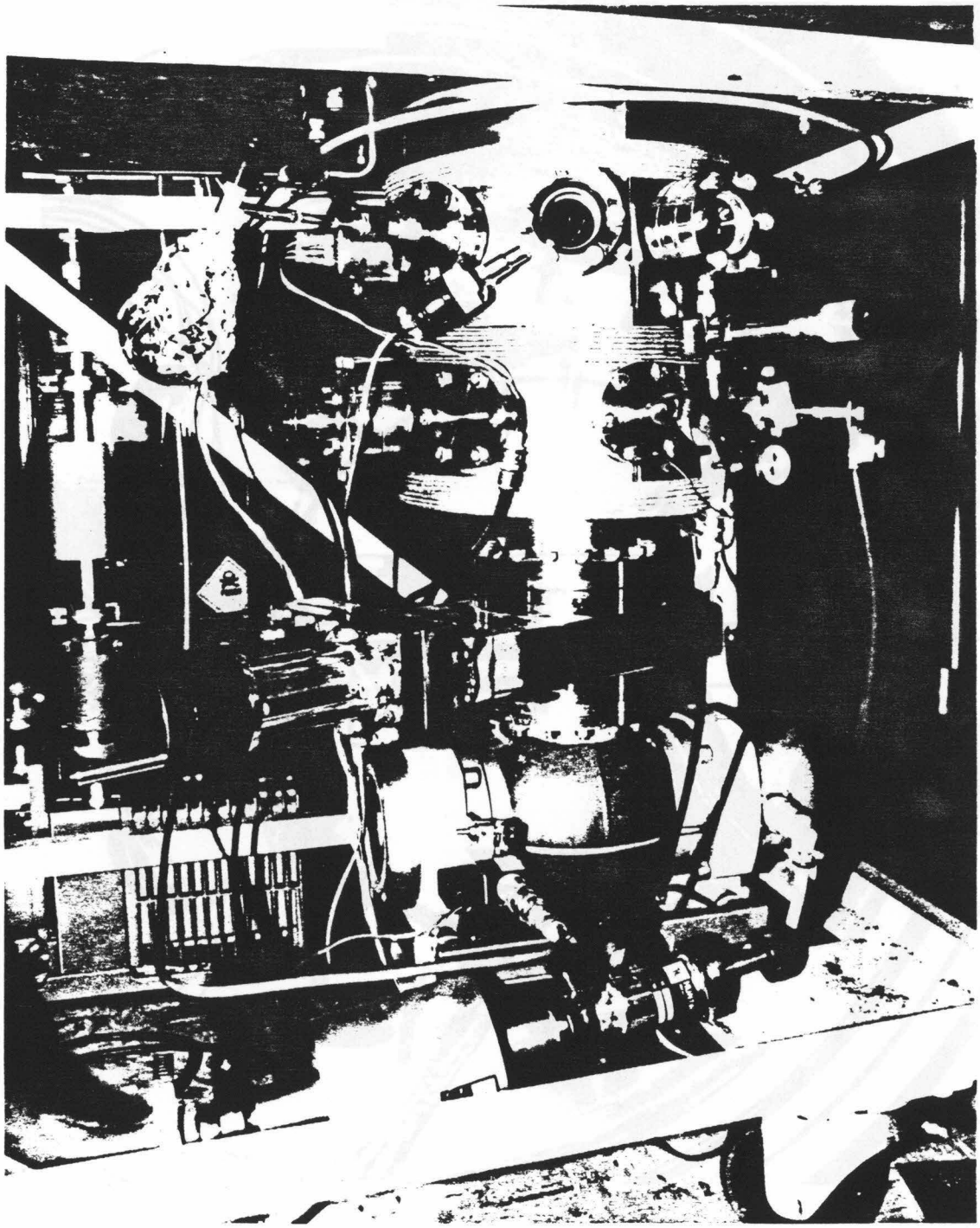

Fig. 2

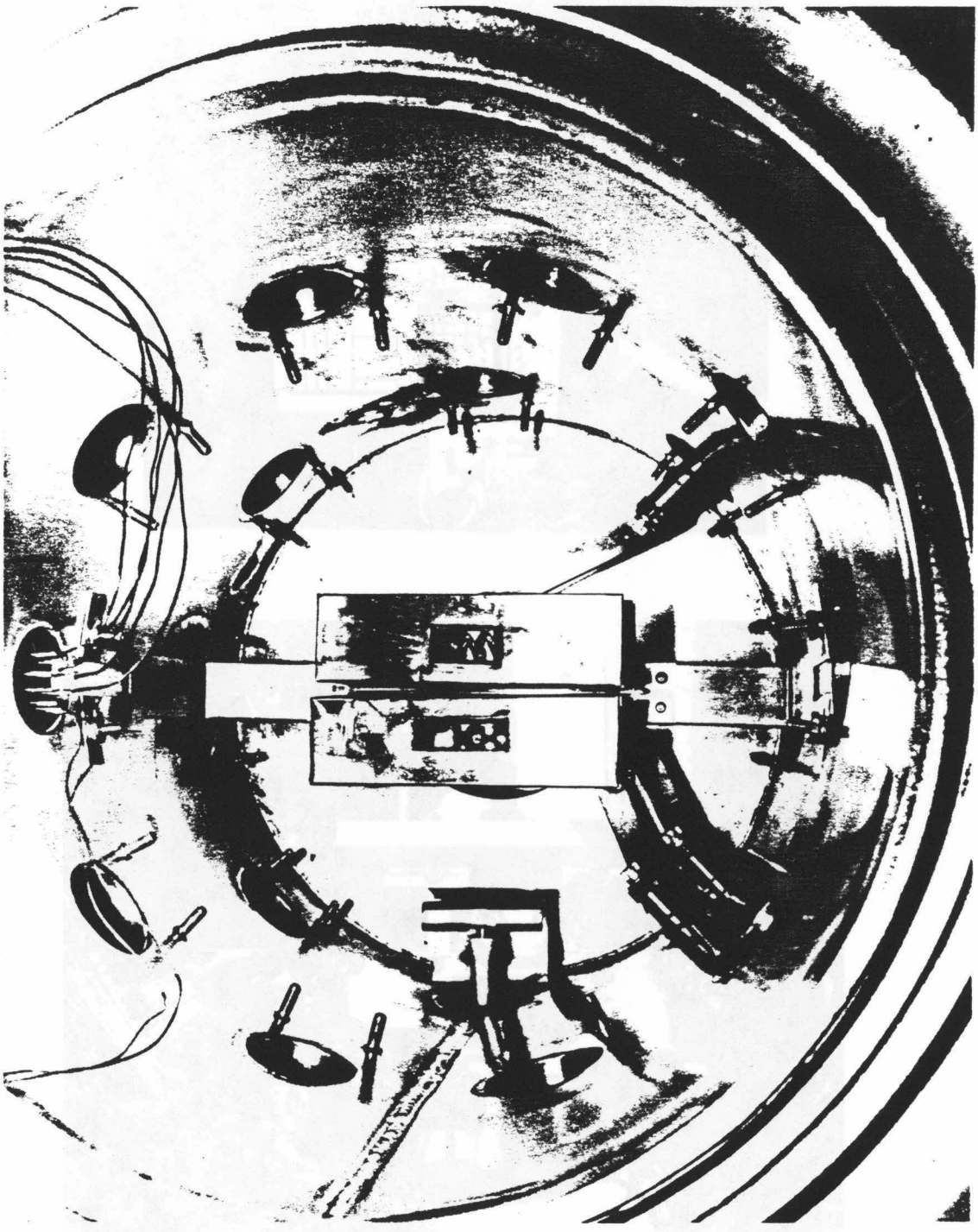

Fig. 3

A)

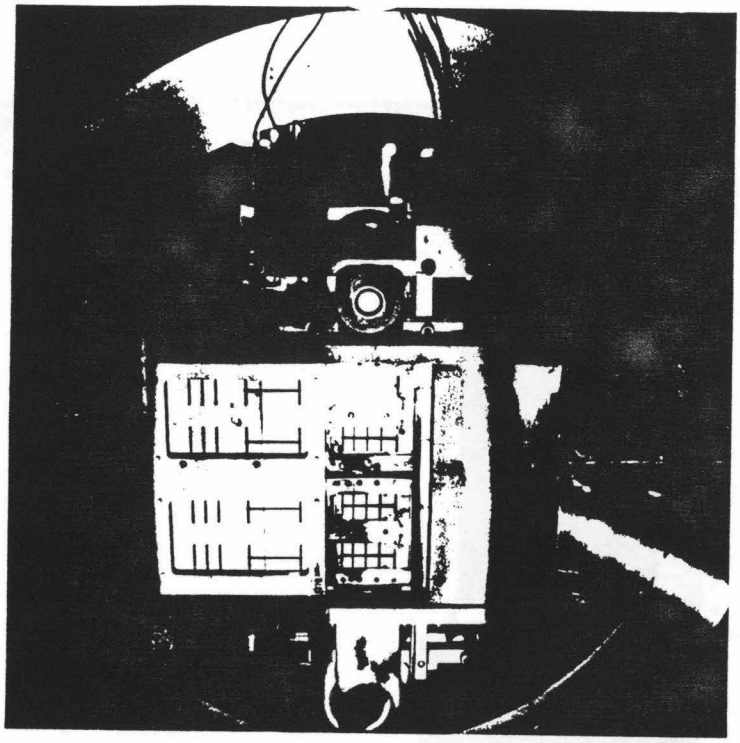

B)

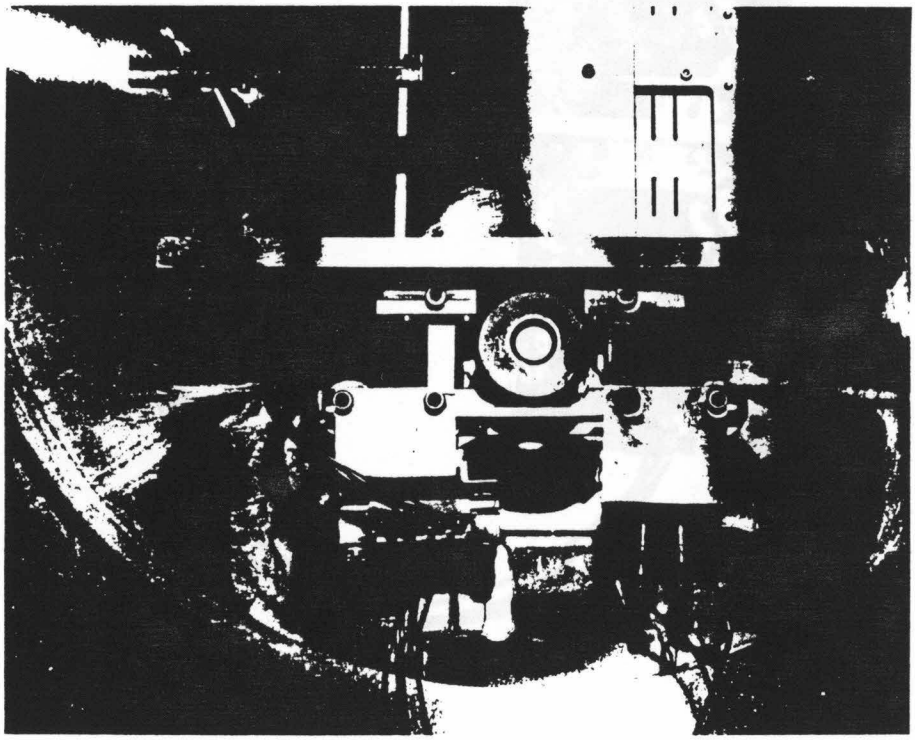

Fig. 4

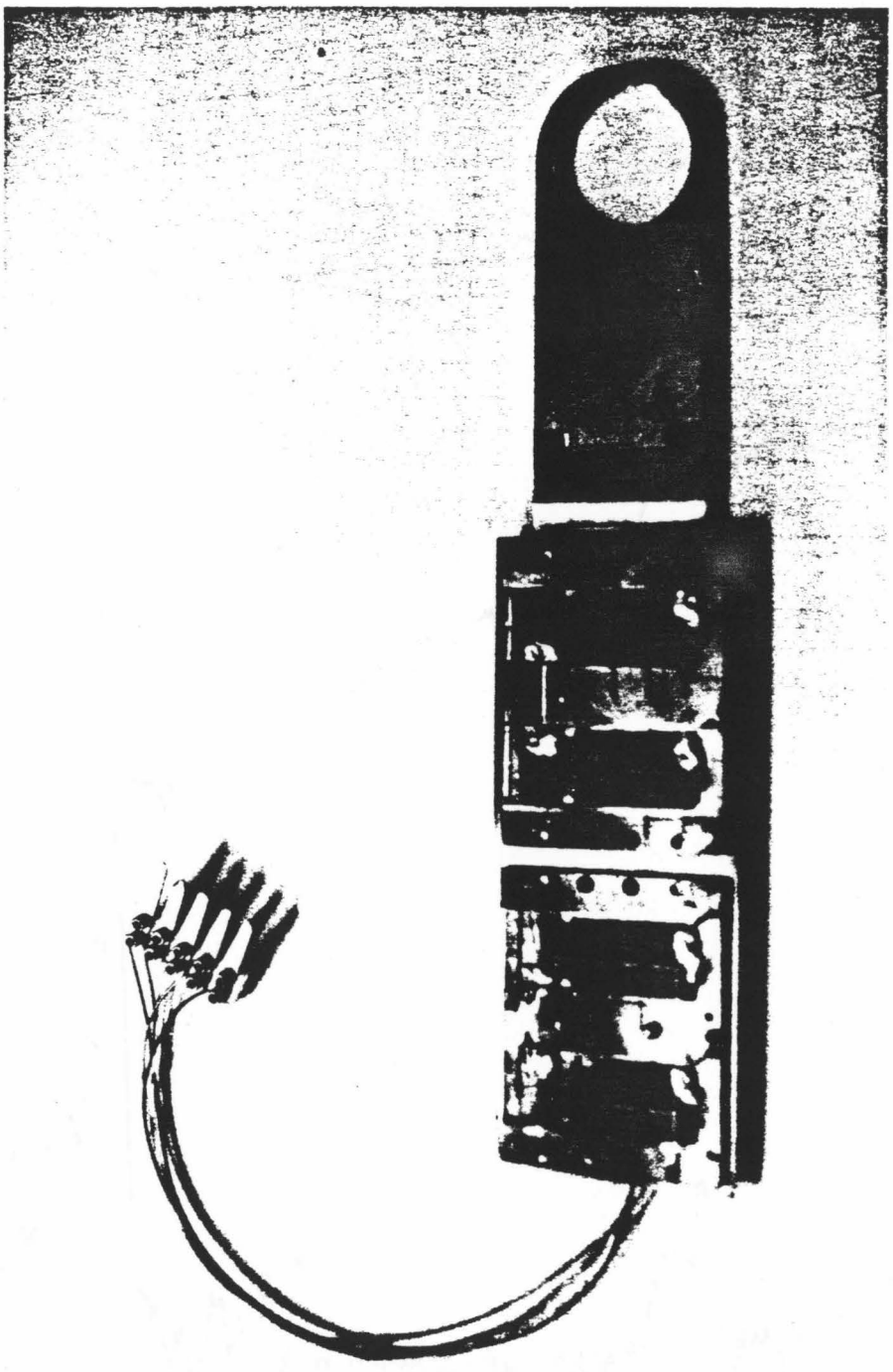

Fig. 5

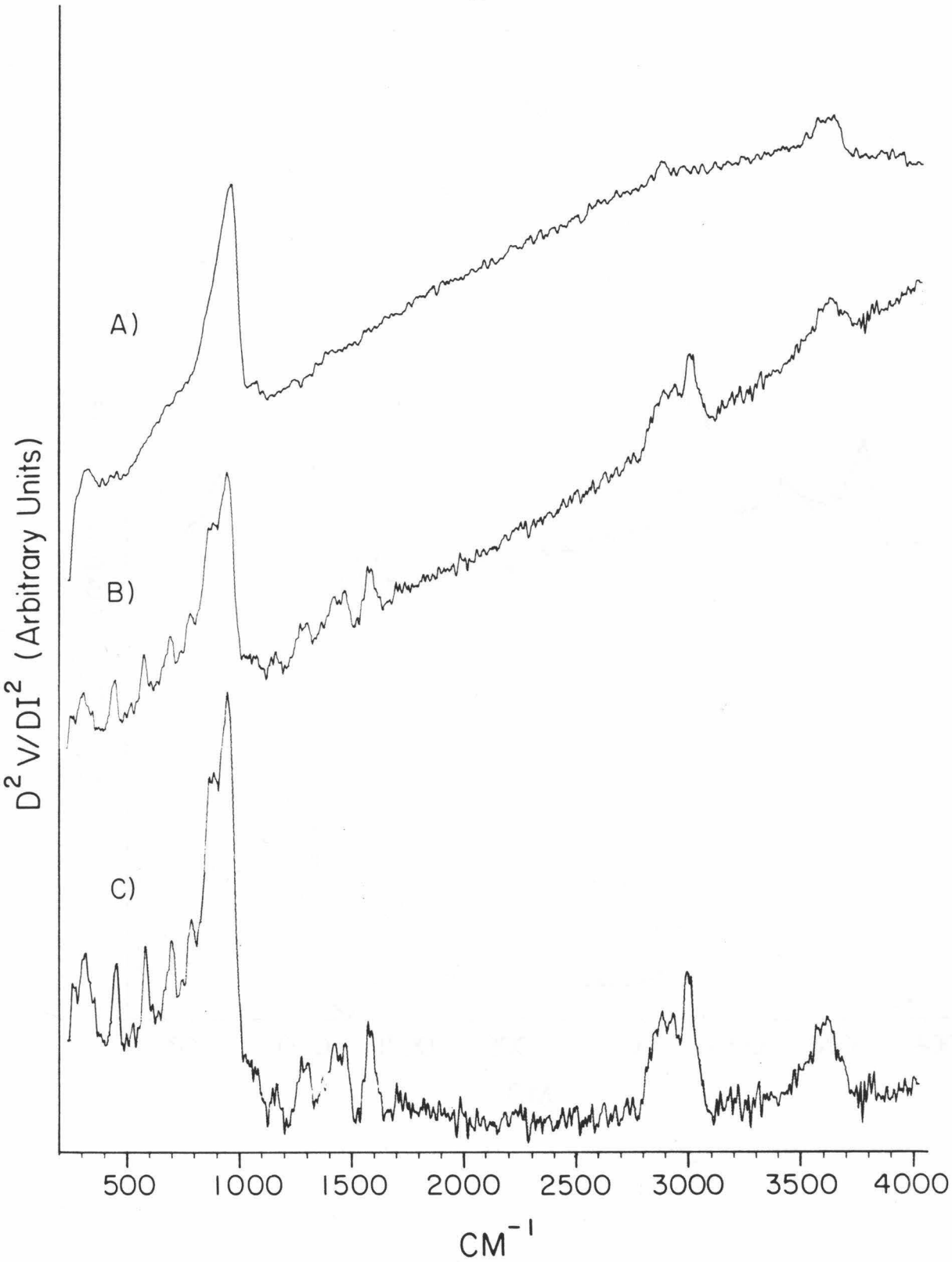
A)
B)
C)
D^2V/DI^2 (Arbitrary Units)
500
1000
1500
2000
2500
3000
3500
4000
CM^{-1}

Fig. 6

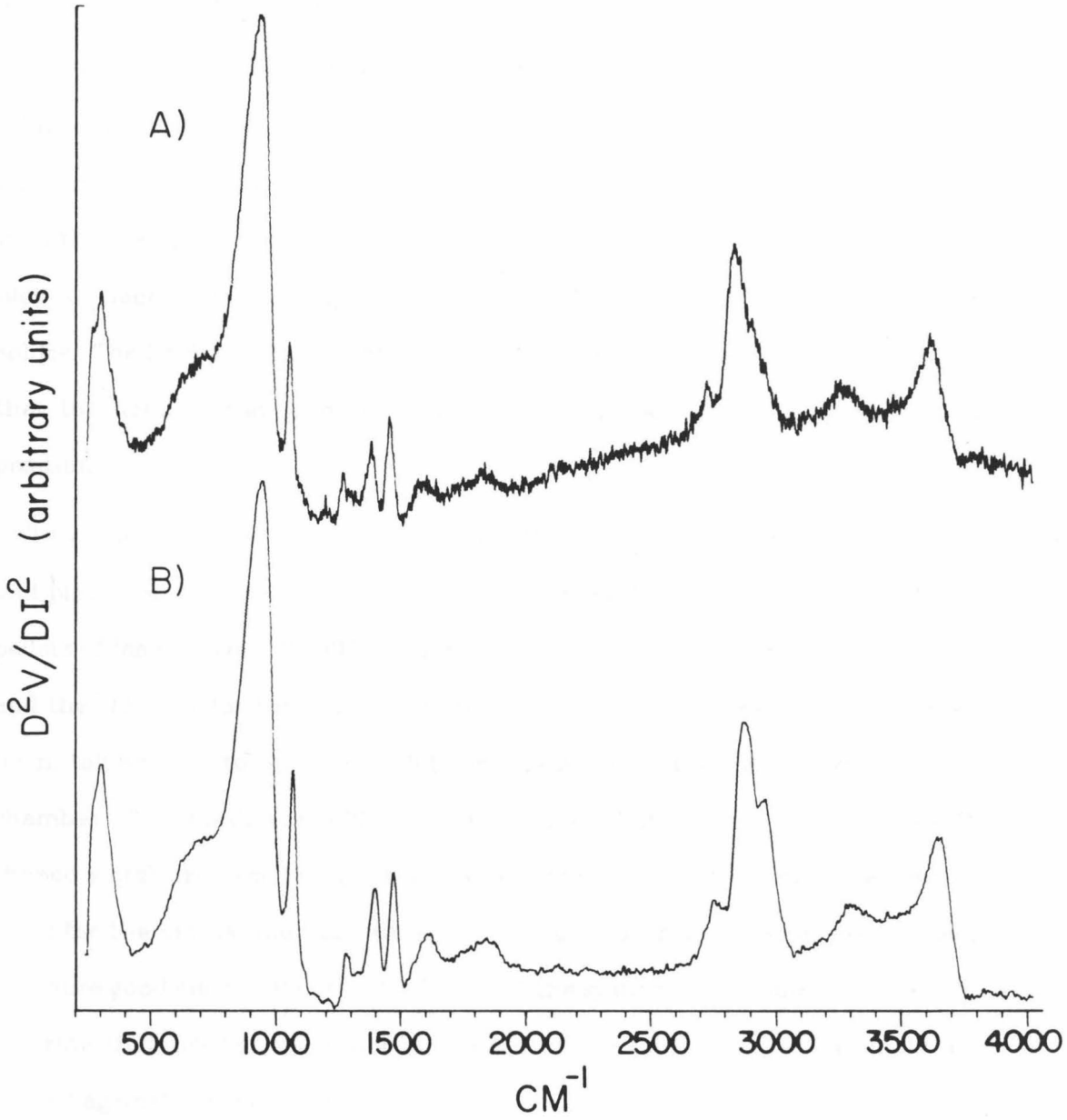
A)
B)
D^2V/DI^2 (arbitrary units)
500
1000
1500
2000
2500
3000
3500
4000
CM^{-1}

Fig. 7

APPENDIX

Junction Fabrication Procedure

Four 1" x 1/2" glass slides (Corning 9053) are cleaned, if necessary, in a dilute solution of detergent (Alconox), rinsed with distilled water, then methanol and dried under nitrogen. They are inserted into the substrate holder which uses the spring tension of the slotted intermediate metal sheet to hold the samples in place. The heating wire leads are soldered to the slides with indium solder. The holder is then inserted into the mask/shutter assembly, taking care that the heating leads are not damaged. The quick-connect is tightened into position.

Two 1" long rods of aluminum (Balzers 99.995%) are bent into U-shaped forms and placed on the two center coils of the tungsten filament. Approximately ten pellets of lead (Balzers 99.995%) are placed on the molybdenum boat. The boxes and the chimney for the aluminum are placed on the evaporation support platform, taking care to orient the slots on the box tops toward the center of the chamber. The mask assembly is positioned so that the aluminum masks (I-shaped slots) are over the glass slides, and the shutter is closed. The connections for the crystal monitor wires and the junction heating wires are checked to insure good electrical contact. The lid of the system is then lowered carefully, insuring that neither wires nor the edges of the mask/shutter assembly are pinned against the chamber flange.

The pumpdown is started by opening the gate valve, by pressing the "pump" switch on the turbomolecular pump control unit, and then opening the valve in the turbo-pump foreline. This sequence is necessary since the vent valve on the turbopump will not close unless the pump is on, and an unnecessarily large

amount of argon will be drawn through the mechanical pump if the sequence is reversed. The pressure in the chamber can be monitored on the thermocouple gauge, and should drop below ten microns in approximately one minute for proper operation. The turbopump itself requires three minutes to reach maximum velocity. The control circuit incorporates a safety feature which will shut off the turbopump and vent the system if 80% of full speed is not reached in eight minutes. It is important to monitor the pump speed during this period to avoid problems with inadvertent leaks (e.g. leaving the manifold valve open or a burned out vent valve).

After approximately fifteen minutes, the pressure in the system should be less than 10^{-5} Torr, and the glove box can now be purged. The main external door on the glove box is tightened down until the metal retaining strips for the O-ring seal have stopped against the metal frame. The covers for the gloves are tightened carefully, making sure that the gloves are not trapped between the cover and its seal. If necessary, the glove box can be evacuated *slightly* — only enough to pull the gloves inward and clear of their covers. Once the covers are sealed, the pressure equalization valve is opened, and the gloves should deflate. The manifold is sealed off from the vacuum pump and the glove box opened to the vacuum pump. It will require approximately ten minutes for the box to be evacuated below 1 Torr, and the box should be left under vacuum for 30 to 60 minutes.

Prior to refilling the box with argon, insure that the pressure in the tank is greater than 500 psi. If the pressure is insufficient, switch to the back-up tank. The main valve on the glove box is then turned slowly toward the argon setting, and argon is bled into the chamber at a rate slow enough for the pressure control unit to respond. The rate can be increased with time as the pressure difference will become smaller. It will require five to ten minutes to refill the box

completely, and the valve should be left in the 'argon' position. The main door must *not* be opened until the experiment is finished.

If desired, the vacuum chamber and/or the manifold can be baked out. The vacuum chamber requires a variac setting of 130 and should be baked out for at least eight hours, together with a bakeout of the turbo pump. The turbo pump bakeout is controlled by the 'heater' push button on the pump control unit. The vacuum chamber pressure should be less than 10^{-5} Torr before starting the bakeout, and a bakeout should not be attempted during the glove box purge. It should be noted that at least two hours will elapse after termination of the bakeout before the chamber and its internals will be cooled enough to use. The manifold requires a variac setting of 70 and approximately two hours for a good bakeout. It will require about 15 minutes to cool.

The preparation of a set of junctions can now begin. The pressure equalization valve on the glove box is closed, and the glove box covers are opened. The gloves should expand outward due to the slightly greater than atmospheric pressure in the box. Any supplies placed in the vacuum box can now be transferred into the main box. Leaving the interchamber door open provides better regulation of the pressure in the vacuum box.

Double check that the masks are set to the *aluminum* position, the shutter is closed, and that the high current power supply is connected to the *lead* electrode. Be certain that the high current supply is turned off before switching electrodes! Turn on the frequency counter, crystal monitor power supply and ionization gauge, if not on already. The ionization gauge will require approximately five minutes to stabilize due to local heating of the wall by the filament. When all indicators are stable, make sure the high current supply is turned off and the variac is turned down to zero. Turn the supply on and slowly increase

the variac setting until the current meter reads approximately 40 amps. The pressure in the vacuum chamber will rise, and at or slightly above 40 amps, evaporation of the lead will begin, as seen by a decrease in the frequency on the frequency counter. Continue to allow the lead to evaporate until the frequency has decreased by approximately 100-200 Hz. Note the maximum pressure reached in the chamber, and smoothly turn the power down to zero. Then turn off the power supply. This procedure degasses the lead so that adsorbed molecules will not interfere when the lead is evaporated later to form the upper electrode.

The supply current is now shifted to the aluminum electrode. Note the frequency of the crystal. It should be approximately 5 MHz. The thicknesses of the aluminum and lead strips are determined by the frequency change in Hertz during their deposition. All of the following frequency changes are based on an initial frequency of 5 MHz.

Turn on the power supply and increase the current slowly to 20 amps. Pause a moment and then continue to increase the current two amps at a time, pausing after each increment. This procedure insures that the aluminum melts and wets the tungsten filament. If the current is increased too rapidly, the aluminum rods will simply melt through and fall off the filament. At approximately 45 amps, a steady aluminum evaporation should occur. Adjust the current to achieve a rate of 5-10 Hz/second. Open the shutter and note the frequency. Continue the evaporation until 800--1000 Hz of aluminum is deposited. Turn down the current smoothly to zero and turn off the power. Note the final frequency and subtract to obtain the actual aluminum deposition.

When a fresh tungsten filament is used, a slight modification of the above procedure is necessary. Increase the current to 24 amps and wait for the pressure in the chamber to rise to 10^{-6} Torr, and then fall back to about 5×10^{-7}

Torr. This takes about one hour. Raise the current to 28 amps and allow the pressure to rise to approximately 2 x 10^{-6} Torr; when attained, slowly increase the current (about 2 amps/min) to 45 amps where steady evaporation should occur.

For experiments involving the heating of the junctions, it is necessary to anneal the aluminum strips before oxidizing. The junctions are annealed by heating the aluminum strips for 50 seconds to the highest temperature planned for the experiment, then allowing the electrodes at least 300 seconds to cool to room temperature before oxidizing. The heating is accomplished by passing a current through the aluminum strip, which has a typical resistance of 25 ohms. The temperature is determined by measuring the voltage drop across a precision resistor in series with the aluminum strip to determine the current. A second measurement of the voltage drop across the aluminum strip provides the voltage. From these two values, the dynamic resistance ($R_D = V/I$) is determined. Using a formula determined by Bowser and Weinberg **(14)**, the temperature is calculated as

$$T = T_o + \left(\frac{R_D - R_0}{R_0} \right) \times 558.66 ,$$

where T_o is the initial temperature, and R_0 is the initial resistance of the strip.

Now the junctions are oxidized using a glow discharge in an oxygen/water mixture. To prepare the mixture, close the manifold valve leading to the vacuum pump. Add 300 microns of water vapor to the manifold from the water supply attached to ultratorr No. 2. Then add sufficient oxygen from line No. 5 to bring the pressure in the manifold to 300 Torr. Connect the Simpson analog volt meter to the glow discharge electronics and set it to 50 V DC full scale. Turn on the high voltage power supply and set it for -1100 V output. When the high

voltage supply reaches the standby mode, switch the frequency counter to the reset position, turn off the ionization gauge and close the gate valve. Set the masks to the open position and open the shutter.

Slowly open the main shut-off valve on the system, and adjust the metering valve to allow a gradual increase in pressure as monitored by the thermocouple gauge. At approximately 30 microns, switch the high voltage power supply from 'stand-by' to 'on'. Quickly adjust the metering valve to bring the voltage reading on the DVM to -30 V (within 0.5 V is sufficient). Switch the frequency counter from 'reset' to count, and it will function as a stopwatch. The standard oxidation time is 300 seconds, but it may be increased or decreased to form a thicker or thinner oxide, as required. Thinner oxides are used with larger adsorbate molecules to keep the junction resistance below 3000 ohms, which is the upper limit for the measurement electronics. For 'clean' junctions (i.e. no intentionally added molecules), oxidation times of 800-1000 seconds are required to produce junctions with resistances of more than 10 ohms, the lower limit of the measurement electronics.

When the desired time has elapsed, the oxidation is stopped by switching the high voltage power supply back to 'standby'. The shut-off valve is closed, and the metering valve is opened. The gate valve is then opened, allowing the oxidation mixture to be pumped out. The frequency counter is switched back to the frequency mode to monitor the crystal oscillator. The gas manifold is also evacuated. The ion gauge can be turned on after five minutes, and the system left to pump down (for adsorption from the gas phase) or shutdown (for adsorption from the liquid phase).

For adsorption from the gas phase, the system is left to pump down to the desired background pressure. To reach a pressure of 5×10^{-7} Torr requires

approximately 30 minutes. Meanwhile, the adsorbate to be introduced should be placed on the manifold and placed through several freeze-degas-thaw cycles to remove trapped air, etc. If the adsorbate is reactive, the manifold must be presaturated by filling the manifold with the vapor and pumping it out several times.

When the appropriate background pressure is reached, the gate valve is closed, and the vapor added to the chamber through the metering valve. Be certain to close the metering valve before opening the shut-off valve. The most convenient way to introduce condensed adsorbates is at their equilibrium vapor pressure, so that the ion gauge and thermocouple gauge can be turned off. If reduced pressures are needed, either the thermocouple gauge or the ion gauge must be used. These, however, can cause significant decomposition of sensitive molecules. The length of exposure is timed, using the frequency counter as a stopwatch, as for oxidation. When completed, the system is pumped down following the procedure from the oxidation. A background pressure of $\leq 5 \times 10^{-7}$ Torr is necessary prior to the lead evaporation. The manifold should be baked out for several hours if particularly 'sticky' compounds are used. A similar procedure is followed for the mini-manifold.

Adsorption from the liquid phase may be carried out by allowing the fabrication system to equalize in pressure with the vacuum box. The necessary materials are transferred from the atmosphere box to the vacuum box, and the interchamber door is closed to minimize solvent contamination. The lid of the fabrication system is opened, and the quick-connect is disconnected. The sample holder can be removed and placed on a suitable tray to catch any spills. The prepared solutions are then placed on the aluminum strips with a gas-tight syringe, and any excess is allowed to run off. The holder is returned to the mask/shutter assembly and the quick-connect is retightened. The lid is closed,

and the pumpdown is started as described above. The solutions are returned to the atmosphere box, and the excess solvent and syringes are neutralized with ethanol if necessary (e.g. when metal alkyls are used). After insuring that the interchamber door is closed, the system is pumping down, and the vacuum/inert gas valve for the vacuum box is in the off (center) position; the vacuum box may be opened and the used materials retrieved for cleaning or disposal.

When the fabrication system pressure has been reduced to below 2 x 10^{-7} Torr, the remaining steps of the fabrication can be completed. Many experiments require long preparation sequences. For example, the reaction sequence of molybdenum hexacarbonyl involves: (1) dehydrate the junctions at 200°C for ten minutes, (2) expose to $Mo(CO)_6$ at 100 μ for five minutes, (3) pump down to below 1 x 10^{-7} Torr, (4) heat to 100°C for ten minutes, (5) heat in 2 Torr ethylene for 1800 seconds, and (6) pump down for lead evaporation.

After the final fabrication step, the system is pumped down to below 10^{-7} Torr (preferably below 5 x 10^{-8} Torr) for the lead evaporation. The lead evaporation is straightforward. Set the mask for lead and close the shutter. Connect the heating lead to the lead evaporation source and raise the current to 45 amps. When evaporation starts, as indicated on the crystal monitor, open the shutter and deposit 10 KHz of lead. Turn off the power and close the shutter. Allow the system to cool for 15 minutes, and then shut down the system as follows. Turn off the ion gauge, close the right-angle valve for the turbopump, and turn off the turbopump power supply. The system will backfill automatically, taking about two minutes to reach atmospheric pressure. The sample holder is removed (as described above for the solution dosing step) and the individual samples desoldered from the heating leads. They are then mounted for measurement as described by Bowser **(15)**.

Table A1. Fabrication Summary

1. Mount slides to heating leads with indium solder.
2. Insert holder into track, being careful with heating leads.
3. Connect heater quick-connect and tighten screws with allen wrench.
4. Set mask to aluminum position.
5. Replace aluminum and lead.
6. Clean O-rings with acetone.
7. Pump down system (open gate valve, start turbopump, open right-angle valve).
8. Bake out system overnight.
9. Insert materials into glove box and pumpdown glove box.
10. Refill glove box with argon.
11. Degas lead (40 A, ΔHz = 0.1 kHz).
12. Evaporate aluminum (28A $\rightarrow$ 5 x 10^{-7} Torr, $\rightarrow$ 45A evap, ΔHz = ~600 Hz) for a new filament (24A $\rightarrow$ 1 x 10^{-6} Torr, $\rightarrow$ 45A evap).
13. Anneal strips (~100 mA, 200°C).
14. Prepare oxygen:water mixture (300 μ H_2O + 300 Torr O_2).
15. Oxidize (60-80 μ H_2O/O_2 mixture, -1100 V, -30 V/R, (= 12 mA), 300s.
16. Heat strips.
17. Expose to reactants.
18. Pump out system (90-120 min P < 5.0 x 10^{-7} Torr for Pb).

19. Evaporate lead (40 A, ΔHz = 10 KHz).

20. Open system (close right-angle valve, turn off turbo pump).

21. Disconnect quick-connect with allen wrench.

22. Open glove box.

23. Remove sample holder and mount slides for measurement

Table A2. Measurement Summary

1. Insert sample holder into liquid helium.
2. Measure 4-wire resistances.
3. Turn on terminal.
4. Connect DVM to mod port to measure AC and DC volts.
5. Start computer program (R IETS).
6. Number of scans: 100.
7. Connect measurement leads to box and set to first junction.
8. Set sine-wave voltage to 3 V.
9. High resolution: N (no).
10. Enter file name, IVMIN, IVMAX, IVMOD, adjusting the modulation voltage to ~1.50 mV RMS.
11. Step through spectrum.
12. Run junction: Y, take spectrum; N, step through spectrum (for scaling, etc.); R, reject, go to next junction; O, show spectrum on oscilloscope
13. Make necessary adjustments for best spectrum.
14. Take spectrum (100 scans x 10 ms, 500 scans x 3 ms for good junctions).
15. Next junction (set R to 10 KΩ, V mod to O).
16. When finished, reconnect measurement leads to dummy junction, sensitivity to 100 μV, V mod to O, R to 10 KΩ, offset to 0, turn sine wave voltage to 0.
17. Turn off terminal; do not turn off computer or disk drive.

Table A3. Maintenance Summary

1. After each fabrication:

   — Check for loose screws, wires, etc.; repair or replace as necessary.

   — Replace aluminum and lead for next fabrication.

2. Irregularly:

   — Replace the quartz crystal when the frequency is ~4.5 MHz.

   — Replace the tungsten filament when it breaks or does not evaporate the aluminum (about 5-6 evaporations).

   — Replace the molybdenum boat when the lead no longer evaporates (about every six months).

   — Regenerate the oxygen and water adsorbers after ten cylinders of inert gas.

3. Every six months:

   — Change the oil in the turbo pump bearings.

   — Clean the aluminum and lead evaporation shields by soaking them in 10% NaOH solution.

4. Every year:

   — Change the oil in the mechanical pumps and check for wear.

Chapter Three.

Rapid Measurement of Inelastic Electron Tunneling Spectra

Rapid measurement of inelastic electron tunneling spectra

G. J. Gajda[a] and W. H. Weinberg

Division of Chemistry and Chemical Engineering, California Institute of Technology, Pasadena, California 91125

(Received 19 November 1984; accepted for publication 26 December 1984)

The design and the operation of a rapid (~ 10 s), accurate ($\pm 1\%$), moderate resolution (~ 50 cm^{-1}) system for measuring inelastic electron tunneling spectra are described. The utility of this system is discussed, and an example of its use is presented.

INTRODUCTION

Inelastic electron tunneling spectroscopy is a versatile, high-sensitivity technique for obtaining vibrational spectra of adsorbates on oxide surfaces, especially aluminum oxide. The theory and practice of tunneling spectroscopy have been reviewed extensively.[1-10] The design and operation of several tunneling spectrometers have been described in the literature.[11-15]

The development of a rapid and accurate method to obtain moderate resolution inelastic electron tunneling spectra provides a convenient, practical method to screen tunnel junctions rapidly in order to eliminate poor quality scans and to optimize the phase setting of the lock-in detector in order to obtain the best possible data from a given junction. The measurement of inelastic electron tunneling spectra requires the adjustment of the phase setting of the lock-in amplifier to provide optimum results. Traditionally, this has been accomplished by maximizing the signal at a fixed bias voltage.[16] In practice, the maximum signal occurs over a range of approximately 30° in phase angle. Thus the average of the endpoints is used at the optimum phase. However, optimization at one point does not necessarily optimize the phase for the entire scan.

I. SYSTEM DESCRIPTION

A schematic of the system, which has been described in detail elsewhere[16,17] is shown in Fig. 1. The modifications to this system are detailed in the Appendix. The basic philosophy is the use of a moderately fast (1200 Hz), highly accurate analog-to-digital converter combined with the ability to trade-off resolution for an improvement in the signal-to-noise ratio through the amplifier time constant in order to provide rapid (~ 10 s) and accurate ($\pm 1\%$) spectra of moderate resolution (~ 50 cm^{-1}).

The electronics employed in the measurement of the tunneling spectra are controlled by a Digital Equipment Corporation LSI-11/23 microcomputer with an RT-11 V4.0B operating system running FORTRAN IV V2.1. The computer is equipped with 128 kbytes of semiconductor memory, a DLV11-F console terminal interface, a DRV11-J 64-line parallel I/O interface, and a Data Translation DT2781 analog I/O card which provides eight differential input, 16-bit analog-to-digital (ADC) data channels and two 12-bit digital-to-analog (DAC) output channels. Data are stored on a Data Systems Design 210 floppy disk drive in single density (RXO1) format. The console terminal is a Lear Siegler ADM 5.

The inputs to the electronics are supplied by the parallel I/O card. Four reed relays select the total range of the bias voltage for the narrow DAC (± 0.1, ± 0.2, ± 0.5, and ± 1.0 V), and one of these relays is set through the *C* output port of the DRV11. The wide DAC provides the overall offset for a scan and can be set to ± 1 V. It is driven by the *B* output port. The narrow DAC actually steps through the spectrum and, in conjunction with the reed relays, determines the minimum step size. It is driven through the A output port. Typically, the No. 2 reed relay is set, and the wide DAC is set to 0 V. The narrow DAC then provides approximately a 2 cm^{-1} step size (0.5 V/2047 steps = 0.244 mV/step = 1.97 cm^{-1}/step).

The output from the Princeton Applied Research HR-8 lock-in amplifier is sent to channel 0 of the DT2781 ADC. The resulting data can be displayed selectively on the Tektronix 564 storage oscilloscope, as used for the quick scans, or can be plotted on the Hewlett-Packard 7035B *X*–*Y* recorder. The *X* and *Y* axes are driven by the two DT2781 DAC channels, and they may be connected to one or the other of the output devices. The data files containing the spectra are transferred to floppy disks in image format (I *4) to save space over ASCII format. They can be transferred to a VAX 11 780 computer for further processing of the data.

A scan consists of 965 points, equally spaced over the

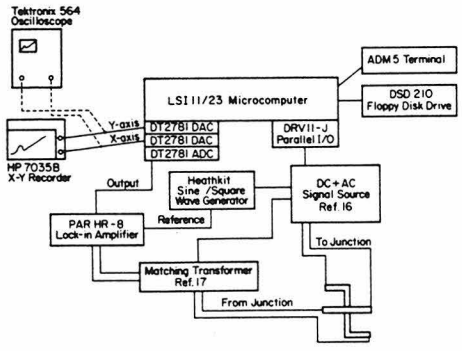

FIG. 1. Block diagram of computer-controlled inelastic electron tunnel junction measurement system.

 0034-6748/85/050700-03$01.30

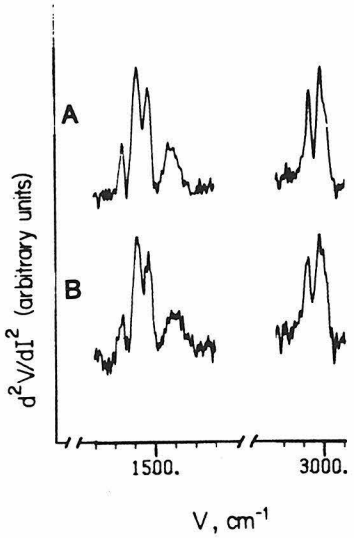

FIG. 5. Data processed to remove the background slope. The figure shows the spectral regions from 1200–1800 and 2750–3100 cm^{-1}. (a) $\varphi = 41.1°$; (b) $\varphi = 11.1°$.

detailed scans of inelastic electron tunnel junctions is presented. It can be very valuable both in optimizing spectral quality and in quickly screening out low-quality junctions.

ACKNOWLEDGMENT

This work was supported by the Army Research Office under Grant No. DAAG29-83-K-0094.

APPENDIX

The major changes in the measurement electronics that have occurred since the previous descriptions[16,17] were published are detailed below.

(1) The output from the lock-in amplifier is now sampled by a Data Translation DT2781. This is a 16-bit, 1200 sample per second ADC that is directly interfaced to the DEC LSI-11/23 computer.

(2) The data signals to drive the wide DAC, narrow DAC, and reed relays are now supplied by a DRV11-J parallel I/O interface which is controlled directly by the LSI-11/23 computer.

(3) A Hewlett–Packard 7035B X–Y recorder has been interfaced to the system through the Data Translation DT2781 control board. The latter provides two 12-bit DACs which provide the analog signal to drive the recorder. The recorder is used to provide a hard copy of the raw data from the scans.

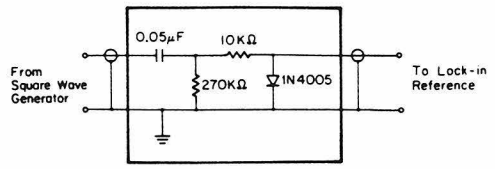

FIG. 6. Schematic diagram of simplified frequency doubler circuit.

(4) The entire system is now under the control of the dedicated DEC LSI-11/23 microcomputer running the RT-11 V4.0B operating system. The resulting data files are output in a form suitable for transfer to a VAX-11/780 computer where they are further processed to remove the sloping background and to identify the peaks.[17]

(5) The frequency doubler circuit[16] has been simplified considerably and is shown in Fig. 6. The new circuit uses the square-wave output from a Heathkit IG-18 sine/square wave generator. This signal is maximized and sent to the reference channel of the PAR HR-8 lock-in amplifer. The lock-in amplifier continues to operate in the selective external mode which uses a filter (set to 94.46 kHz[16]) to extract the second-harmonic reference signal.

(6) A Tektronix 564 storage oscilloscope with a 3A1 vertical module and a 2B67 time base module has been added to the system for the quick scans described above. It is controlled by the same DACs that drive the X–Y recorder, and the cables must be manually switched between the two devices.

[a] National Science Foundation Predoctoral Fellow
[1] P. K. Hansma, Phys. Rep. C **30**, 146 (1977).
[2] W. H. Weinberg, Annu. Rev. Phys. Chem. **29**, 115 (1978).
[3] *Inelastic Electron Tunneling Spectroscopy*, edited by T. Wolfram (Springer, Berlin, 1978).
[4] P. K. Hansma and J. R. Kirtley, Acc. Chem. Res. **11**, 440 (1978).
[5] H. W. White and T. Wolfram, Methods Exp. Phys. A **16**, 149 (1980).
[6] S. Ewert, Appl. Phys. A **26**, 63 (1981).
[7] H. W. White, L. M. Godwin, and R. Elliatioglu, J. Adhes, **13**, 177 (1981).
[8] *Tunneling Spectroscopy*, edited by P. K. Hansma (Plenum, New York, 1982).
[9] W. H. Weinberg, in *Vibrational Spectra and Structure*, edited by J. R. Durig (Elsevier, Amsterdam, 1982), Vol. 11, p. 1.
[10] S. K. Khanna and J. Lambe, Science **220**, 1345 (1983).
[11] P. N. Shott and B. O. Field, Spectrochim. Acta Part A **35**, 301 (1979).
[12] A. B. Dargis, Rev. Sci. Instrum. **52**, 46 (1981).
[13] H. S. Gold and L. J. Hilliard, Chem. Biomed. Environ. Instrum. **12**, 1 (1982).
[14] D. G. Walmsley, I. W. N. McMorris, W. E. Timms, W. J. Nelson, J. L. Tomlin, and T. J. Griffin, J. Phys. E **16**, 1052 (1983).
[15] N. K. Eib, T. Furukawa, and K. L. Mittal, Rev. Sci. Instrum. **55**, 1161 (1984).
[16] W. M. Bowser, Ph. D. thesis, California Institute of Technology, 1980.
[17] M. K. Templeton, Ph. D. thesis, California Institute of Technology, 1984.
[18] G. J. Gajda and W. H. Weinberg (to be published).

spectral range from 240–4000 cm^{-1}. The ADC sequentially samples each point 12 times at 1200 Hz or 10 ms per point. A delay of 1 ms separates each point for a sample time of 11 ms, or 10.62 s for a complete scan. The effects of varying the time constant are shown in Fig. 2. These results indicate an optimum time constant of 30 ms giving the best trade-off of resolution versus signal-to-noise ratio. A faster ADC could be operated at lower time constants for better resolution.

The data are ordinarily displayed on the Tektronix oscilloscope, operated in the storage mode. The 2B67 time base converter allows an external input which is used to provide the bias voltages. The oscilloscope thus acts as a rapid (< 1 s) and asccurate ($\pm 0.5\%$) X–Y recorder or point plotter. It requires < 1 s to plot the data, giving a usable scan in approximately 12 s. The results are best viewed at low electron beam intensity in a partially darkened room. The photographs were prepared by setting the oscilloscope to its normal scan mode and maintaining a long pause at each point to provide a 15-s plotting time. The intensity was reduced as much as possible to provide an indication of the sharpness actually obtained. The rapid scanning provides the ability to adjust the phase setting and observe the results virtually immediately. It can also rapidly screen out poor quality junctions.

II. SYSTEM OPERATION

As an example of the utility of the system, the results obtained in scanning an $Al/Al_2O_3/Pb$ junction, prepared with acetic acid adsorbed from the vapor phase on the Al_2O_3, are presented. The junction had a resistance of 283 Ω and, since the step-up transformer is optimized for approximately 1000 Ω, would be expected to be optimized ($\pm 5°$) at the average phase setting. Low-resistance ($R \lesssim 100\ \Omega$) junctions display significant deviations ($> 15°$) from this setting. The maximum value, $+32\%$ of full scale, was obtained at phase settings from $-9.9°$ to $+32.1°$. This gives an optimum at $+11.1°$ with an rms modulation voltage of 1.5 mV. The quick scan is displayed in Fig. 3 (b). A setting of $+1.1°$ results in the spectrum shown in Fig. 2 (b) and the optimum by the quick scan method is obtained at 41.1° and shown in Fig. 3 (a).

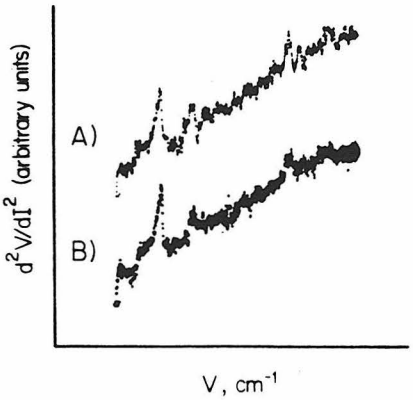

FIG. 3. Quick-scan spectra (1 scan, $\tau = 30$ ms, $V_{mod} = 1.5$-mV rms). Negatives of Polaroid photographs of the oscilloscope screen. (a) $\varphi = 41.1°$, quick-scan optimum; (b) $\phi = 11.1°$, average phase optimum (X axis: 240–4000 cm^{-1}).

Conventional detailed scans were obtained by co-adding 50 scans at 1.5-mV modulation and a time constant of 3 ms. The raw data are presented in Fig. 4. In addition each spectrum has had a linear function subtracted in order to remove the background. The details of the background subtraction are presented elsewhere.[18] The spectral regions encompassing the ν_s and ν_a O–C-O modes and the νC–H modes of the surface acetate from the processed spectra are detailed in Fig. 5. The results are both acceptable, but the "quick-scan optimum" [Fig. 5 (a)] displays somewhat greater resolution and signal-to-noise than the "average optimum" [Fig. 5 (b)]. This is not caused by slow deterioration of the junction, since the scan in Fig. 4 (b) was taken before that in Fig. 4 (a).

In summary, a rapid, accurate method for obtaining

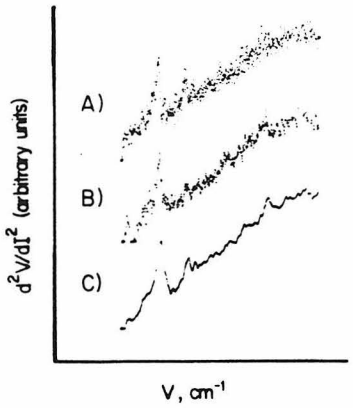

FIG. 2. Effect of changing the lock-in amplifier time constant on the quality of the data (1 scan, $\varphi = 1.1°$). Negatives of Polaroid photographs of the oscilloscope screen (a) 10 ms; (b) 30 ms; (c) 100 ms (X axis: 240–4000 cm^{-1}).

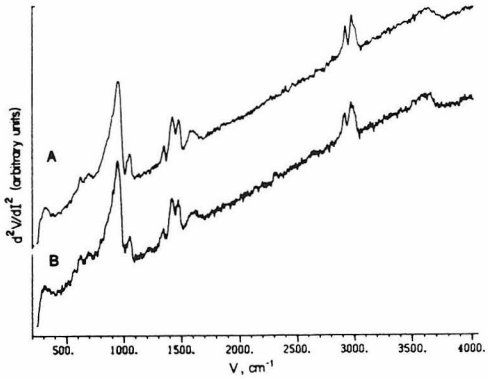

FIG. 4. Raw data (50 scans, $\tau = 3$ ms, $V_{mod} = 1.5$-mV rms). (a) $\varphi = 41.1°$; (b) $\varphi = 11.1°$.

Chapter Four.

An Effective Background Removal Technique for Inelastic Electron Tunneling Spectra

An effective background removal technique for inelastic electron tunneling spectra

G. J. Gajda and W. H. Weinberg
Division of Chemistry and Chemical Engineering, California Institute of Technology, Pasadena, California 91125

(Received 25 March 1985; accepted 28 June 1985)

This report describes a simple, rapid, and effective computer algorithm for background removal in inelastic electron tunneling spectra.

I. INTRODUCTION

Inelastic electron tunneling spectroscopy (IETS) is a highly sensitive surface vibrational spectroscopy of moderate resolution. As such, it has been applied to a wide variety of problems in surface science, and has been reviewed extensively.[1,8] As in the case of all surface sensitive vibrational spectroscopies (e.g., IRAS, Raman, and EELS), IETS provides information on the molecular nature of the surface species. Unlike other vibrational spectroscopies, IETS has an intrinsically upward sloping background with increasing frequency. Several methods have been used to remove this background slope, including trial and error slope subtraction,[9] Tchebycheff polynomials,[9] and subtraction of one tunneling spectrum from another.[10] Each of these methods has drawbacks due to excessive time of interactive trial and error methods, inaccuracy, or problems in matching spectra. In addition, some methods depend on a subjective determination of the "best" spectrum. This report describes a simple and rapid computer algorithm for the efficient, objective re-

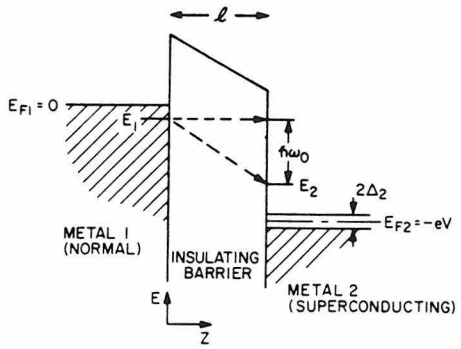

FIG. 1. Schematic energy diagram for the inelastic electron tunneling between energy level E_1 in a normal metal, and energy level E_2 in a superconducting metal of energy gap $2\Delta_2$. The Fermi level of the normal metal is $E_{F1} = 0$, while that of the superconducting metal is $E_{F2} = -eV$, where eV is the applied bias voltage. Elastic tunneling is represented by the horizontal dashed line, whereas inelastic tunneling is represented by the oblique dashed line resulting in a vibrational excitation of energy $\hbar\omega_0$. The width of the insulating barrier is given by 1.

moval of the background slope.

The upward sloping background characteristic of IET spectra is produced by the elastic tunneling which occurs in the junction. A schematic energy diagram of the tunnel junction is given in Fig. 1. As indicated, both elastic and inelastic tunneling can occur; the latter only if eV_{bias} is greater than $\hbar\omega_0$. Figure 2 schematically depicts the results of measuring the current (I), conductance [dI/d (eV)] or the second derivative of the current [d^2I/d (eV)^2] as a function of bias voltage.

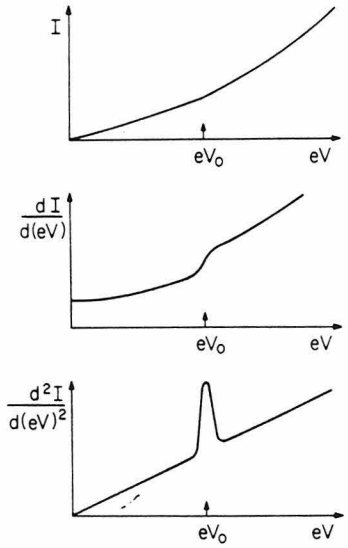

FIG. 2. Schematic representation of the current–voltage, the conductance–voltage and the second derivative of the current with respect to voltage for a tunneling junction. The latter is an "inelastic electron tunneling spectrum."

For small bias voltages (eV < 0.5 V), the elastic background is approximately given by

$$I = \beta(V + \gamma V^3),$$

where β and γ are functions of the barrier properties.[11] This implies that

$$\frac{d^2I}{dV^2} = 6\beta\gamma V,$$

or that the elastic background is a linear function of the bias voltage over the range of interest for vibrational data.

It should be noted that for IET spectra obtained by constant current systems, the background slope often decreases at high bias voltage (eV ~ 0.45–0.5 V). This effect is not due to higher order terms in the expansion since all coefficients are positive and would thus predict an increasing slope. The flattening of the background is an artifact produced by measuring

$$\frac{d^2V}{dI^2} = \frac{1}{\sigma^3}\frac{d^2I}{dV^2}.$$

For low resistance junctions, $\sigma_{500\text{ mV}} - \sigma_{30\text{ mV}} \sim (0.1)\sigma_{30\text{ mV}}$. Unless the second derivative spectra are corrected, errors of $(1.1)^3 - 1 \sim 30\%$ can occur. A more complete discussion of errors and the necessary corrections is given by Adler.[12] These methods, while devised for line shape analysis, can also be used to obtain background removed spectra. However, they require a measurement of the first harmonic spectrum as well as the second harmonic spectrum.

II. DESCRIPTION

The basic idea of any background correction routine in IETS is to calculate the average slope of the background. The quickest, and surprisingly accurate, method is to calculate the average first derivative of the spectrum. This is accomplished by using the least squares convolution method of Savitsky and Golay.[13] A cubic derivative function 11 points

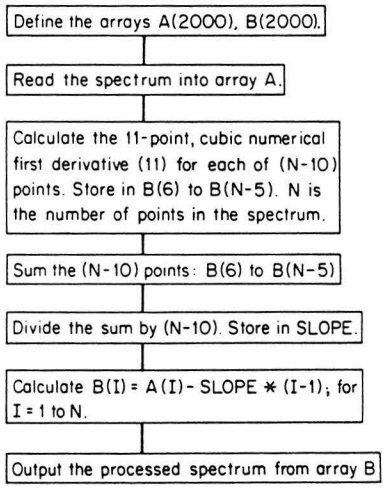

FIG. 3. Simplified flow chart of background slope removal subroutine.

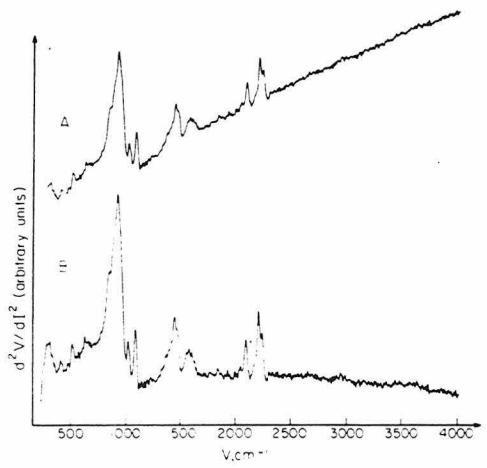

FIG. 4. Inelastic electron tunneling spectrum of CD_3COOD adsorbed on Al_2O_3. [Lock-in time constant $\tau = 1$ ms, 3500 scans.] (A) Raw data. (B) Data processed to remove background slope.

in length is used. The 11 points represent a compromise between smoothing spectra to minimize the effects of noise, and minimizing broadening to allow the first derivative to calculate peak positions, as described by Templeton.[9] The values calculated at the $N - 10$ fitting points are summed and then divided by $(N - 10)$, where N is the number of data points in the spectrum. The resulting value is the average slope and is the magnitude of a linear function which is then subtracted from the original data. This provides a flat background for the spectrum which facilitates comparison of the data with other spectra.

The routine easily handles large asymmetric peaks if the peaks start and end at the base line. Shoulders and poorly resolved peaks are also handled properly. The presence of a partial peak that occurs at the start of the spectrum (240 cm^{-1}) will cause problems due to the slope of the peak not averaging to zero. The program checks to see if the spectrum starts at a value close to the minimum value in the entire spectrum, which indicates the absence of an interfering peak. If a peak occurs at 240 cm^{-1}, it is skipped, and the correction routine starts at the minimum amplitude point in the spectrum. A flow chart of the routine employed is given in Fig. 3. The computer programs used to process the data are available upon request.

III. RESULTS AND DISCUSSION

As an example of this background removal technique, the results obtained from an $Al/Al_2O_3/Pb$ tunnel junction, the Al_2O_3 surface of which was exposed to CD_3COOD from the vapor phase, are presented. The junction had a resistance of 992 Ω. The spectrum was obtained with the phase optimization technique described elsewhere.[14] The raw data are presented in Fig. 4(A). This 965 point spectrum was then processed by the background removal routine, which required 4 s to execute on an LSI 11/23 microcomputer using FORTRAN IV with an RT-11SJ V4.0B operating system. The final spectrum is presented in Fig. 4(B).

The processed spectrum, with a relatively flat background, permits easier location of peak maxima, especially with a numerical derivative evaluation routine,[9] and determination of "shoulders" on peaks. In addition, it removes the change in background values as the limiting factor in vertical spectrum expansion. [In Fig. 4(A), the spectrum amplitude is determined by the background value at 4000 cm^{-1}. In Fig. 4(B), it is determined by the height of the Al–O stretching mode at 940 cm^{-1}.] This permits finer detail to be observed throughout the entire spectrum.

In summary, a rapid and simple computer algorithm for the removal for the sloping background from inelastic electron tunnel junction spectra has been presented. This algorithm allows easier evaluation of the data contained in the spectra, while providing an objective method of eliminating the sloping background in a single tunnel junction.

ACKNOWLEDGMENT

This work was supported by the Army Research Office under Grant No. DAAG29-83-K-0094.

[1] S. K. Khanna and J. Lambe, Science **220**, 1345 (1983).
[2] *Tunneling Spectroscopy*, edited by P. K. Hansma (Plenum, New York, 1982).
[3] W. H. Weinberg, Vib. Spectra Struct. **11**, 1 (1982).
[4] W. H. White and T. Wolfram, Methods Exp. Phys. A **16**, 149 (1980).
[5] *Inelastic Electron Tunneling Spectroscopy*, edited by T. Wolfram (Springer, Berlin, 1978).
[6] W. H. Weinberg, Annu. Rev. Phys. Chem. **29**, 115 (1978).
[7] P. K. Hansma and J. R. Kirtley, Acc. Chem. Res. **11**, 440 (1978).
[8] P. K. Hansma, Phys. Rep. **30C**, 146 (1977).
[9] M. K. Templeton, Ph. D. thesis, California Institute of Technology, 1984.
[10] W. M. Bowser and W. H. Weinberg, J. Am. Chem. Soc. **102**, 4720 (1980).
[11] J. G. Simmons, J. Appl. Phys. **34**, 238 (1963).
[12] J. G. Adler, in *Tunneling Spectroscopy* (Plenum, New York, 1982).
[13] A. Savitzky and M. J. E. Golay, Anal. Chem. **36**, 1627 (1964).
[14] G. J. Gajda and W. H. Weinberg, Rev. Sci. Instrum. **56**, 700 (1985).

Chapter Five.

An Inelastic Electron Tunneling Spectroscopic Investigation of the Interaction of Molybdenum Hexacarbonyl with an Aluminum Oxide Surface

I. Introduction

Inelastic electron tunneling spectroscopy is a highly sensitive, moderate resolution vibrational technique for studying molecules adsorbed on insulator surfaces. Although many substrates can be used, the majority of the existing studies have been concerned with adsorption on aluminum oxide employing aluminum-aluminum oxide-lead tunnel junctions. Several recent reviews discuss the theory and practice of tunneling spectroscopy **(1-10)**, as well as a recent overview of tunneling spectroscopy **(11)**.

Tunneling spectroscopy has been applied to the study of both adsorbed metal carbonyls and evaporated metal clusters with postadsorbed carbon monoxide **(9,12)**. Specific systems include $Ru_3(CO)_{12}$ **(13)**, $[Rh(CO)_2Cl]_2$ **(14)**, and CO adsorbed on alumina supported Rh **(15)**, Fe **(16)** and Ni **(17)** crystallites. The sensitivity and wide spectral range (240-4000 cm^{-1} in our experiments) permit the observation of the ν(CO), δ(M-C-O) and ν(M-CO) vibrational modes. Broadening and downshifting of the ν(CO) modes limits, however, the spectral resolution. A discussion of the perturbation on vibrational frequencies by the upper metal electrode has been given by Kroecker and Hansma **(18)**.

The extensive study of molybdenum hexacarbonyl adsorbed on aluminum oxide and its decomposition products dates back to the observation by Banks and Bailey **(19)** of catalytic metathesis of propylene by alumina supported molybdenum hexacarbonyl decomposition products. This catalyst was prepared by impregnating an activated alumina (approximately equivalent to partially dehydroxylated alumina discussed below) with a solution of $Mo(CO)_6$ in cyclohexane at 65°C. The cyclohexane was removed by flushing the catalyst with dry nitrogen and then evacuating at 120-140°C. The catalyst was activated with dry air at 540°C for five hours. Although various decomposition products of the

adsorbed molybdenum hexacarbonyl can catalyze other reactions such as isotopic exchange between deuterium and alkanes **(20)** or Fischer-Tropsch synthesis **(21)**, much of the work has centered on identification of the species responsible for the metathesis reaction **(22,23)**.

The metathesis reaction may be written as

$$2\ RCH{=}CH_2 \rightarrow RCH{=}CHR\ (\text{cis and trans}) + CH_2{=}CH_2\ , \qquad (1)$$

where the ratio of the cis-to-trans olefin that is formed is a function of both the reactant and the catalyst. The Chauvin-Herisson (carbene) mechanism **(24)**,

has been established by a series of isotopic labeling experiments **(25)**. Based on the work of Mocella et al. **(26)**, this mechanism was extended for the molybdenum catalyzed systems in order to explain the necessary presence of oxygen to activate the catalyst. This led to the oxo-molybdenum carbene hypothesis which was given theoretical support by Goddard and Rappe´ **(27)** who determined that the reaction mechanism

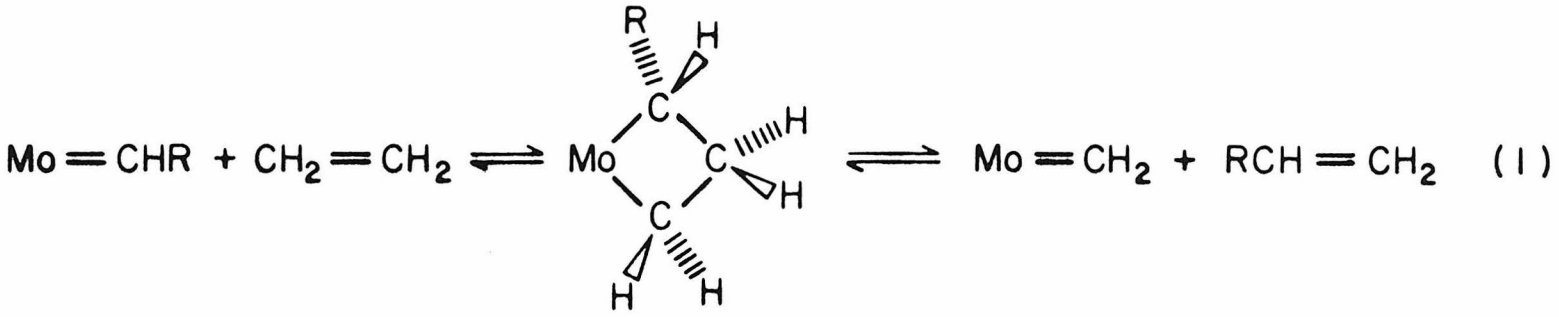

(1)

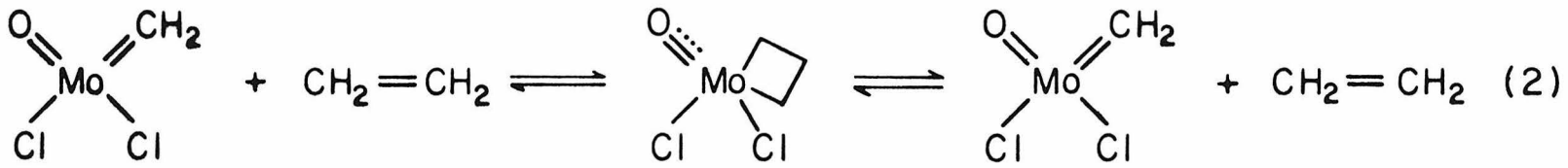

(2)

(2)

was favored due to the change in the nature of the molybdenum oxygen bond in the metallacycle. This calculation explained the origin of the reduction in the activation energy for the insertion reaction. Recently, isolatable tungsten oxo-alkylidene complexes, which are quite active for metathesis in solution, have been synthesized and characterized **(28,29)**. A review of the field has been given by Grubbs **(30)**.

The study of the adsorption and reaction of molybdenum hexacarbonyl has involved primarily the use of transmission infrared spectroscopy of the carbonyl stretching region (1700-2100 cm^{-1}), in addition to an analysis of desorbed thermal decomposition products. The majority of the experiments have involved partially or fully dehydroxylated aluminas as opposed to fully hydroxylated alumina. These materials are prepared by heating γ-alumina in flowing helium to a temperature of 500°C (partially dehydroxylated) or 1000°C (fully dehydroxylated) for one hour **(31)**. The reaction of the hexacarbonyl proceeds quite differently on the three supports. On hydroxylated alumina, the hexacarbonyl adsorbs weakly and readily decomposes with loss of carbon monoxide at 25°C and oxidation of molybdenum at 265°C (monitored by the desorption of hydrogen) **(22)**. On partially dehydroxylated alumina, the initial adsorption is stronger, and the subsequent thermal decomposition produces a variety of surface species, e.g. $Mo(CO)_3(ads)_3$, $Mo(O)_2(CO)_2(ads)_2$ and $(Al\text{-}O)_2Mo$ **(22)** [(ads) represents a surface Lewis base site]. Since this surface produces the most active metathesis catalysts, it has been studied extensively **(22,23,31-34)**. The exact species that form and their relative concentrations appear to depend critically on initial preparation conditions and thermal decomposition parameters such as temperature and time of decomposition.

Under conditions of rigorous water removal, the hexacarbonyl decomposes to zero valent molybdenum at submonolayer coverages. Residual hydroxy protons produce some oxidation, yielding an average oxidation number of 0.4 **(22)**. The average oxidation number is the formal oxidation state, as determined by quantitative oxidation of the surface species to MoO_3. The oxygen uptake, corrected for other oxidation products (such as hydrogen) is converted to an oxygen/molybdenum ratio, and then subtracted from three (MoO_3 has an O/Mo ratio of three) and doubled (since the formal oxidation state of oxygen is -2). We emphasize that the oxidation number represents a *formal* oxidation state and does not imply, for example, that Mo^{+6} exists on the surface. The chemistry of the fully dehydroxylated species corresponds to that of dispersed molybdenum metal, although the extent of dehydroxylation must be extremely high to avoid significant side reactions from the residual oxidized species.

The accumulated data from the decomposition studies on various alumina surfaces has led to the development of models for the adsorption and decomposition reactions by Brown **(35)**, Bailey and Langer **(36)**, and Phillips and Dumesic **(37)**, the latter summarizing available experimental evidence for characterizing the adsorption and decomposition of various carbonyls (including molybdenum hexacarbonyl) on alumina surfaces. In addition to structural information derived from transmission infrared spectroscopy of thin pressed alumina disks, information is available concerning the oxidation state of the molybdenum species from X-ray photoelectron spectroscopy (XPS) and electron spin resonance (ESR) measurements [on molybdenum (V) species]. These data support the carbene mechanism indirectly by indicating both a correlation of the metathesis activity with the molybdenum (IV) concentration and also the difficulty of oxidizing the molybdenum species beyond molybdenum (V) under all but the most severe conditions. For example, decomposition at 600°C in helium

produces an average oxidation number of 4.6 **(34)**, while heating in oxygen at 500°C is necessary to produce molybdenum (VI) **(23)**.

Brown **(35)** also provides a summary of work on alumina supported carbonyl complexes, emphasizing molybdenum hexacarbonyl, and formulates a series of plausible mechanisms for the adsorption and decomposition reactions consistent with the experimental data. This includes the initial adsorption (through a Lewis acid-carbonyl interaction, a molybdenum carboxylate species, or a surface hydroxyl-carbonyl interaction), the formation of various gas-phase products (CO, CO_2, H_2 and CH_4), and the formation of a surface carbene species for the metathesis reaction. We will be concerned here with the initial adsorption reaction and the final decomposition to molybdenum oxide.

Bailey and Langer **(36)** report a comprehensive review of supported carbonyl catalysts. They include systems supported on functionalized polymers and inorganic supports, including the alumina system considered here. They provide an exhaustive summary of the research performed on the molybdenum hexacarbonyl-aluminum oxide system, including discussions of models proposed by experimentalists but do not provide a formalism to unify the data.

Finally, the synthesis and vibrational characterization of stable metal carboxylic acids [MCOOH, e.g. Pt **(38)**] and their considerably more stable esters [MCOOR, e.g. Co **(39)**] provide direct information concerning the vibrational frequencies of carboxylate species. In general, the high frequency bands [ν_a(OCO) ~1550 cm^{-1} or ν(C=O) ~1650 cm^{-1}] are observable in the high surface area alumina transmission infrared spectra. Lower frequency modes (including the metal-carboxyl stretch and deformations and the δ(OCO) mode) occur in regions that are highly absorbing in the high surface area systems and are rarely

observed for the organometallic complexes. The identification of intermediate frequency modes ν(CO) ~1200 cm^{-1}, δ(COH) at ~1350 cm^{-1} or ν_s(OCO) at ~1400 cm^{-1}, which are known from homogeneous systems and several supported systems, can be used to link the high surface area alumina data with the information from the wider spectral range of inelastic electron tunneling spectroscopy.

II. Experimental Procedures

The inelastic electron tunnel junction fabrication system and experimental procedures are described in detail elsewhere **(40)**. Briefly, a lower aluminum electrode is formed by evaporating high purity aluminum metal through a mask onto a clean glass slide. The aluminum surface is oxidized in an oxygen/water vapor glow discharge to form the thin insulating aluminum oxide film. The molecule under study is then deposited on this aluminum oxide surface either by adsorption from the vapor phase or by exposure to a solution of the molecule in an inert solvent (hexane). Heating, if used, is accomplished by the resistive heating method of Bowser and Weinberg **(41)**. The system is then evacuated to below 5 x 10^{-7} Torr and the upper lead electrode is vacuum evaporated to complete the tunnel junction.

The tunneling spectra are measured using a constant current modulation system described elsewhere **(42)**. This system incorporates near-real-time viewing of the spectra to aid in optimizing the phase setting of the lock-in detector. The spectra are processed using an algorithm **(43)** to remove the linear background slope from the measured spectra.

The molybdenum hexacarbonyl from Pressure Chemical was purified by the method of Laniecki and Burwell **(29)** (sublimed twice in vacuo). The ethylene was CP grade (99.9%) from Matheson, and the hexane was Photrex grade (99%) from Baker. Both were used as received.

III. Results

A. Surface Carbonyl Hydroxy Reaction

Due to the nature of tunneling spectroscopy, it is impossible to follow the course of a surface reaction on a single junction. Several junctions prepared under different conditions must be used to study dynamic processes, such as reversible adsorption as well as sequential irreversible reactions. The tunneling spectrum of molybdenum hexacarbonyl adsorbed at 22°C on a fully hydroxylated ($\theta_{OH} = 1$) aluminum oxide surface is shown in Fig. 1(A). This spectrum was obtained by minimizing the time (15 min) between the end of the carbonyl exposure and the start of the lead electrode evaporation. An intermediate stage in the desorption is observed with a 22 min delay, and the spectrum is shown in Fig. 1(B). The tunneling spectrum that results from a 25 min delay is shown in Fig. 1(C). The spectrum in Fig. 1(C) is comparable to the spectrum of a clean junction shown in Fig. 1(D). This suggests that the reaction of the carbonyl with the fully hydroxylated surface is reversible at room temperature. The spectrum in Fig. 1(A) has been processed to remove the background, and the region from 240 to 1050 cm^{-1} is shown in Fig. 2.

B. Surface Carbonyl Decomposition Reaction

The tunneling spectrum that results after heating the junction to 200°C for 600 s to partially dehydroxylate ($\theta_{OH} \cong 0.85$) the alumina surface, followed by adsorption of molybdenum hexacarbonyl at 22° C, is presented in Fig. 3(A). An unheated blank junction is shown for comparison in Fig. 3(B). The partially dehydroxylated surface produces a very small amount of decomposition of the carbonyl. The extent of dehydroxylation is approximately 15% as judged by a comparison of the intensities of the (Al)OH stretching mode at approximately 3600 cm^{-1}. The time delay is not important because we are interested in

irreversibly chemisorbed products, as discussed in Sect. IV.C.

C. Activated Adsorption and Decomposition

Pure molybdenum hexacarbonyl has been reported to decompose at its own vapor pressure at 150°C **(44)**. The tunnel junctions shown in Fig. 4 (left) and (center) were heated to approximately 140°C for 5 min and 30 sec, respectively. The molybdenum hexacarbonyl has decomposed to form a molybdenum metal zone, which appears darker than the aluminum strip by reflected light. A standard, unexposed junction is shown for comparison in Fig. 4 (right). These experiments also indicate qualitatively the thermal gradient present in the junctions during heating.

The molybdenum hexacarbonyl decomposes without metal deposition when the junctions are heated to approximately 100°C. The tunneling spectrum that results after exposure to 10^{-1} Torr of molybdenum hexacarbonyl vapor for 300 s at 100°C is shown in Fig. 5(A). The decomposition can be carried to completion by heating the junction in vacuum at 100°C for 300 s after prior hexacarbonyl exposure at 100°C (post-heating). The tunneling spectrum that results from this treatment is shown in Fig. 5(B).

D. Attempted Activation of Decomposition Products of Molybdenum Hexacarbonyl with Ethylene

Molybdenum oxides, primarily ammonium molybdate, have been used as metathesis catalyst precursors **(45)**. After calcining to remove ammonia and water, the resulting molybdenum oxide is activated with an olefin, typically propylene, at a temperature of 400°C in one atmosphere of olefin for one to four hours **(45)**.

The molybdenum hexacarbonyl decomposition products formed in the activated adsorption experiments described in Sect. III.C were exposed to 2 Torr

of ethylene vapor at 100°C for 900 to 3600 s. The tunneling spectrum that results from the 900 s exposure is shown in Fig. 5(C). There is no evidence of reaction of the ethylene wth the surface under these conditions. Longer exposures also showed no evidence of hydrocarbon or carbene formation.

In the fabrication system, as currently configured, pressures up to 2 Torr can be measured by using a thermocouple gauge, and correcting for differing gauge sensitivities. This pressure is accurate to approximately ±10%.

The maximum temperature is limited by the method of heating the junctions **(41)**. The electrical lead wires are soldered to the glass slide using Indaloy 1 solder, a eutectic mixture of indium (52%) and tin (48%), which melts at 117°C **(46)**. This solder is used because it wets the glass, and this is necessary to provide a smooth transition from solder pad to glass slide for the aluminum strip **(41)**. Since the aluminum strip is only 800-1000 Å in thickness, the sharp transition produced by a nonwetting solder would result in a discontinuity in the strip.

The stability of the solder joint is determined by the strip temperature, the adsorbate pressure in the system, and the rate of heat transfer from the solder joint through the glass slide and heating wires. We have observed solder joint failure at approximately 200°C at 10^{-1} Torr and 110°C at 1 Torr. The higher temperatures at lower pressures are possible due to the decrease in convective heat transfer at reduced pressures. In vacuum (pressures below 10^{-7} Torr), failure occurs at approximately 400°C.

E. Attempted Decomposition of Molybdenum Hexacarbonyl via UV Photolysis

A series of junctions were prepared by depositing 10 μl of a 1% (w/v) $Mo(CO)_6$/hexane solution (approximately 0.04 M) on the aluminum oxide surface at 22°C, allowing the solvent to evaporate (~30 s), and exposing the junctions to 366 nm (3.39 eV) ultraviolet radiation through a Huntington Mechanical Labs

VP-151 viewport constructed of type 7056 glass. This viewport has a minimum transmission coefficient of 0.8 from 320 to 2700 nm. The source has a stated light intensity of 330 $\mu W/cm^2$ at six inches. The junctions were positioned approximately four inches from the source, which provided an intensity of 594 $\mu W/cm^2$ [330 $\mu W/cm^2$ x $(6/4)^2$ x 0.8]. The exposure to this UV irradiation was 300 s in duration. The delay time between the end of the UV exposure and the start of the lead evaporation was approximately 60 min. The tunneling spectra of a UV-exposed junction and a non-UV-exposed junction, prepared at the same time, are shown in Fig. 6 (A), represented by a resonance structure, and (B), respectively.

IV. Discussion

A. Molybdenum Hexacarbonyl - Surface Complex Formation

As discussed by Brown **(35)**, three major types of surface carbonyl complexes can occur: (1) a carboxylate-type species which can be subdivided into a "carboxylic acid" (IA), represented by a resonance structure, that can occur on partially or fully hydroxylated oxide surfaces, and a carboxylate (IB) that can occur on partially or fully dehydroxylated oxide surfaces,

IA IB

(2) a carbonyl-Lewis acid adduct (II) that can occur on partially or fully dehydroxylated oxide surfaces,

II

or (3) a carbonyl-surface hydroxyl adduct (III) that can occur on partially or fully hydroxylated oxide surfaces.

III

Each structure has certain characteristic vibrational frequencies that, if sufficiently intense, can be used to identify the species. The "carboxylic acid" (IA) would have modes from ν(C=O) [~1600-1680 cm^{-1} **(38,39)**], ν(C-O) [~1200 cm^{-1} **(38)**] and δ(C-O-H) [~1350 cm^{-1} **(47)**], as well as lower frequency carboxylic acid deformation modes, which will occur in the metal-carbonyl bending region [~600-800 cm^{-1} **(47)**]. The carboxylate (IB) would have asymmetric and

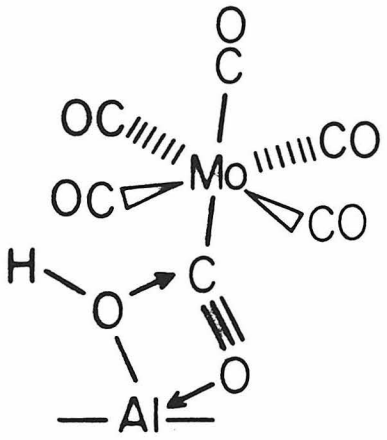

IA

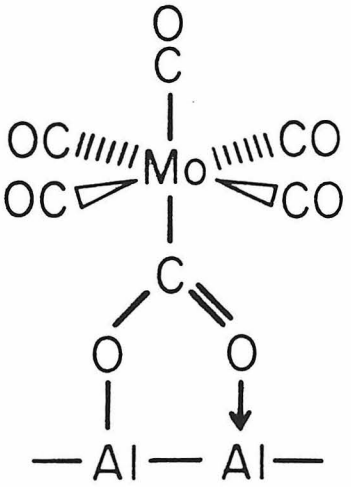

IB

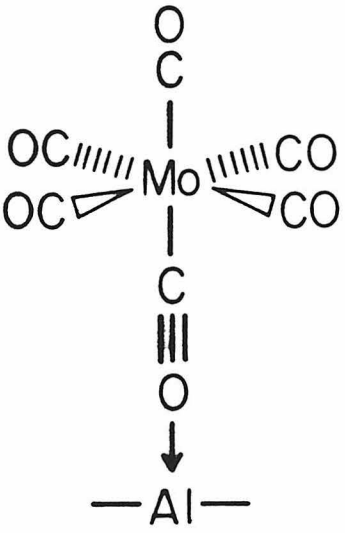

II

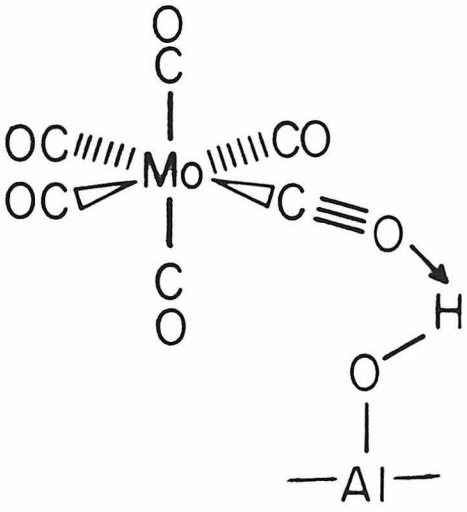

III

Fig. 7

symmetric carboxylate stretching modes [ν_a(OCO) ~1580 cm^{-1} and ν_s(OCO) ~1460 cm^{-1} for formate on alumina **(48)**]. The carbonyl-Lewis acid adduct (II) would produce a broad, down-shifted carbonyl stretch, extending as low as 1700 cm^{-1} **(33)**. Finally, the carbonyl-surface hydroxyl adduct (III) would, in addition to a carbonyl downshift, produce the characteristically downshifted ν(OH) modes of a hydrogen-bonded complex [ν(OH) ~3400 cm^{-1} **(47)**].

The tunneling spectrum of the surface molybdenum carbonyl complex adsorbed at 22°C is shown in Fig. 1(A), with the spectral region from 240 to 1050 cm^{-1} shown in greater detail in Fig. 2. The vibrational frequencies are listed in Table 1. The tunneling spectrum of Fig. 1(A) was obtained by evaporating the lead overlayer 15 min following the molybdenum hexacarbonyl exposure at a system pressure of approximately 5 x 10^{-7} Torr. Shorter delay times produce poor quality junctions due to a higher background pressure. The tunneling spectrum in Fig. 1(C) was obtained with a delay time of 25 min prior to the lead evaporation. By comparison with the tunneling spectrum of the blank junction shown in Fig. 1(D), there is no evidence of any molybdenum hexacarbonyl (or decomposition products therefrom) remaining on the surface. From this, we infer that the interaction of the molybdenum hexacarbonyl with the fully hydroxylated alumina surface is rather weak and completely reversible. Based on these data we can calculate an approximate heat of adsorption. If we assume a steady state between a 5 x 10^{-7} Torr background molybdenum hexacarbonyl partial pressure and a fractional surface coverage of 0.01 (the detection limit of 10^{12} molecules/cm^2) with a preexponential factor of the desorption rate coefficient of 10^{13} s^{-1} and a probability of adsorption of unity, we calculate E_{ads} = 15.1 kcal/mol. By varying the approximations, we find E_{ads} = 15 ± 3 kcal/mol. As noted in Sect. III.A, the need to deposit the lead upper electrode to synthesize the tunneling junction does not allow a single junction to be observed as a

function of time. Rather, a series of junctions must be prepared with increasing delay times between the end of the vapor phase exposure to the molybdenum hexacarbonyl and the beginning of the lead evaporation. An example is given in Fig. 1(B) for which the delay time is 22 min.

Both Burwell and co-workers **(22,31)**, and Howe and co-workers **(23,32,33)** have reported the formation of a $Mo(CO)_3(ads)_3$ type species on partially dehydroxylated alumina surfaces on the basis of CO desorption studies. The $Mo(CO)_3(ads)$ complex is formed over approximately one hour by sweeping the alumina supported carbonyl with pure helium at 100°C. Molybdenum hexacarbonyl can be recovered quantitatively by flowing CO containing helium through the sample cell. However, $Mo(CO)_3(ads)_3$ is reported to be stable indefinitely to flowing helium below 100°C on hydroxylated aluminas **(31)**. Since the desorption observed in this work occurs under vacuum and hence does not involve recarbonylation by CO, and considering the short time (~20 min) and low temperatures (~22°C) involved, the surface species formed here cannot be $Mo(CO)_3(ads)_3$.

The vibrational frequencies of the surface species are compared with the frequencies of gas-phase molybdenum hexacarbonyl in Table 1. The free molybdenum hexacarbonyl frequencies **(49)** are listed with the assignments and mode symmetry given by Shimanouchi **(49)**. Unlike infrared or Raman spectroscopy, inelastic electron tunneling spectroscopy has no strict selection rules comparable to the dipolar allowed modes of infrared spectra or the polarization rules of Raman spectra **(50)**. Thus the number of observed modes is not a useful guide to the symmetry of the adsorbed molecule in tunneling spectroscopy.

The relatively good correspondence between the low frequency modes of the surface species and the free hexacarbonyl suggest, in agreement with the obser-

vation of reversible adsorption, that relatively minor modifications in the structure of the molecule have occurred. In addition to several new low frequency modes (below 1000 cm^{-1}), a broad mode occurs from approximately 1200 to 1650 cm^{-1} and a second from approximately 1650 to 2100 cm^{-1}. The hydroxyl stretching mode at 3550-3700 cm^{-1} is essentially unshifted from its position on the clean alumina surface [cf. Fig. 1(D)].

Of the three surface species discussed above, only the surface carboxylic acid (IA) or the surface carboxylate (IB) would be expected to produce vibrational frequencies in the 1200-1600 cm^{-1} range. Relatively few carboxylic acid complexes (as opposed to carboxylate esters) are sufficiently stable for infrared spectra to be obtained. The platinum complex $Pt(COOH)(C_6H_9)(P\text{-}P)$, [(P-P) = $Ph_2P(CH_2)_nPPh_2$, n = 2,3,4] discussed in Sect. I has a ν(C=O) of 1555-1651 cm^{-1} and a ν(C-O) of 1137-1215 cm^{-1} **(38)**. In addition, $CpFe(CO)(PPh_3)(COOH)$ has a ν(C=O) of 1565 cm^{-1} **(51)**. Several additional examples of carboxylate esters are known with most having a ν(C=O) of approximately 1685 cm^{-1} **(37,52,53)**, due primarily to the lack of hydrogen bonding that exists in the carboxylic acid dimer. In the surface species, the carbonyl frequency is downshifted by the analogous interaction with the aluminum site.

Two bulk oxide systems provide additional evidence for metal carboxylate formation. Fubini et al. **(54)** have studied the adsorption of chromium hexacarbonyl on calcium oxide. The oxide was dried by heating in vacuum to remove all hydroxyl groups, and provides a useful infrared range down to 900 cm^{-1}. They assign broad modes at 1425 [ν_s(OCO)], 1075 [δ_a(OCO)] and 975 cm^{-1} [δ_s(OCO)] to a surface carboxylate similar to (IB). In addition, they observe a series of broad infrared bands from 2120 cm^{-1} to 1715 cm^{-1} in the carbonyl stretching frequency region. Guglielminotti and Zecchina **(55)** have studied the adsorption of molybdenum hexacarbonyl on magnesium oxide and observed similar bands at

1472-1436 cm^{-1} [ν_s(OCO)] and 1060 cm^{-1} [δ_s(OCO)] which they assigned to a surface carboxylate. Their magnesium oxide surface was stated to be free of hydroxyl groups, precluding the formation of a carboxylic acid species (IA).

The broad mode at 1200-1650 cm^{-1}, produced by the surface molybdenum hexacarbonyl, precludes any attempt to differentiate between (IA) and (IB) on the basis of the carboxyl modes. However, the carboxylic acid, as opposed to the carboxylate, would be expected to produce a downshifted ν(OH) mode due to the surface hydroxyl-carbonyl carbon interaction and reduce the intensity of the ν(Al)OH mode. Although the downshifted ν(OH) mode is too weak to observe, the 3650 cm^{-1} ν(OH) mode in the carboxylic acid spectrum is attenuated relative to a blank junction spectrum. Since our surfaces are fully hydroxylated in the untreated state, we favor the assignment of the 'carboxylic acid' type structure.

Finally, the broad carbonyl stretching mode from approximately 1700 to 2100 cm^{-1} may be due to an interaction with the surface aluminum sites, as in (II), or a downshift caused by the lead upper electrode **(18)**. Generally, the lead-induced downshift is ≤6% **(18)** which cannot account for these observed shifts. Rather, the observed low frequency of ν(C≡O) is consistent with a Lewis acid induced downshift [e.g. Kazusaka and Howe **(33)**] as in (II). A surface species such as (III) is unlikely due to the lack of a broad ν(OH) mode at approximately 3300 cm^{-1}.

On the basis of these combined observations, we propose a surface "carboxylic acid" (IV) to best represent the structure of the surface species:

(IV)

It incorporates both the carboxylic acid moiety as well as the aluminum-carbonyl acid-base adduct. The vibrational modes are too broad to exclude the alternative of two species (IA) and (II) the vibrational modes of which are superposed to give the observed spectrum.

B. Carbonyl Adsorption on the Partially Dehydroxylated Surface

The high surface area alumina studies of Burwell et al. **(22,31)** and Howe et al. **(23,32,33)** have each demonstrated significantly greater reactivity on partially or fully dehydroxylated alumina surfaces compared to the fully hydroxylated surface. To investigate this possibility, we attempted to partially dehydroxylate our alumina surface by heating the junctions to 200°C for 300 to 600 s prior to exposure to the molybdenum hexacarbonyl vapor. A comparison of the resulting tunneling spectrum in Fig. 3(A) with that of a blank junction in Fig. 3(B) indicates that very few decomposition products are observed.

The extent of dehydroxylation, as judged by the relative areas of the ν(OH) mode centered at 3650 cm^{-1}, is rather small (approximately 15% or $\theta_{OH} \sim 0.85$ after annealing to 200°C). The partially dehydroxylated aluminas used by Burwell et al. **(31)**, for example, were prepared by heating the alumina to 450°C in flowing helium for one hour, while the fully dehydroxylated aluminas were heated to 1000°C for one hour. As discussed in Sect. III.D, the method of heating the junctions prevents us from reaching these elevated temperatures.

C. Reaction at Elevated Temperatures

Molybdenum hexacarbonyl vapor is reported to decompose at 150°C **(44)** to give molybdenum metal and CO. To test the reactivity of molybdenum hexacarbonyl with the alumina surface, we prepared several tunneling junctions by exposing them to 10^{-1} Torr of molybdenum hexacarbonyl

vapor while heating the aluminum strips from 100 to 150°C. The measured temperatures show significant (±10°C) fluctuations when the temperature reaches 140°C. The result of heating for five minutes and for 30 s beyond the observation of the first fluctuations is shown in Fig. 4 (left) and (center), respectively. This figure is a photograph of the completed junctions after removal from the vacuum system. The negative heating lead is connected at the upper left of each junction as oriented in the figure, while the positive lead is connected at the lower right. The junction in Fig. 4 (left) shows a large, approximately oval metal film deposited asymmetrically with respect to the heating leads. In addition, a small metal film is deposited on the back side of the glass slide and located on the central aluminum strip lines near the upper crossbar of the I-shaped aluminum strip. The formation of this second film, between the glass slide and the slide holder (see Ref. 40 for details), indicates that decomposition of the vapor produced the film, and the source was the heat produced by the aluminum strip heating, transmitted through the glass slide. No direct line of sight exists between the second metal film and any metal evaporation source.

The 30 second heating exposure shown in Fig. 4 (center) depicts the initial stages of the film formation and also indicates the asymmetric nature of the deposition. The localized nature of the metal film deposition suggests that a thermal gradient exists along the heated aluminum strip. Comparison of the measured decomposition temperature on the alumina surface, 140 ± 2°C [±2 being the calibration accuracy **(41)**], as indicated by the start of the temperature fluctuations caused by the metal deposition, and the measured decomposition temperature of $Mo(CO)_6$ vapor at its own vapor pressure [150 ± 1°C **(44)**], indicates that the maximum local deviation from the average temperature (140°C) is approximately 10°C.

Heating the junctions to 100°C for 300 s during the molybdenum hexacarbonyl vapor exposure results in decomposition of the carbonyl with no evidence of metal deposition. The tunneling spectrum of the decomposition product is shown in Fig. 5(A). Heating the junction to 100°C in vacuum for 300 s after the original thermal decomposition produces the tunneling spectrum in Fig. 5(B). We note the weak carbonyl vibrations in Fig. 5(A), with the presence of hydroxyl vibrations; while the reverse is true in Fig. 5(B). This apparent discrepancy is explained by the presence of chemisorbed hexacarbonyl on the alumina surface for approximately 15 min after the initial pumpdown. The hexacarbonyl decomposes with loss of CO by reaction with surface hydroxyl groups **(37)**. In the case of no postheating, excess hexacarbonyl desorbs leaving a molybdenum suboxide and unreacted hydroxyl groups. The postheating allows the reaction between the residual chemisorbed hexacarbonyl and the surface hydroxyl groups to continue, until all of the hydroxyl groups are reacted. This produces a mixture of molybdenum suboxides and subcarbonyls **(37)**. A similar result is obtained if the initial heating in hexacarbonyl vapor is for 600 s. This suggests that the decomposition of the carbonyl is limited by the availability of protons from hydroxyl groups on the surface. This is in accord with previous observations of molybdenum carbonyl-aluminum oxide systems that all hydroxylated surfaces have a maximum reaction capacity, limited by the number of hydroxyl groups **(37)**. Further reaction requires much higher temperatures, or the addition of oxygen or water vapor to the system.

The complex nature of the spectra render more detailed assignments impossible. In particular, the very broad carbonyl stretching modes prevent any correlation with the oxidized subcarbonyls, such as $Mo(O)_2(CO)_2(ads)_2$, postulated by Brenner and Burwell **(22)**.

D. Reaction of Decomposed Molybdenum Hexacarbonyl with Ethylene

As noted in Sect. III.C, several tunneling junctions were prepared by reacting molybdenum hexacarbonyl vapor with the alumina surface heated to 100°C. After evacuation of the vacuum system to a pressure below 5×10^{-8} Torr, the junctions were exposed to 2 Torr of ethylene vapor while heated to 100°C for 900 to 3600 s. Ethylene was used rather than propylene since the catalyst "activation" was reported to occur at lower temperatures for this olefin **(23)**, although the resulting metathesis reaction cannot be observed by standard gas chromatographic detection (ethylene metathesis is degenerate). The tunneling spectrum that results from such a 900 s "activation" is shown in Fig. 5(C). None of the activation experiments provided any indication of hydrocarbon or carbene formation as judged by the absence of C-H stretching modes in the 2800-3100 cm^{-1} region of the spectrum. Considering the rather severe conditions (400°C and one atm propylene) used to activate molybdenum (VI) oxide metathesis catalysts **(45)**, evidently our experimental conditions were insufficient to activate the decomposition product(s) of the molybdenum hexacarbonyl to the metathesis catalyst.

E. UV-Exposure of Chemisorbed Molybdenum Hexacarbonyl

Photolysis of alumina supported molybdenum hexacarbonyl by UV-irradiation has been observed to produce CO and yield the proposed $Mo(CO)_3(ads)_3$ species **(36)**. We have attempted to prepare irreversibly adsorbed molybdenum hexacarbonyl by exposure to 366 nm radiation. Details of the experiment were given in Sect. III.E. The sample holder was oriented so that two junctions would be exposed to the light source and two junctions would be shielded. The resulting tunneling spectra for the exposed and unexposed junctions are shown in Fig. 6(A) and (B), respectively. The similarity in the spectra

indicates that the UV source was insufficiently intense to photolyze the carbonyl. Typically, light intensities of 4 mW/cm^2 (vs. 594 $\mu W/cm^2$ in our experiments) are used to initiate decomposition **(56)**. The observed weak modes are probably hydrocarbon contaminants from the solvent.

V. Summary

We have obtained the vibrational spectrum of a transient complex formed between molybdenum hexacarbonyl and a fully hydroxylated alumina surface. The spectrum shows significant similarities to the gas phase or solid state hexacarbonyl, and is consistent with the carboxylic acid-type intermediate (IV) proposed by Burwell **(31)** and by Brown **(35)**. The complex is formed by the interaction of a surface hydroxyl group and a carbonyl from the molybdenum hexacarbonyl. Both the ease of desorption (~25 min at 22°C) and small perturbations from the gas phase spectrum indicate relatively weak chemisorption on the surface. Attempts to partially dehydroxylate the surface or expose the adsorbed complex to ultraviolet irradiation proved insufficient to increase the reactivity of the carbonyl at room temperature. Heating the surface during the vapor exposure of molybdenum hexacarbonyl produced molybdenum metal films at a temperature of 140°C and a mixture of molybdenum suboxides and subcarbonyls at 100°C. An attempt to react the molybdenum suboxides with ethylene to produce a molybdenum carbene species (the proposed metathesis catalyst) was unsuccessful. No evidence of hydrocarbon or carbene vibrational modes was observed.

Acknowledgment

This research was supported by the National Science Foundation under Grant No. 8500789.

References

1. P. K. Hansma, Phys. Rep. C **30**, 146 (1977).
2. W. H. Weinberg, Ann. Rev. Phys. Chem. **29**, 115 (1978).
3. "Inelastic Electron Tunneling Spectroscopy", T. Wolfram, Ed., Springer, Berlin (1978).
4. P. K. Hansma and J. R. Kirtley, Acc. Chem. Res. **71**, 440 (1978).
5. H. W. White, L. M. Godwin and R. Elliatioglu, J. Adhes. **13**, 177 (1981).
6. H. W. White and T. Wolfram, Methods Exp. Phys. A **16**, 149 (1980).
7. S. Ewert, Appl. Phys. A, **26**, 63 (1981).
8. "Tunneling Spectroscopy", P. K. Hansma, Ed., Plenum, New York (1982).
9. W. H. Weinberg, Vibrational Spectra and Structure, **11**, 1 (1982).
10. S. K. Khanna and J. Lambe, Science **220**, 1345 (1983).
11. "Principles of Electron Tunneling Spectroscopy", E. L. Wolf, Ed., Oxford, New York (1985).
12. R. M. Kroecker, Ref. 8, Chap. 13.
13. W. M. Bowser and W. H. Weinberg, J. Am. Chem. Soc. **102**, 4720 (1980).
14. W. M. Bowser and W. H. Weinberg, J. Am. Chem. Soc. **103**, 1453 (1981).
15. R. M. Kroecker, W. C. Kaska and P. K. Hansma, J. Catal. **63**, 487 (1980), and references therein.
16. R. M. Kroecker, W. C. Kaska and P. K. Hansma, J. Chem. Phys. **72**, 4845 (1980).
17. R. M. Kroecker, W. C. Kaska and P. K. Hansma, J. Chem. Phys. **74**, 732 (1981).
18. R. M. Kroecker and P. K. Hansma, Catal. Rev. Sci. Eng. **23**, 553 (1981).

19. R. L. Banks and G. C. Bailey, Ind. Eng. Chem., Prod. Res. Dev. **3**, 170 (1964).

20. C. Defosse, M. Laniecki and R. L. Burwell, Jr., 7th Int. Cong. Catal. Preprints, Tokyo (1980).

21. S. Sivasanker, E. P. Yesodharian, C. Sudhaker, A. Brenner and C. B. Murchison, J. Catal. **87**, 514 (1984).

22. A. Brenner and R. L. Burwell, Jr., J. Catal. **52**, 364 (1978).

23. R. F. Howe and I. R. Leith, J. Chem. Soc. Faraday Trans. **69**, 1967 (1973).

24. J. Herisson and Y. Chauvin, Makromol. Chem. **141**, 161 (1970).

25. R. H. Grubbs, P. L. Burk, D. D. Carr, J. Am. Chem. Soc. **97**, 3265 (1975).

26. M. T. Mocella, R. Rovner and E. L. Muetterties, J. Am. Chem. Soc. **98**, 4689 (1976).

27. A. K. Rappe´ and W. A. Goddard III, J. Am. Chem. Soc. **102**, 5114 (1980).

28. J. H. Wengrovius, R. R. Schrock, M. R. Churchill, J. R. Missert and W. J. Youngs, J. Am. Chem. Soc. **102**, 4515 (1980).

29. R. R. Schrock, S. Rocklage, J. Wengrovius, G. Rupprecht and J. Fellman, J. Mol. Catal. **8**, 73 (1980).

30. R. H. Grubbs, in "Comprehensive Organometallic Chemistry", G. Wilkinson, Ed., Pergamon, Oxford (1982) Chap. 54.

31. M. Laniecki and R. L. Burwell, Jr., J. Colloid Interface Sci. **75**, 95 (1980).

32. R. F. Howe, Inorg. Chem. **15**, 486 (1976).

33. A. Kazusaka and R. F. Howe, J. Mol. Catal. **9**, 183 (1980).

34. D. A. Hucul and A. Brenner, J. Phys. Chem. **85**, 496 (1981).

35. T. L. Brown, J. Mol. Catal. **12**, 41 (1981).

36. D. C. Bailey and S. H. Langer, Chem. Rev. **81**, 109 (1981).

37. J. Phillips and J. A. Dumesic, Appl. Catal. **9**, 1 (1984).

38. M. A. Bennet and A. Rokicki, Organomet. **4**, 180 (1985).

39. M. Tsai and G. Palyi, Organomet. **4**, 1523 (1985).

40. G. J. Gajda and W. H. Weinberg, Rev. Sci. Instrum., submitted.

41. W. M. Bowser and W. H. Weinberg, Rev. Sci. Instrum. **47**, 583 (1976).

42. G. J. Gajda and W. H. Weinberg, Rev. Sci. Instrum. **56**, 700 (1985).

43. G. J. Gajda and W. H. Weinberg, J. Vac. Sci. Technol. A **3**, 2208 (1985).

44. E. M. Fednova and J. V. Krykova, Russ. J. Inorg. Chem. **11**, 141 (1966).

45. "Catalysis by Supported Complexes", Yu. I. Yermakov, B. N. Kuznetsov and V. A. Zakharov, Eds., Elsevier, New York (1981).

46. "CRC Handbook of Chemistry and Physics", 55th ed., R. C. Weast, Ed., CRC Press, Cleveland (1974).

47. See, for example, J. B. Lambert, H. F. Shurvell, L. Verbit, R. G. Cooks and G. H. Stout, "Organic Structural Analysis", Macmillan, New York (1976).

48. D. G. Walmsley, W. J. Nelson, N. M. D. Brown and R. B. Floyd, Appl. Surface Sci. **5**, 107 (1980).

49. T. Shimanouchi, J. Phys. Chem. Ref. Data **6**, 993 (1977).

50. See, for example, Ref. 8, Chap. 1.

51. N. Grice, S. C. Kao and R. Pettit, J. Am. Chem. Soc. **101**, 1627 (1979).

52. T. Yoshida, Y. Veda and S. Otsuka, J. Am. Chem. Soc. **100**, 3941 (1978).

53. C. P. Cosey, M. A. Andrews and J. E. Rinz, J. Am. Chem. Soc. **101**, 741 (1979).

54. B. Fubuni, E. Giamello, E. Guglielminotti and A. Zecchina, J. Mol. Catal. **32**, 219 (1985).

55. E. Guglielminotti and A. Zecchina, J. Chim. Phys. **78**, 891 (1981).

56. P. George, PhD Thesis, California Institute of Technology, 1981.

Table 1. Vibrational Frequencies of Gas Phase and Adsorbed Molybdenum Hexacarbonyl

	Gas Phase **(49)**			Chemisorbed on Alumina	
Mode	Symmetry	Assignment[a]	Frequency (cm^{-1})	Frequency (cm^{-1})	Assignment[a]
13	f_{2u}	δ(CMoC)	60		
9	f_{1u}	δ(CMoC)	82		
11	f_{2g}	δ(CMoC)	86		
5	f_{1g}	β(MoCO)	342	298	β(MoCO)
8	f_{1u}	β(MoCO)	367	366	β(MoCO)
4	e_g	ν(MoC)	392	398	ν(MoC)
2	a_{1g}	ν(MoC)	402		
10	f_{2g}	β(MoCO)	448		
12	f_{2u}	β(MoCO)	507	491	β(MoCO)
7	f_{1u}	ν(MoC)	596	585br	ν(MoC)
				725 819	carboxylic acid deformation modes
				945	νAl-O
				1166w 1200- 1650vbr	carboxylic acid stretching modes
6	f_{1u}	ν(CO)	2003	1650-	ν(CO)
3	e_g	ν(CO)	2019	2100vbr	
1	a_{1g}	ν(CO)	2117		
				3650vbr	νOH

[a] ν = stretching mode, δ = deformation mode, β = bending mode, w = weak, br = broad, vbr = very broad.

Figure Captions

Figure 1. Tunneling spectra of molybdenum hexacarbonyl adsorbed from the vapor phase on alumina at 22°C with increasing time delays between the end of the exposure and the start of the lead evaporation. Exposure of 30 Torr-s (10^{-1} Torr for 300 s). (A) Delay ~15 min, (B) Delay ~22 min, (C) Delay ~25 min, (D) Blank (unexposed) junction for comparison. 1000 scans, τ = 1 ms and V_{mod} = 1.7 mV rms.

Figure 2. Spectrum from Fig. 1(A) with the background removed for the region between 240 and 1050 cm^{-1}.

Figure 3. (A) Tunneling spectrum of molybdenum hexacarbonyl adsorbed from the vapor phase on an alumina surface heated to 200°C for 600 s to partially dehydroxylate it. Exposure of 30 Torr-s (10^{-1} Torr for 300 s). 750 scans, τ = 3 ms, and V_{mod} = 1.7 mV rms. (B) Tunneling spectrum of a blank junction for comparison. 1000 scans, τ = 1 ms and V_{mod} = 1.7 mV rms.

Figure 4. (A,B) Photograph of actual junctions heated to 140°C during exposure to molybdenum hexacarbonyl in the vapor phase. Vapor pressure = 10^{-1} Torr. (A) Heated for 300 s. (B) Heated for 30 s. (C) Unexposed junction for comparison.

Figure 5. (A) Tunneling spectrum of molybdenum hexacarbonyl adsorbed from the vapor phase at 100°C. Exposure of 30 Torr-s (10^{-1} Torr for 300 s). 1000 scans, τ = 3 ms and V_{mod} = 1.7 mV rms. (B) As in (A) except the junction was then heated in vacuum at 100°C for 300 s to further decompose the adsorbed species. 100 scans, τ = 10 ms and V_{mod} = 1.7 mV rms. (C) As in (A) except the surface species was exposed to

ethylene at 100°C. Exposure of 1800 Torr-s (2 Torr for 900 s). 1000 scans, τ = 3 ms and V_{mod} = 1.7 mV rms.

Figure 6. (A) Tunneling spectrum of a junction exposed to molybdenum hexacarbonyl in the liquid phase, (1% w/v [0.04 M] $Mo(CO)_6$ in hexane, 10^{17} molecules/cm^2), then ~600 $\mu W/cm^2$ of 360 nm UV light for 300 s. 100 scans, τ = 10 ms and V_{mod} = 1.7 mV rms. (B) As in (A) without exposure to UV light.

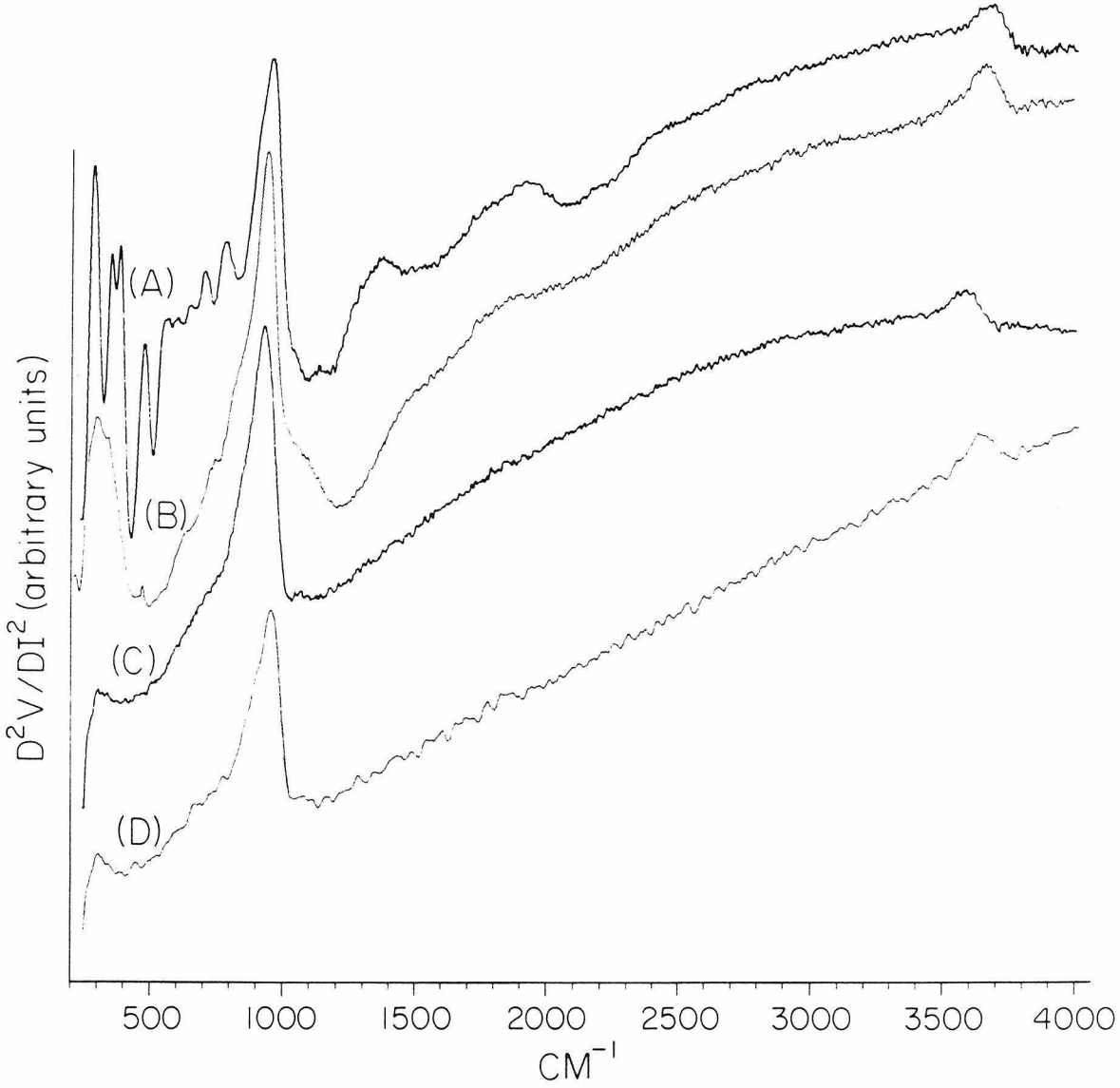
(A)
(B)
(C)
(D)
D^2V/DI^2 (arbitrary units)
500
1000
1500
2000
2500
3000
3500
4000
CM^{-1}

Fig. 1

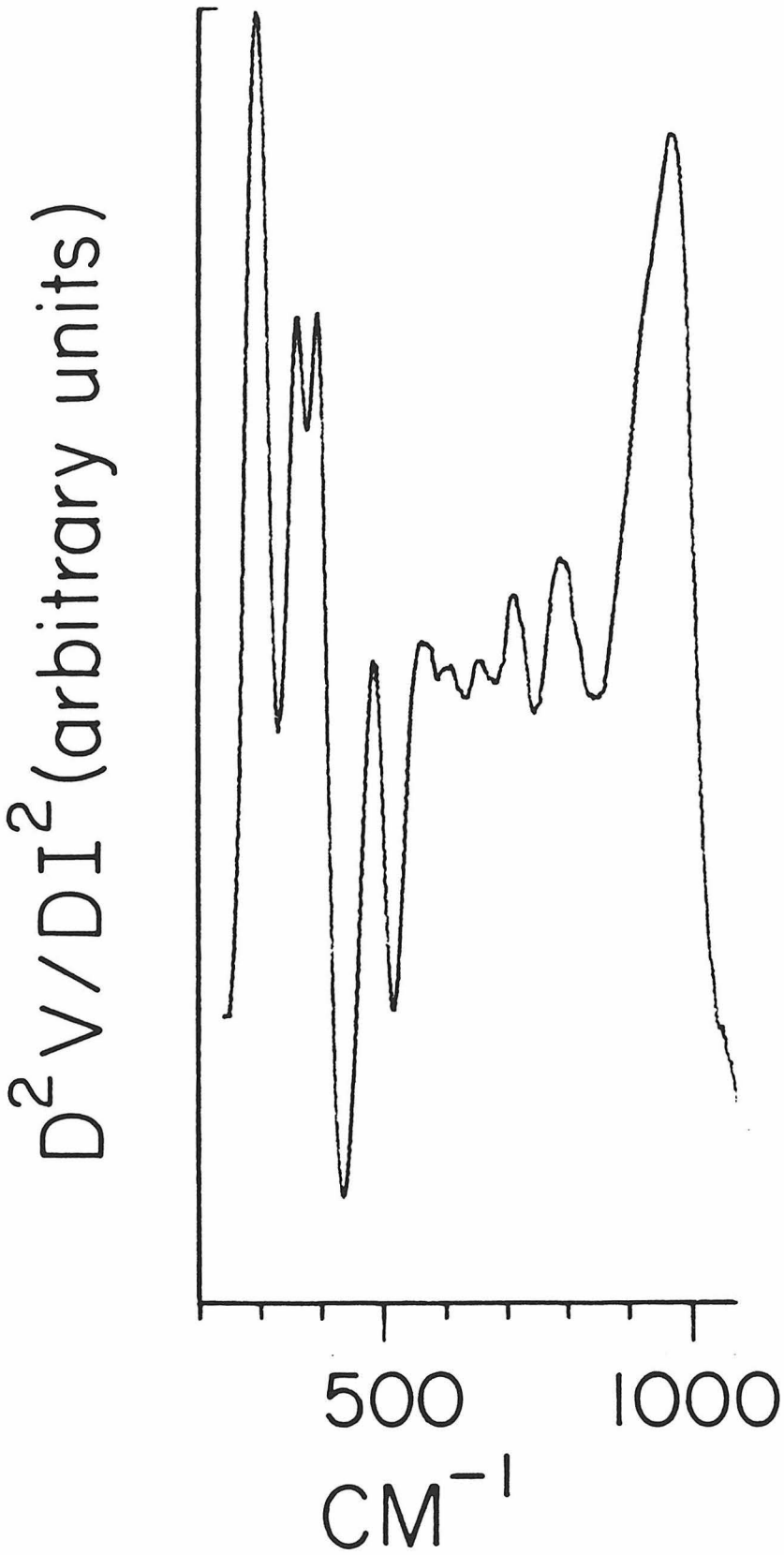

Fig. 2

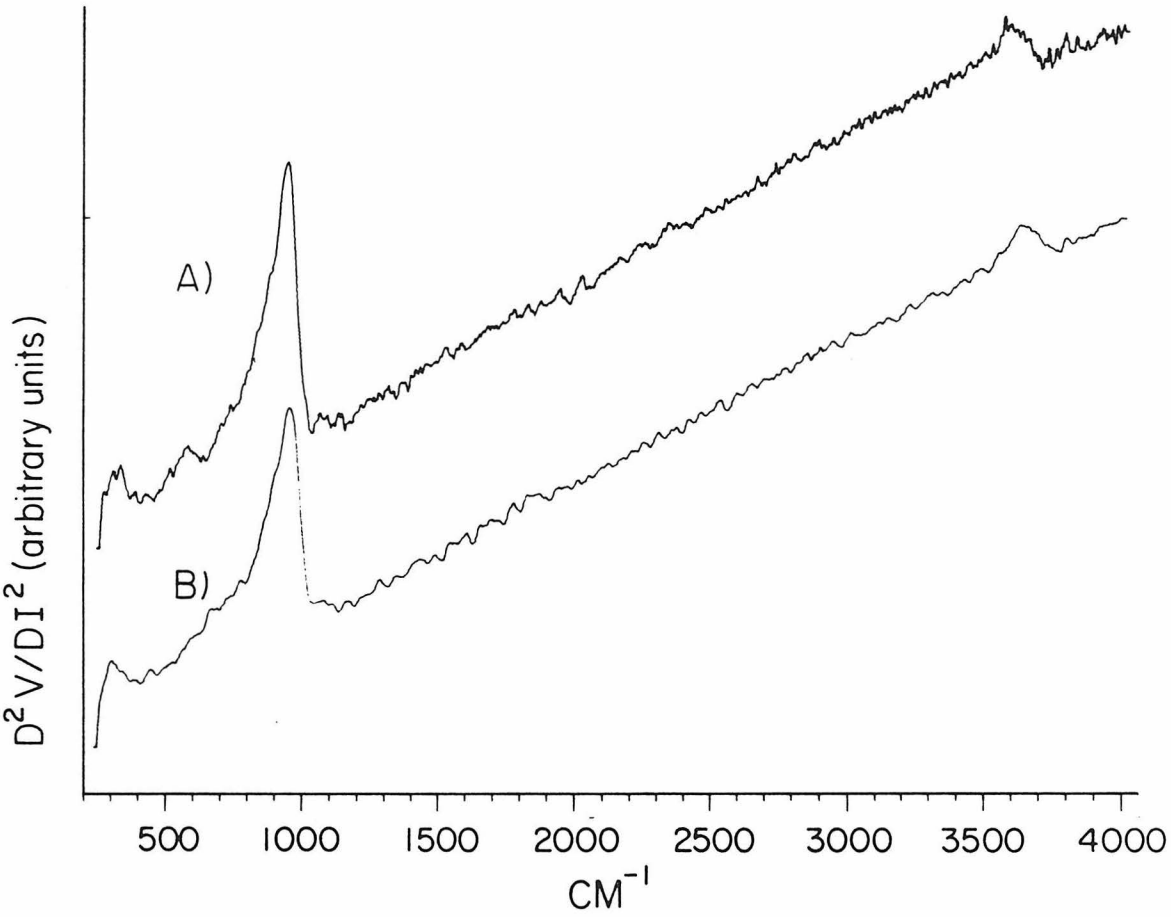
A)
B)
D^2V/DI^2 (arbitrary units)
500
1000
1500
2000
2500
3000
3500
4000
CM^{-1}

Fig. 3

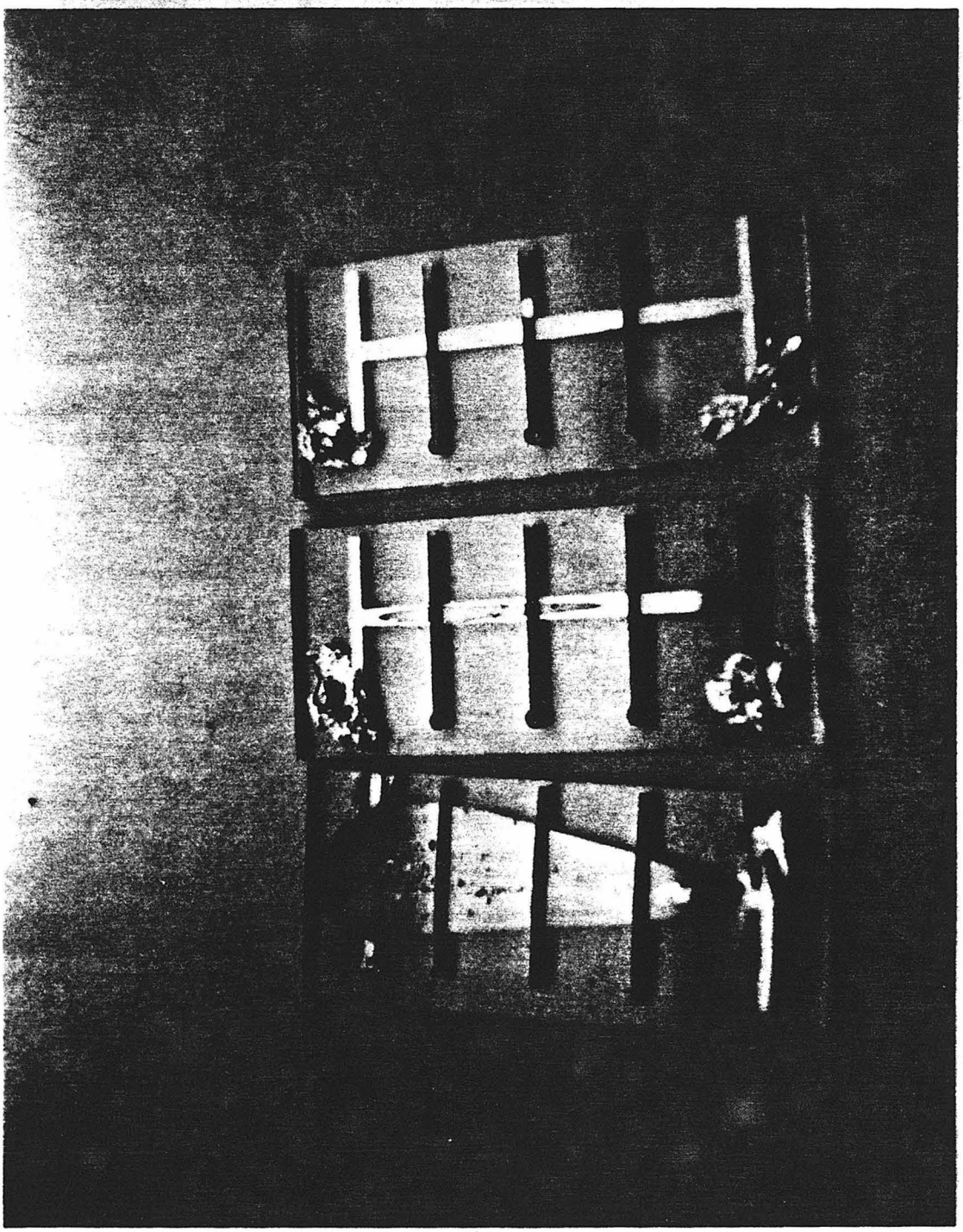

Fig. 4

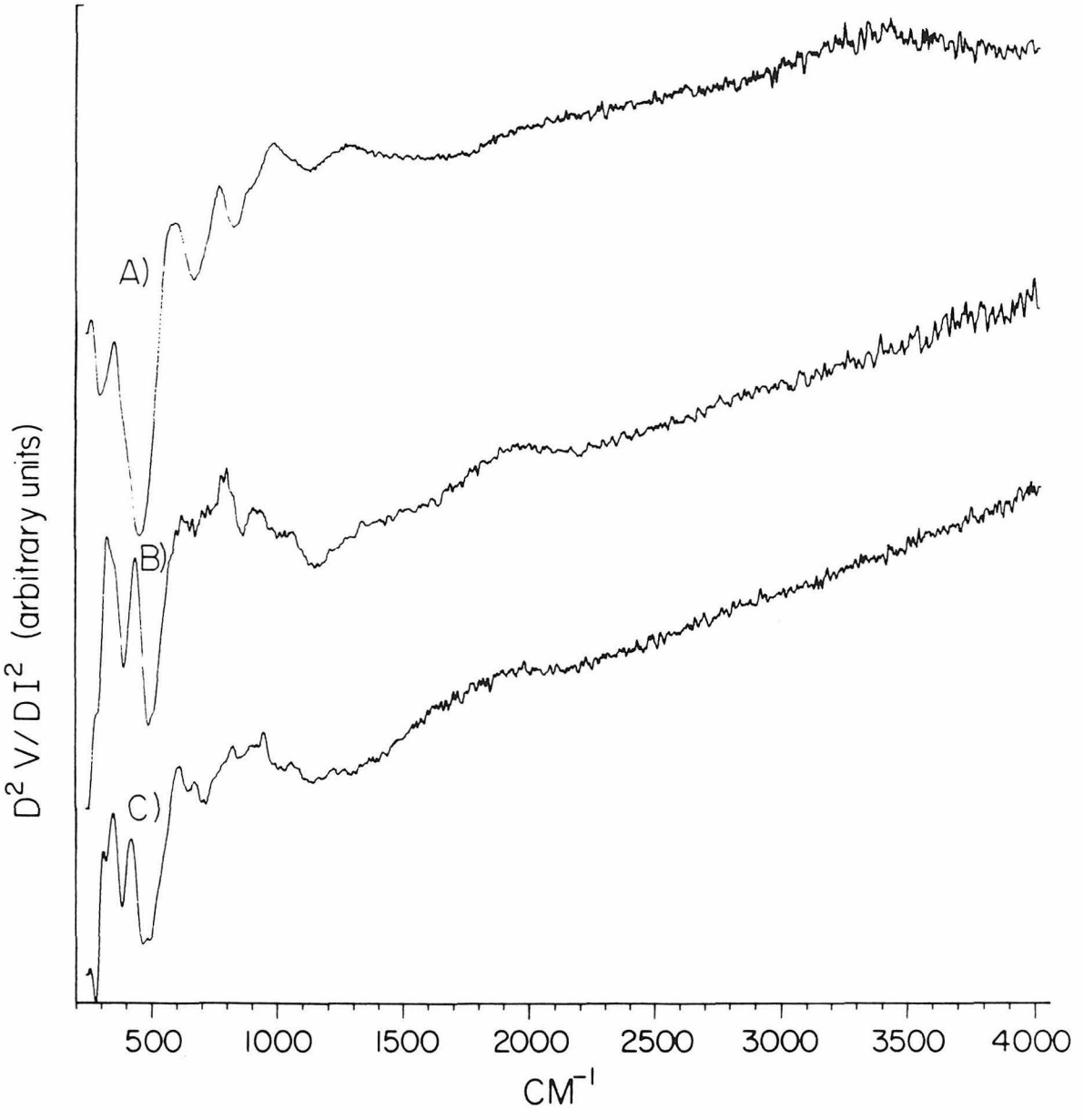
A)
B)
C)
$D^2 V / DI^2$ (arbitrary units)
500
1000
1500
2000
2500
3000
3500
4000
CM^{-1}

Fig. 5

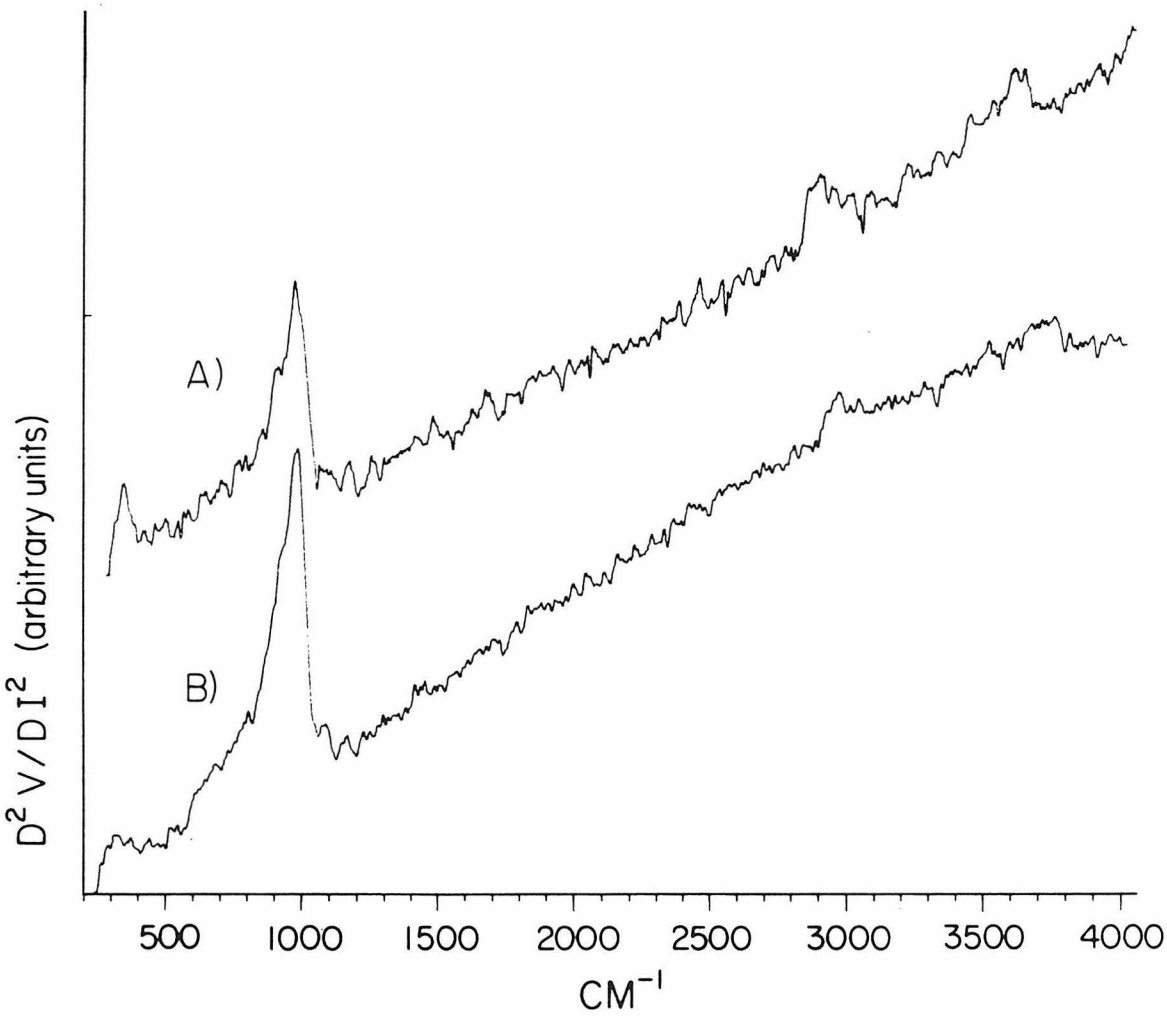
A)
B)
D^2V/DI^2 (arbitrary units)
500
1000
1500
2000
2500
3000
3500
4000
CM^{-1}

Fig. 6

Chapter Six.

An Inelastic Electron Tunneling Spectroscopic Investigation of the Reaction of Molybdenum Oxychlorides with a Hydroxylated Aluminum Oxide Surface

I. Introduction

Inelastic electron tunneling spectroscopy is a moderate resolution (full-width at half-maximum below 20 cm^{-1}), high sensitivity (fractional surface coverages on the order of 10^{-2} monolayer) technique for measuring the vibrational spectra of molecules adsorbed on insulating surfaces. The theory and practice of inelastic electron tunneling have been reviewed extensively **(1-10)**, as has the more general class of tunneling spectroscopies **(11)**. The basic requirement of the technique is the formation of a tunnel junction consisting of two conductors separated by a thin insulating barrier. The surface of this insulator is the one upon which adsorption and reaction occurs.

Although many substrates have been used [e.g. Cr **(12)**, Y **(12)**, Ho **(13)**, Er **(13)**, Al **(14)** and Mg **(14)**], the insulator in most cases has been the metal oxide formed by oxidation in air or a glow discharge. The majority of tunneling spectra have been obtained on the surfaces of Al_2O_3 and MgO **(14)**. This restriction has led to an investigation of non-oxide insulators and alternative junction geometries (involving movable electrodes) in a search to broaden the range of applications accessible to tunneling spectroscopy.

Non-oxide barriers have been synthesized primarily by employing reagents other than oxygen in the glow discharge treatment of the metal film electrode. For example, by using CF_4, a barrier similar to AlF_3 is formed **(15)**, while using $SO_2 + O_2$ produces an AlS_xO_y barrier similar to aluminum disulfate **(16)**. A second approach has been the evaporation of low-volatile oxides [e.g. SiO **(17)**] onto the metal substrate. Variations in the junction geometries are represented by the 'squeezable' electron tunnel junctions **(18)**. In this technique, two separate metal film electrodes are fabricated and mechanically positioned crosswise, similar to a standard junction geometry but with an air-gap between

them. The supported films are then squeezed together by an electromagnet to reduce the gap between the electrodes to approximately 10-20 Å, necessary for electron tunneling to occur. Although no vibrationally inelastic tunneling spectra have yet been reported by this technique, experiments continue **(18)**. Similarly, theoretical work has appeared suggesting the measurement of inelastic spectra via scanning tunneling microscopy **(19)**. An additional technique is field emission energy distribution measurements, which is especially applicable to the surfaces of refractory metals. A review of this spectroscopy is given by Gadzuk and Plummer **(20)**.

Molybdenum oxide is used widely as a catalyst for oxidation reactions either by itself or in the form of a mixed oxide **(21)**. We have observed the formation of molybdenum suboxides by decomposition of molybdenum hexacarbonyl on alumina surfaces **(22)**, but these suboxides were not suitable insulators for tunneling spectroscopy. We have observed also that metal chloride complexes [e.g. $[Rh(CO)_2Cl]_2$ **(23)**] will react with the hydroxylated aluminum oxide surface present in our tunnel junctions. The reaction produces HCl and forms a metal-oxygen bond, anchoring the complex to the surface. By using the molybdenum oxychlorides MoO_2Cl_2 and $MoOCl_4$, we would expect to form a molybdenum oxide surface and be able to investigate its properties. This would allow us to characterize the interactions of the molybdenum oxychlorides with alumina, and possibly expand the range of usable surface oxides.

Molybdenum dioxodichloride and molybdenum oxotetrachloride are well suited for use in these experiments: both are monomeric in the vapor phase **(24)**, and both react with hydroxyl groups **(25)**. The oxotetrachloride reacts with water to form 'molybdenum blues' **(25)**, which are a series of mixed molybdenum (V)/molybdenum (VI) oxides. It has been suggested that the blue color is due to the formation of Mo_3 metal atom clusters **(26)**. Further

information concerning these molybdenum blues is reviewed elsewhere **(26,27)**.

The two oxychlorides and the molybdenum (VI) oxide are strong Lewis acids and react readily with Lewis bases. A substantial number of $MoO_2Cl_2 \cdot 2L$ type complexes are known, where L = ether, ketone or ester **(28)**, tetrahydrofuran **(29)**, pyridine **(30)**, N,N-dimethylformamide or N,N-dimethylacetamide **(25)**. Each of these complexes is monomeric, in contrast to MoO_2Cl_2 in chloroform **(31)** or in a Nujol mull **(31)**, where it is dimeric or polymeric with oxygen bridges. Similarly, the molybdenum (VI) oxide is polymeric in the solid state but forms monomeric species when complexed with strong Lewis bases such as diethylenetriamine **(32)**. A considerable number of molybdenum oxides are known with composition intermediate between MoO_2 and MoO_3. Of these, six have been reasonably well characterized, usually by X-ray crystallography, namely Mo_4O_{11}, $Mo_{17}O_{47}$, Mo_5O_{14}, Mo_8O_{23}, Mo_9O_{26} and $Mo_{18}O_{52}$ **(33-36)**. These oxides are based primarily on MoO_6 octahedra, but $Mo_{17}O_{47}$ and Mo_5O_{14} are based both on MoO_6 and MoO_7 (pentagonal bipyramidal) subunits **(35,37,38)**. These materials exhibit a wide variation in resistivity (at 0°C), e.g. from 250 $\Omega \cdot$cm for $Mo_{18}O_{52}$ to 5×10^{-3} $\Omega \cdot$cm for $Mo_{17}O_{47}$ **(35-37,39)**, and 2.98×10^{-4} $\Omega \cdot$cm for MoO_2 **(40,41)** which is comparable to bismuth (1.07×10^{-4} $\Omega \cdot$cm) **(42)**. Thus, these materials have rather low resistivities and may exhibit small band gap (semiconductor) rather than large band gap (insulator) characteristics. This requires the presence of an insulator support to provide acceptable voltage characteristics for use in inelastic electron tunneling spectroscopy. Further details and numerous references to the molybdenum suboxides are given by Manthiram and Gopalakrishnan **(43)**.

II. Experimental Procedures

A. Materials

The molybdenum dioxodichloride (MoO_2Cl_2, minimum purity 99%) and molybdenum oxytetrachloride ($MoOCl_4$, minimum purity 99%) were purchased from Alfa. The ethylene was Matheson CP grade (99.5% min.). The acetic acid was Fischer Scientific reagent grade (assay 99.7% min.). The 4-t-butylpyridine was purchased from Aldrich (minimum purity 99%).

B. Junction Fabrication

The fabrication system and detailed fabrication procedures are given elsewhere **(44)**. Briefly, the procedure is as follows. A lower aluminum electrode, approximately 800 Å in thickness, is evaporated through a pattern forming mask onto a glass substrate. The electrode is then annealed by heating to 100°C for 300 s using the method of Bowser and Weinberg **(45)**. This electrode is oxidized in a glow discharge (-1100 eV, 12 mA, 300 s) at a pressure of 10^{-1} Torr in a 1000:1 mixture of oxygen and water vapor. This produces an aluminum oxide film approximately 20 Å in thickness, with properties similar to those of bulk γ-alumina **(46,47)**. The surface of this oxide is hydroxylated due to the presence of the water vapor in the plasma discharge.

Either molybdenum dioxodichloride or molybdenum oxytetrachloride is then adsorbed on the oxide surface from the vapor phase. Adsorption was carried out both at room temperature (22°C), and at elevated temperatures (usually 100°C) by resistive heating of the aluminum electrode. Some junctions were completed at this point, whereas most were subjected to further reaction. By evacuating the system to a pressure below 5×10^{-8} Torr, exposed junctions could be post-heated in vacuum.

All junctions were completed by evaporating a lead upper electrode, approximately 2500 Å in thickness, and then removed from the vacuum system and mounted on a sample holder for measurement.

C. Spectral Measurements and Data Processing

The tunneling spectra were measured using a computer controlled data acquisition system described in detail elsewhere **(48)**. The electronics consist of a constant-current modulation, second derivative detection system operated at a junction temperature of 4.2 K in liquid helium. This second derivative (D^2I/DV^2) produces a spectrum that is analogous to an IR or Raman vibrational spectrum. The spectral data over a range between 240 and 4000 cm^{-1} were acquired with a DEC LSI 11/23 microcomputer-based system and displayed in near-real time (~10 s) on a Tektronix oscilloscope to aid in the optimization of the phase setting of the lock-in detector. Typical data collection parameters are the following: 1.7 mV rms modulation voltage (at a bias voltage of 0.250 V), lock-in detector time constant (τ) of 3 ms, and 1000 spectral scans (of 965 points each corresponding to a 4 cm^{-1} point spacing) summed to improve the signal-to-noise ratio. The combination of thermal and modulation broadening yields an instrumental resolution of approximately 20 cm^{-1} for the operating parameters given above.

All tunneling spectra displayed in the figures are unsmoothed. Some spectra were processed further to remove the linear background slope using a least-squares convolution algorithm to extract the average slope. Details of this method are discussed elsewhere **(49)**.

III. Results

A. Molybdenum Oxytetrachloride Adsorption on Alumina

Molybdenum oxytetrachloride was adsorbed on the alumina surface of the tunnel junction from the vapor phase at its (extrapolated) vapor pressure of 27 x 10^{-3} Torr at 22°C **(50)**. Spectra of the decomposition products are shown in Fig. 1(A) and (B). The tunneling spectrum in Fig. 1(A) is from a junction which

was at a temperature of 22°C for 900 s after termination of the $MoOCl_4$ exposure. The tunneling spectrum in Fig. 1(B) is from a junction which was heated to approximately 40°C for 900 s after the termination of the $MoOCl_4$ exposure. The system pressure was below 5 x 10^{-8} Torr before the lead evaporation was begun. A blank junction (with no intentionally added adsorbates) is shown for comparison in Fig. 1(C). The spectrum of Fig. 1(A) was processed to remove the background slope and is shown in Fig. 2 for the spectral region between 240 and 1100 cm^{-1}. The vibrational frequencies from the molybdenum oxytetrachloride junction are listed in Table 1.

Heating the alumina surface during exposure to molybdenum oxytetrachloride vapor results in further reaction. As an example, a junction that was heated to 100°C during exposure for 300 s is shown in Fig. 1(D). The majority of junctions prepared in this way with molybdenum oxytetrachloride displayed very low resistance ($R < 10\ \Omega$) or, for those with sufficient resistance to measure, extreme changes in conductivity (σ) with bias voltage. For a typical tunnel junction prepared with acetic acid, $\Delta\sigma \equiv \frac{\sigma_{500mV} - \sigma_{30mV}}{\sigma_{30mV}}$ ~3-5%. For many of the molybdenum oxytetrachloride junctions, $\Delta\sigma > 200\%$. The tunneling junction spectrum in Fig. 1(D) had a $\Delta\sigma$ of approximately 30%. These large changes in conductance produce significant problems in a constant modulation current measurement system, such as ours, since they cause very large changes in sensitivity over the range of bias voltages. The sensitivity is proportional to the square of the modulation voltage, which in turn is equal to the fixed current divided by the conductance.

B. Molybdenum Dioxodichloride Adsorption on Alumina

As was the case for the molybdenum oxytetrachloride exposures, the molybdenum dioxodichloride was exposed to the alumina surface from the

vapor phase at its (extrapolated) vapor pressure of 59 x 10^{-3} Torr at 22°C **(51)**. The results of various thermal treatments are shown in Fig. 3. The tunneling spectrum resulting from an exposure at room temperature for 300 s, and kept at room temperature, is shown in Fig. 3(A). Exposure at room temperature for 300 s, followed by heating to 100°C for 300 s in vacuum (background pressure below 10^{-7} Torr) produces the tunneling spectrum in Fig. 3(B). Heating the junction to 100°C for 300 s during the dioxodichloride exposure, followed by cooling to room temperature in vacuum, yields the tunneling spectrum in Fig. 3(C). Finally, the result of heating the junction to 100°C for 300 s during the exposure, followed by heating the junction to 100°C for 300 s in vacuum, is shown in Fig. 3(D). Unlike the case of oxytetrachloride exposures, the majority of the junctions produced with dioxodichloride exposures exhibited only moderate ($\Delta\sigma$ < 50%) or small ($\Delta\sigma$ < 10%) conductance changes. All tunneling spectra shown are from junctions with small conductance changes.

C. Attempted Reaction of Decomposition Products of Adsorbed Molybdenum Dioxodichloride with Ethylene

The reaction product formed by heating the alumina substrate to 100°C for 300 s during exposure to molybdenum dioxodichloride [Fig. 3(C)] was reacted further with 2 Torr of ethylene at 100°C for 900 s. The spectrum of the resulting product is shown in Fig. 4. As discussed elsewhere **(22)**, the junction heating method used prevents reaching temperatures above approximately 100°C at these pressures.

D. Reaction of Decomposition Products of Adsorbed Molybdenum Dioxodichloride with Acetic Acid and 4-t-Butylpyridine

The reaction product formed by heating the alumina substrate to 100°C for 300 s during exposure to molybdenum dioxodichloride [Fig. 3(C)] was reacted

further with acetic acid and with 4-t-butylpyridine at room temperature. The tunneling spectrum that results from an exposure to acetic acid at 10^{-1} Torr for 100 s is shown in Fig. 5(A), whereas the tunneling spectrum of acetic acid adsorbed on the alumina surface is shown for comparison in Fig. 5(B). Exposing the decomposition products of adsorbed molybdenum dioxodichloride to 4-t-butylpyridine at 5 x 10^{-2} Torr for 100 s produced the tunneling spectrum in Fig. 6(A). For comparison, exposing an alumina surface to 4-t-butylpyridine (10^{-1} Torr for 1000 s) resulted in the tunneling spectrum of Fig. 6(B), whereas the tunneling spectrum of a blank junction is shown in Fig. 6(C).

IV. Discussion

A. Molybdenum Oxytetrachloride Adsorption on Alumina

Exposing the alumina surface to molybdenum oxytetrachloride ($MoOCl_4$) produced the tunneling spectra in Figs. 1 and 2. The vibrational frequencies listed in Table 1 include those of Fig. 1(A) and Fig. 2, a bidentate bridging formate on alumina due to the dissociative adsorption of formic acid, molybdenum oxytetrachloride (vapor phase), and molybdenum dioxodichloride both in a diethyl ether solution and a Nujol mull.

The tunneling spectra of $MoOCl_4$ adsorbed on alumina at 22° C [Fig. 1(A) and (B)] show evidence of very slight contamination by formate (the peaks at approximately 2900, 1050, 1375 and 1640 cm^{-1}). This species results from an unintentional infusion doping of carbon dioxide in a high relative humidity atmosphere during the transfer of the completed junctions from the fabrication system to the measurement system **(52)**. Under these conditions, carbon dioxide and water vapor in the atmosphere react with the lead electrode during infusion to form formic acid, which in turn reacts with the alumina to form formate and a surface hydroxyl group. Further details are discussed by Field **(52)**.

The major difference between the tunneling spectra in Fig. 1(A) and (B), is the presence of a strong, broad mode at 350-500 cm^{-1} (maximum at 425 cm^{-1}) and two moderately strong modes at 630 and 750 cm^{-1} which appear as shoulders on the 940 cm^{-1} aluminum-oxygen stretching mode in Fig. 1(A). The low frequency modes (240-1100 cm^{-1}) in Fig. 1(A) are shown in detail in Fig. 2. The difference in intensity of the formate modes at 1375 and 1640 cm^{-1} between Fig. 1(A) and (B) is due to a smaller concentration of the formate species in Fig. 1(B). Comparing the tunneling spectrum of Fig. 1(A) or (B) with that of an unexposed (blank) junction, Fig. 1(C), indicates a significant decrease in the area of the hydroxyl peak. This suggests that $MoOCl_4$ reacts with the surface to remove hydroxyl protons and forms a surface species which then desorbs slowly [cf. Fig. 1(B)].

In Table 1, the vibrational frequencies of $MoOCl_4$ adsorbed on alumina are compared with the vapor phase infrared spectra of $MoOCl_4$ and the infrared spectrum of molybdenumdioxodichloride (MoO_2Cl_2) in Nujol (where it is polymeric) and diethyl ether (where it is dimeric) **(31)**.

A comparison between the vapor phase infrared spectrum of $MoOCl_4$ and the tunneling spectrum adsorbed $MoOCl_4$ reveals significant differences between the two [e.g. the lack of a 1015 cm^{-1} (νMo=O) in the adsorbed species]. This indicates a significant structural change in the $MoOCl_4$ upon adsorption. By comparison with the infrared spectra of MoO_2Cl_2 in diethyl ether (where MoO_2Cl_2 is dioxo bridged , but not chlorine bridged) and in a Nujol mull (where MoO_2Cl_2 is tetraoxo bridged and dichlorine bridged to form a polymer), the lack of ν(Mo=O) modes at 928 and 969 cm^{-1} suggests tetraoxo bridging. Although we have no isotopic labeling data to confirm the assignments of the Mo-Cl modes, the formation of a polymolybdate species is unlikely. As discussed in Sect. IV.B, the reaction of MoO_2Cl_2 with the hydroxylated alumina surface does form a

polymolybdate type species, *which does not desorb* when the surface is heated to 100°C for 300 s. One possible admolecule formed is a di(molybdenum oxochloride) complex

(1)

(2)

Reaction (1) is simply that of $MoOCl_4$ with the hydroxylated surface (analogous to the hydrolysis of the $MoOCl_4$), which removes the surface hydroxyl protons as HCl. Reaction (2) is the dimerization of the surface species. This species has a distorted octahedral structure which is known for Mo(VI) complexes **(26)**.

As stated above, both Fig. 1(A) and (B) show evidence of a reduction in the surface concentration of hydroxyl groups. Only Fig. 1(A), however, indicates the presence of the di(molybdenum oxochloride) complex. The lack of modes due to the di(molybdenum oxochloride) complex in Fig. 1(B) suggests that heating to 40°C for 900 s has caused the complex to desorb. One possibility is for the surface complex to de-dimerize and desorb as MoO_2Cl_2, i.e.

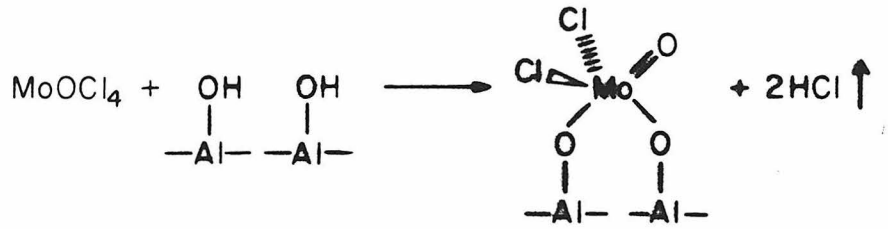

(1)

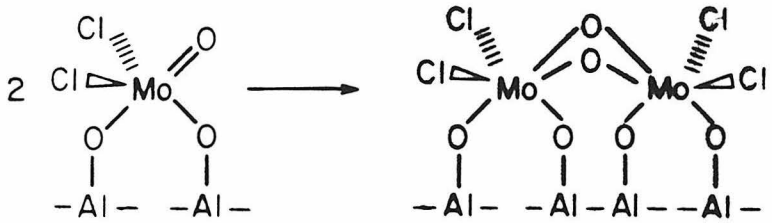

(2)

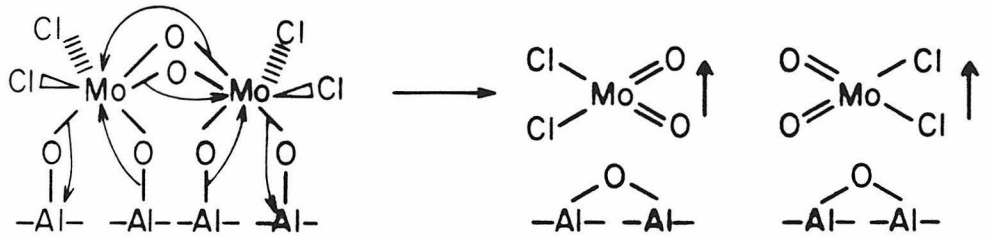

(3)

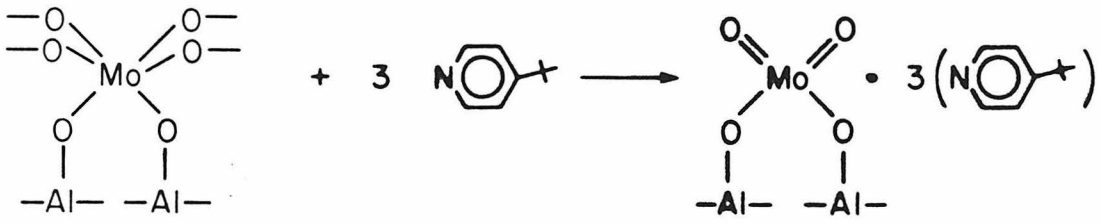

(4)

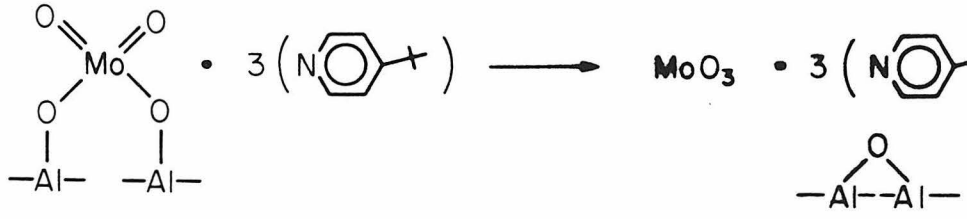

(5)

(3)

If the alumina surface is heated during the $MoOCl_4$ exposure, tunneling spectra similar to that shown in Fig. 1(D) are obtained. As mentioned in Sect. III.A, most of the junctions prepared in this manner have electrical characteristics which make them unsuitable for measuring inelastic tunneling spectra. Due to the large $\Delta\sigma$ which results in substantial background curvature, no structural or mode assignments have been attempted.

B. Molybdenum Dioxodichloride Adsorption on Alumina

The tunneling spectra that result from exposing MoO_2Cl_2 vapor to an alumina surface at either room temperature or 100°C are shown in Fig. 3, and the observed vibrational frequencies are listed in Table 2. The tunneling spectra in Fig. 3(A) and (C) were not heated after exposing the MoO_2Cl_2 to the alumina surface and show evidence of adsorbed water and molybdenum hydroxide formation, which will be discussed below.

These spectra exhibit modes at 1030 cm^{-1} [terminal ν(Mo=O)], 900-950 cm^{-1} [cisν(O=Mo=O)], ~600-850 cm^{-1} [ν(Mo-O-Mo)] and ~300-470 cm^{-1} [δ(Mo-O)] which are characteristic of molybdenum (VI) oxides with varying degrees of oligomerization **(53,54)**. The oligomerized molybdenum oxide formed depends strongly on the conditions of the reaction. Characteristics of limited oligomerization are evident in the oxide formed with exposure and pumpdown at room temperature (RT/RT) (modes at 950 and 910 cm^{-1} indicate cis-molybdenum dioxide groups). By comparison, post-heating to 100°C [RT/100°C, Fig. 3(B)] reveals a loss of intensity near 900 cm^{-1} (the 940 cm^{-1} shoulder is due to the aluminum oxide stretch), and an increase in intensity in the 500-700 cm^{-1} region (indicating bridging oxygen modes) and at 1030 cm^{-1} [probably the terminal molybdenum-oxygen double bond stretch **(54)**].

Similarly, the 100°C exposure without post-heating [100°/RT, Fig. 3(C)] produces no modes characteristic of cis-molybdenum dioxo species, yet has broad modes centered at 590 and 815 cm^{-1} indicating oligomerized molybdenum oxide species (in this case, also with chemisorbed water). Finally, the post-heated junction [100°C/100°C, Fig. 3(D)] gives spectra related both to the RT/100° and 100°C/RT spectra. The extent of oligomerization is quite high **(53,54)** as evidenced by the lack of modes near 900-950 cm^{-1}. The terminal molybdenum oxygen double bond at 1030 cm^{-1} is partially obscured due to the broadness of the δ(Mo-O-H) mode at 1060 cm^{-1}. As in the room temperature post-heated spectrum, there is little evidence of adsorbed water, although the modes at ~1100 and ~1300 cm^{-1} suggest the presence of residual molybdenum hydroxide species. The ν(OH) mode for the hydroxyl groups is too broad to be observed.

Nyquist and Kagel **(53)** discuss the vibrational modes observed in inorganic compounds due to water of hydration and metal hydroxide (formed by the interaction of water and the metal oxide). They assign modes of ν(OH) at 2800-3400 cm^{-1} and δ(H-O-H) at 1590-1660 cm^{-1} as due to the water of hydration (analogous to chemisorbed water on the oxide surface), and ν(OH) at 2000-3200 cm^{-1} and δ(M-O-H) at 950-1200 cm^{-1} as due to metal hydroxide formation. The infrared spectrum of hydrated MoO_3 **(53)** shows modes at 1150, 1350, 1630, 2300 and 3200-3700 cm^{-1}. By comparison, an infrared spectrum of rigorously dried MoO_3 shows no vibrational modes between 1000 and 4000 cm^{-1} **(54)**. The disappearance of the 2930-2950 [ν(HOH)] and 1625 cm^{-1} [δ(HOH)] modes in the tunneling spectrum upon post-heating the tunneling junctions (100°C for 300 s at 1 x 10^{-7} Torr) strongly suggests the interaction of water vapor with the molybdenum oxide that is formed by the hydrolysis of the MoO_2Cl_2 by the surface hydroxyl groups.

The stability of coordinated molecular water in molybdenum complexes is well established. The "hydrates" of MoO_3, $MoO_3 \cdot H_2O$ and $MoO_3 \cdot 2H_2O$, are actually $MoO_2(OH)_2$ and $MoO_2(OH)_2 \cdot H_2O$, respectively. Thermal desorption studies by Sotani et al. **(56)** show desorption maxima of water at 150°C and 400°C for desorption at 10^{-3} Torr. These peaks are attributed to desorption of coordinated water and the recombination of hydroxyl groups, respectively. A transmission infrared study of water chemisorbed on MoO_3 by Chung et al. **(57)** verifies the existence of molecularly chemisorbed water by the presence of the H_2O scissoring mode at approximately 1650 cm^{-1}. The water chemisorbs at coordinatively unsaturated molybdenum sites **(57)**.

These oxide surfaces, unlike those formed by the $MoOCl_4$, produce tunnel junctions with reasonably useful electrical characteristics ($\Delta\sigma \sim$ 5-10%). Some preliminary experiments to investigate the surface properties of these molybdenum oxides are discussed below.

C. Attempted Reaction of the Decomposition of MoO_2Cl_2 Adsorbed on Alumina at 100°C with Ethylene

As discussed elsewhere **(22)**, we have attempted to react a molybdenum oxide surface species, formed by the decomposition of molybdenum hexacarbonyl, with ethylene in order to form an oxomolybdenum carbene species of the type proposed as the active catalyst for metathesis reactions. A discussion of the metathesis reaction and the proposed mechanism is given in the review by Grubbs **(58)**.

Similarly, we attempted to activate with ethylene the oligomerized molybdenum oxide surface produced by surface hydrolysis of MoO_2Cl_2 with ethylene [Fig. 3(C)]. The tunneling spectrum that resulted from a 2 Torr exposure of ethylene at 100°C for 900 s is shown in Fig. 4. Heating times of up to 1800 s were used

with essentially the same result: no evidence of carbene formation. The exposure of the molybdenum oxide surface to ethylene at 100°C has resulted in the desorption of the chemisorbed water (due to the post-heating) as well as most of the hydroxyl groups [indicated by the weak δ(Mo-O-H) modes] at longer heating time. The oxide is also extensively oligomerized as indicated by the weak ν(Mo=O) mode at ~1030 cm^{-1}. These changes are caused by the longer annealing time.

D. Reaction of the Molybdenum Oxide Surface Formd by Decomposition of MoO_2Cl_2 on Alumina at 100°C with Acetic Acid and 4-t-Butylpyridine

The tunneling spectra that result from the hydrolysis of MoO_2Cl_2 display evidence of water chemisorbed on the molybdenum oxide surface. This indicates that the coordinatively unsaturated molybdenum oxide is functioning as a Lewis acid (at the molybdenum center) by coordinating the Lewis base, water. This is in contrast to the coordinatively saturated hydroxylated alumina surface which shows no evidence of coordinated water under normal preparation conditions. The aluminum oxide junctions react with Bronsted acids, such as acetic acid, to form the corresponding conjugate base of the acid (e.g. acetate) and water, which desorbs under vacuum, or an additional surface hydroxyl group. By contrast, Lewis bases such as 4-t-butylpyridine are weakly chemisorbed and readily desorb under vacuum. We thus undertook a preliminary study of the acid/base behavior of the molybdenum surface.

The molybdenum oxide surface that is formed, as noted above, is relatively sensitive to the preparation conditions. Thus all experiments were controlled with the temperatures of exposure maintained at 100 ± 5°C and the times of exposure 300 ±1 s. The temperature in the laboratory was stable to ±0.2°C (at 22.0°C) during the experimental series. This corresponds to a ±1 x 10^{-3} Torr

change in the vapor pressure; or an error in the exposure of ±2%. Thus the initial molybdenum oxide surface corresponds to the tunneling spectrum in Fig. 3(C).

The result of an exposure of acetic acid vapor at 10^{-1} Torr for 300 s is shown in the tunneling spectrum of Fig. 5(A). For comparison, the result of an identical exposure of acetic acid on an alumina surface is shown in Fig. 5(B). The differences are substantial. There are no sharp peaks characteristic of acetate formation on the molybdenum oxide surface. However, the absence of the ν(OH) mode at 3650 cm^{-1}, even though the oxide was not heated, as well as several peaks between 1200 and 3000 cm^{-1} indicate decomposition of the acetic acid. The broad, weak modes produced by the decomposed acetic acid do not allow identification of the decomposition product.

By contrast, the tunneling spectrum that results from an exposure of 4-t-butylpyridine vapor at 5 x 10^{-2} Torr for 100 s on the molybdenum oxide surface is shown in Fig. 6(A). For comparison, the tunneling spectrum from a junction exposed to 10^{-1} Torr of 4-t-butylpyridine vapor for 1000 s on an aluminum oxide surface is shown in Fig. 6(B), and the tunneling spectrum of a blank junction is shown in Fig. 6(C). It is immediately obvious that all modes characteristic of molybdenum oxide are missing in Fig. 6(A), as well as the vibrational modes due to a large fraction (~50-60%) of the surface hydroxyl groups. Exposure of an alumina surface to 200 times as much 4-t-butylpyridine produces a tunneling spectrum, Fig. 6(B), similar to that of a blank junction, Fig. 6(C). The relative surface hydroxyl coverage is determined by comparing the ratio of the area of the ν(OH) peak normalized to the area of the ν(Al-O) mode for the sample spectrum to the corresponding ratio for a blank junction. The MoO_2Cl_2 exposure, followed by 4-t-butylpyridine exposure produces a decrease in the surface hydroxyl coverage of ~50-60%, whereas the 4-t-butylpyridine exposure alone produces a

decrease of ~15-20%. This verifies that, in fact, the MoO_2Cl_2 reacted with the surface hydroxyl groups to form the molybdenum oxide surface and desorb the hydroxyl protons as HCl. The 4-t-butylpyridine then reacted with the oligomerized molybdenum oxide and desorbed the molybdenum oxide from the surface.

Nitrogen-containing bases (e.g. diethylenetriamine) are sufficiently strong to produce depolymerization of molybdenum oxide **(32)**. This suggests the reaction sequence,

(4)

(5)

The ratio of three molecules of 4-t-butylpyridine to one molecule of MoO_3 is hypothetical, but it is based on the observed octahedral coordination of MoO_3 with three basic sites for ligands. There is more than sufficient 4-t-butylpyridine present in the system to satisfy the proposed stoichiometry.

The extremely strong reaction of the molybdenum oxide with Lewis bases suggests that further investigations with weaker bases or much lower exposures

may produce data complementing the primarily Bronsted acid nature of adsorbates on hydroxylated aluminum oxide. In addition, molybdenum oxide is used widely as a catalyst for oxidation reactions either by itself or in the form of a mixed oxide **(21)**. The availability of relatively volatile (e.g. vapor pressure $>10^{-2}$ Torr) halogen or other salts of many metals suggests the possibility of generalizing this method of oxide generation to other metal systems and the formation of mixed metal oxide surfaces. Finally, the availability of dehydroxylated alumina surfaces provides the opportunity for comparison with the hydroxylated alumina surfaces used heretofore in tunneling spectroscopy.

V. Conclusions

The reaction of $MoOCl_4$ with the hydroxylated alumina surface produces a dimeric, oxygen bridged surface species analogous to dimeric MoO_2Cl_2. This species is unstable with respect to desorption under vacuum. Heating the surface during exposure to $MoOCl_4$ produces a molybdenum oxide surface which is poorly suited to tunneling spectroscopy.

Reacting MoO_2Cl_2 with the hydroxylated alumina surface produces a series of molybdenum oxide surface species. The degree of oligomerization depends on the extent of heating. Surface species which have not been post-heated in vacuum give spectral evidence for adsorbed water and molybdenum hydroxide formation. Post heating removes the chemisorbed water.

The molybdenum oxide surface displays little reactivity toward ethylene exposed at 100°C. The molybdenum oxide surface surface causes decomposition of acetic acid adsorbed at 22°C. The oxide reacts with 4-t-butylpyridine, present in substantial excess, causing desorption of the molybdenum oxide, probably as a volatile $MoO_3 \cdot 3$(pyridine) complex. The resulting surface is dehydroxylated aluminum oxide.

The use of volatile metal oxochlorides to form suitable metal oxide surfaces for study by tunneling spectroscopy has been established. Future work on molybdenum and other metal oxide surfaces formed by halide hydrolysis, as well as the availability of dehydroxylated alumina surfaces, has the potential to expand significantly the variety of surfaces capable of being studied by inelastic electron tunneling spectroscopy.

Acknowledgment

This research was supported by the National Science Foundation under Grant No. DMR-8500789.

References

1. P. K. Hansma, Phys. Rep. C **30**, 146 (1977).
2. W. H. Weinberg, Ann. Rev. Phys. Chem. **29**, 115 (1978).
3. "Inelastic Electron Tunneling Spectroscopy", T. Wolfram, Ed.; Springer, Berlin, 1978.
4. P. K. Hansma and J. R. Kirtley, Acc. Chem. Res. **71**, 440 (1978).
5. H. W. White and T. Wolfram, Methods Exp. Phys. A, **16**, 149 (1980).
6. H. W. White, L. M. Godwin and R. Elliatioglu, J. Adhes. **13**, 177 (1981).
7. S. Ewert, Appl. Phys. A, **26**, 63 (1981).
8. "Tunneling Spectroscopy", P. K. Hansma, Ed.; Plenum, New York, 1982.
9. W. H. Weinberg, Vibrational Spectra and Structure, **11**, 1 (1982).
10. S. K. Khanna and J. Lambe, Science **220**, 1345 (1983).
11. "Principles of Electron Tunneling Spectroscopy", E. L. Wolf, Ed.; Oxford, New York, 1985.
12. D. G. Walmsley and J. L. Tomlin, Prog. Surface Sci. **18**, 247 (1985).
13. R. C. Jaklevic and J. Lambe, Phys. Rev. B **2**, 808 (1970).
14. A. Adane, Solid State Commun. **16**, 1071 (1975).
15. See, for example, the spectra in Ref. 12.
16. S. Gauthier, S. De Cheveigne, G. Salace, J. Klein and M. Belin, Surface Sci. **155**, 31 (1985).
17. M. Suzuki, U. Mazur and K. Hipps, Surface Sci. **161**, 156 (1985).
18. U. Mazur and K. Hipps, J. Phys. Chem. **85**, 2244 (1981).

19. J. Moreland, S. Alexander, M. Cox, R. Sonnenfeld and P. K. Hansma, Appl. Phys. Lett. **43**, 387 (1983).

20. G. Binnig, N. Garcia and H. Rohrer, Phys. Rev. B **32**, 1336 (1985).

21. See, for example, "Fourth International Conf.: The Chemistry and Uses of Molybdenum", Climax, Ann Arbor, 1982.

22. G. J. Gajda, R. H. Grubbs and W. H. Weinberg, J. Am. Chem. Soc., submitted.

23. W. M. Bowser and W. H. Weinberg, J. Am. Chem. Soc. **103**, 1453 (1981).

24. B. G. Ward and F. E. Stafford, Inorg. Chem. **7**, 2569 (1968).

25. M. L. Larson and F. W. Moore, Inorg. Chem. **5**, 801 (1966).

26. F. A. Cotton and G. Wilkinson, "Advanced Inorganic Chemistry", 4th ed.; Wiley, New York, 1980.

27. M. B. Rubin and P. Day, Adv. Inorg. Chem. Radiochem. **10**, 335 (1967).

28. H. L. Krauss and W. Huber, Chem. Ber. **94**, 2864 (1961).

29. K. Freeman and G. W. A. Fowles, Inorg. Chem. **4**, 310 (1965).

30. J. Bernard and M. Camelot, Compt. Rend. Acad. Sci. Paris, Ser. C. **263**, 1068 (1966).

31. C. S. Barraclough and J. Stals, Austr. J. Chem. **19**, 741 (1966).

32. W. F. Mazluft, Inorg. Chem. **3**, 395 (1964).

33. A. Magneli, Acta Chem. Scand. **2**, 501 (1948).

34. A. Magneli, Acta Cryst. **6**, 495 (1953).

35. L. Kihlborg in, "Nonstoichiometric Compounds", R. Ward, Ed.; Am. Chem. Soc., Washington, 1963.

36. L. Kihlborg, Acta Chem. Scand. **13**, 954 (1959).

37. L. Kihlborg, Acta Chem. Scand. **14**, 1612 (1960).

38. L. Kihlborg, Arkiv. Kemi. **21**, 427 (1963).

39. M. A. Khilla, H. Mikhail, A. Abul-El-Soud and Z. M. Hanafi, Czeck. J. Phys. B **30**, 1039 (1980).

40. B. G. Brandt and A. C. Skapski, Acta Chem. Scand. **21**, 661 (1967).

41. L. Benadar and Y. Shimony, Mat. Res. Bull. **9**, 837 (1974).

42. "Handbook of Chemistry and Physics", 55th ed., R. C. West, Ed.; CRC Press, Cleveland, 1974.

43. A. Manthiram and J. Gopalakrishan, Rev. Inorg. Chem. **6**, 1 (1984).

44. G. J. Gajda and W. H. Weinberg, Rev. Sci. Instrum., submitted.

45. W. M. Bowser and W. H. Weinberg, Rev. Sci. Instrum. **47**, 583 (1976).

46. W. M. Bowser and W. H. Weinberg, Surface Sci. **64**, 377 (1977).

47. H. E. Evans, W. M. Bowser and W. H. Weinberg, Appl. Surface Sci. **5**, 258 (1980).

48. G. J. Gajda and W. H. Weinberg, Rev. Sci. Instrum. **56**, 700 (1985).

49. G. J. Gajda and W. H. Weinberg, J. Vacuum Sci. Technol. A **3**, 2208 (1985).

50. Y. Sacki and R. Matsuzaki, J. Electrochem. Soc. Jap. **34**, 115 (1966).

51. Y. Sacki and R. Matsuzaki, J. Electrochem. Soc. Jap. **34**, 180 (1966).

52. B. O. Field, R. Hart and D. M. Lewis, Spectrochim. Acta **41A**, 1069 (1985).

53. R. A. Nyquist and R. O. Kagel, "Infrared Spectra of Inorganic Compounds"; Academic, New York, 1971.

54. R. I. Buckley and R. J. H. Clark, Coord. Chem. Rev. **65**, 167 (1985).

55. See, for example, Sadtler Infrared Spectrum Y924K.

56. N. Sotani, S. Masuda, S. Kishimoto and M. Hasegawa, J. Colloid Int. Sci. **70**, 595 (1979).

57. J. S. Chung, R. Miranda and C. O. Bennett, J. Chem. Soc. Faraday Trans. I **81**, 19 (1985).

58. R. H. Grubbs, in "Comprehensive Organometallic Chemistry", G. Wilkinson, Ed.; Academic, New York, 1982, Vol. 8, pp. 499-551.

59. D. G. Walmsley, W. J. Nelson, N. M. D. Brown and R. B. Floyd, Appl. Surface Sci. **5**, 107 (1980).

Table 1. Vibrational Frequencies in Wavenumbers of Molybdenum Complexes and Formate Anion.

MoO_2Cl_2 Gas Phase **(29)**		MoO_2Cl_2 Nujol Mull **(29)**		MoO_2Cl_2 Diethylether Solution **(29)**		$MoOCl_4$ Gas Phase **(22)**	
				2991	$\nu_s(CO_2^-)$ + $\nu_a(CO_2^-)$?		
				2875	ν(CHH)	2935	ν(CH)
				2724	δCH overtone		
				1580	$\nu_a(CO_2^-)$	1639	$\nu(CO_2^-)$
				1456	$\nu_s(CO_2^-)$		
				1370	δ(CH)	1377	δ(CH)
				1038	γ(CH)	1053	γ(CH)
						1015	νMo=O
996	ν_sMo=O			969	ν_sMo=O		
972	ν_aMo=O	910	νMo-O	928	ν_aMo=O		
		864	νMo-O				
		827	νMo-O	830	νMo-O-Mo		
		781	νMo-O	777	νMo-O-Mo		
		600	ν_sMo-O-Mo			628	νMo-O-Mo
453	ν_aMo-Cl					450	νMo-Cl
437	ν_sM-Cl						
		401	νMo-Cl				
		376	+			396	νMo-Cl
		372	defor-	361	νMo-Cl		
		344	mation	358	νMo-Cl		
		284	modes				

(Table 1 continued)

MoO_4^{2-} Solid State **(58)**		$Mo_2O_3^{2-}$ Solid State **(58)**		$HCOO^-$/Alumina IETS **(59)**		$MoOCl_4$/Alumina IETS Fig. 1(A)	
		990	νMo-O				
		950	νMo-O	940	νAl-O	940	νAl-O
		910	νMo-O				
897	ν_sMo=O						
858	ν_aMo=O	825	ν_asMoO_3				
830	ν_aMo=O	780	ν_asMoO_3			752	νMo-O-Mo
		465				400-	νMo-Cl
						500	δ-Mo-Cl+
407	δO=Mo-O						
		360	δMoO_3				
330	δO=Mo-O	333	δMoO_3				
318	δO=Mo-O	315	δMoO_3			307	δ-Mo-Cl
				242	CO_2^-rock		

Table 2. Vibrational Frequencies (in cm^{-1}) of Molybdenum Oxide Surface Complexes Formed from MoO_2Cl_2.

RT/RT	RT/100°C	100°C/RT	100°C/100°C	Tentative Assignment **(53,54)**
3680		3680		ν(OH)
2950		2930		ν(H-O-H)
2400		2460		ν[(Mo)-O-H]
1625		1625		δ(H-O-H)
1440		1440		δ(H-O-H)
			1320	δ(Mo-O-H)
	1300		1225	δ(Mo-O-H)
1090	1105	1150	1060	δ(Mo-O-H)
	1030		1030	ν(Mo=O)
950				ν_a(O=Mo=O)
	940	940	940	ν(Al-O)
910				ν_s(O=Mo=O)
815		815	815	ν(Mo-O)
	770			ν(Mo-O)
			740	ν(Mo-O-Mo)
665	645		665	ν(Mo-O-Mo)
590	590	590	590	ν(Mo-O-Mo)
	535		535	ν(Mo-O-Mo)
500	440	455	470	δ(Mo-O)
385	385			δ(Mo-O)
		340	345	δ(Mo-O)
260	285	270	280	δ(Mo-O)

Figure Captions

Figure 1. Tunneling spectra produced by adsorption of $MoOCl_4$ on aluminum oxide. (A) Adsorption at 22°C, (B) Adsorption at 22°C, followed by heating in vacuum to 40°C for 900 s, (C) Tunneling spectrum of a clean aluminum oxide surface (blank junction), (D) Adsorption at 100°C. Pressure of $MoOCl_4$ = 27 x 10^{-3} Torr, time of exposure = 300 s.

Figure 2. Tunneling spectrum from Fig. 1(A) processed to remove the background slope. The spectral region from 240 to 1100 cm^{-1} is shown.

Figure 3. Tunneling spectra produced by adsorption of MoO_2Cl_2 on aluminum oxide. (A) Adsorption at room temperature, no post-heating, (B) Adsorption at room temperature, post-heated to 100°C for 300 s in vacuum, (C) Adsorption at 100°C, no post-heating, (D) Adsorption at 100°C, post-heated to 100°C for 300 s in vacuum. Pressure of MoO_2Cl_2 = 59 x 10^{-3} Torr, time of exposure = 300 s.

Figure 4. Tunneling spectrum of molybdenum oxide surface prepared as in Fig. 3(C) and heated to 100°C in 2 Torr ethylene for 900 s.

Figure 5: (A) Tunneling spectrum of molybdenum oxide surface prepared as in Fig. 3(C) and exposed to 10^{-1} Torr acetic acid for 300 s. (B) Tunneling spectrum of aluminum oxide surface exposed to acetic acid as in (A).

Figure 6: (A) Tunneling spectrum of molybdenum oxide surface prepared as in Fig. 3(C) and exposed to 5 x 10^{-2} Torr 4-t-butylpyridine for 300 s. (B) Tunneling spectrum of aluminum oxide surface exposed to 10^{-1} Torr 4-t-butylpyridine for 1000 s. (C) Tunneling spectrum of a clean aluminum oxide surface (blank junction).

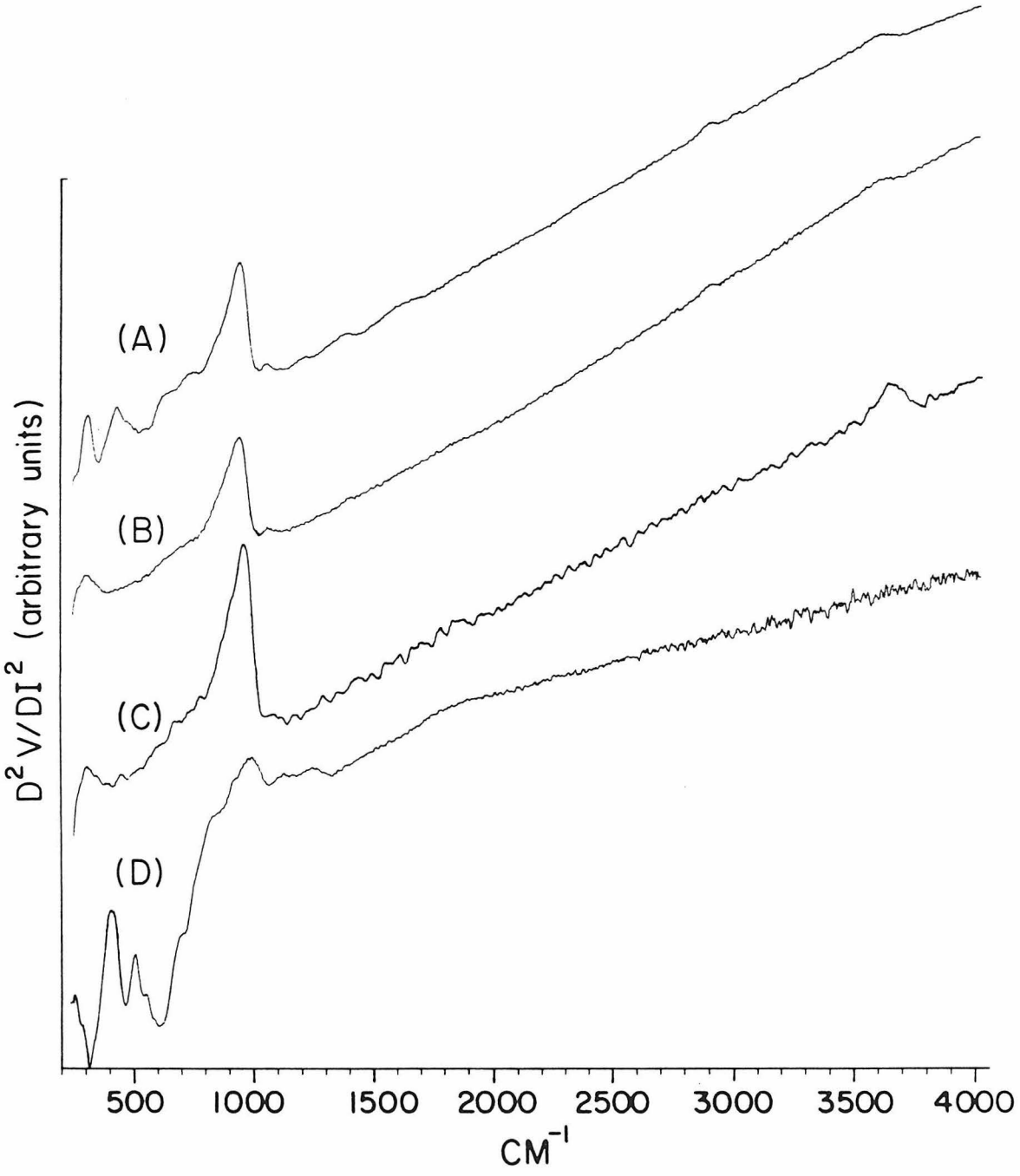
(A)
(B)
(C)
(D)
D^2V/DI^2 (arbitrary units)
500
1000
1500
2000
2500
3000
3500
4000
CM^{-1}

Fig. 1

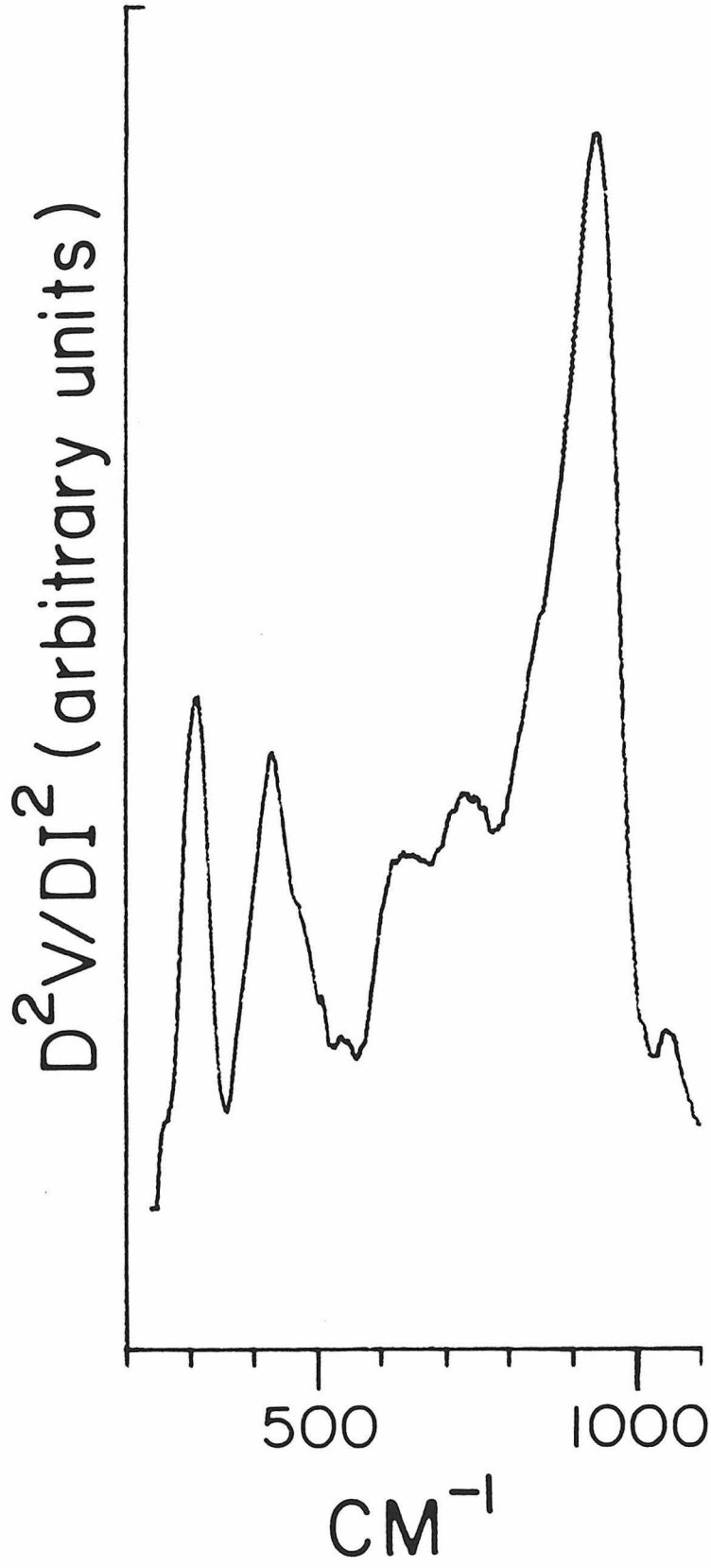

Fig. 2

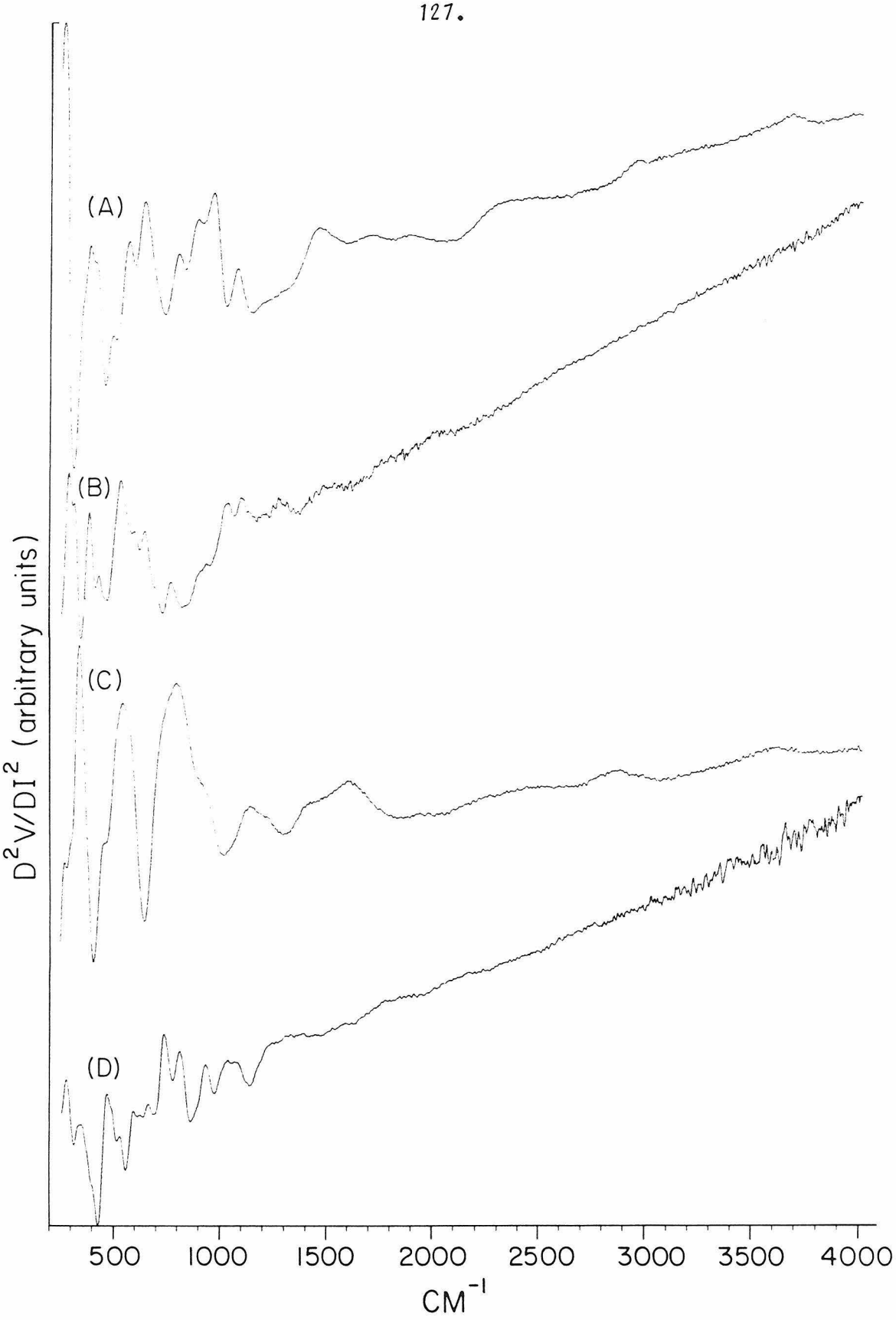
(A)
(B)
(C)
(D)
D^2V/DI^2 (arbitrary units)
500
1000
1500
2000
2500
3000
3500
4000
CM^{-1}

Fig. 3

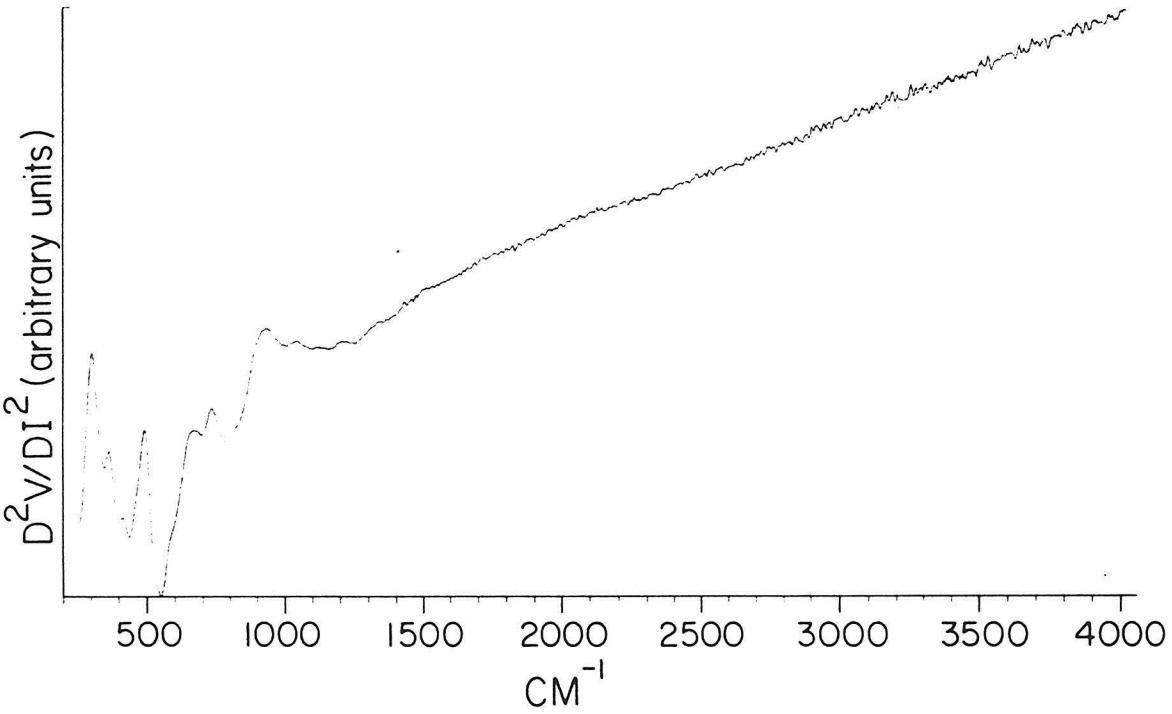
D^2V/DI^2 (arbitrary units)
500
1000
1500
2000
2500
3000
3500
4000
CM^{-1}

Fig. 4

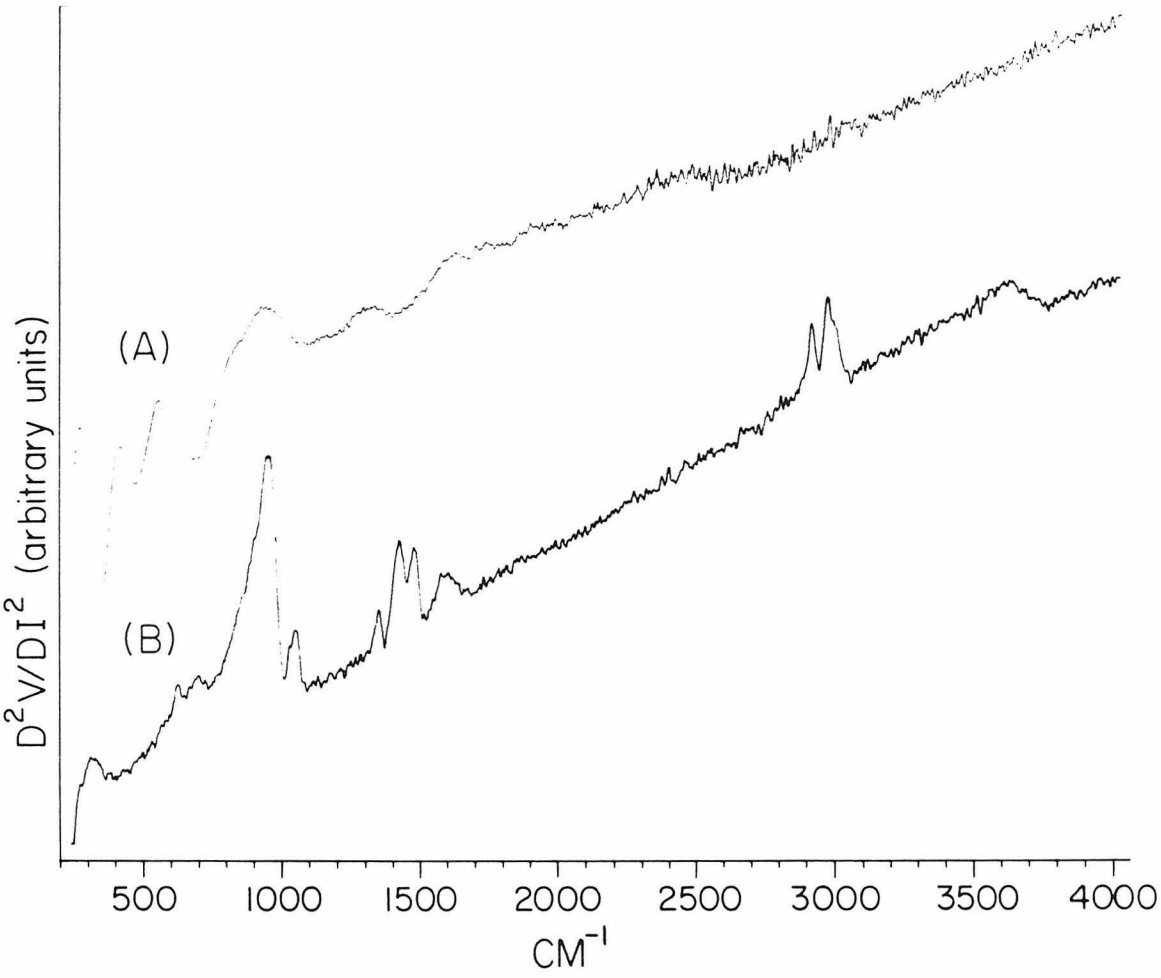
(A)
(B)
D^2V/DI^2 (arbitrary units)
500
1000
1500
2000
2500
3000
3500
4000
CM^{-1}

Fig. 5

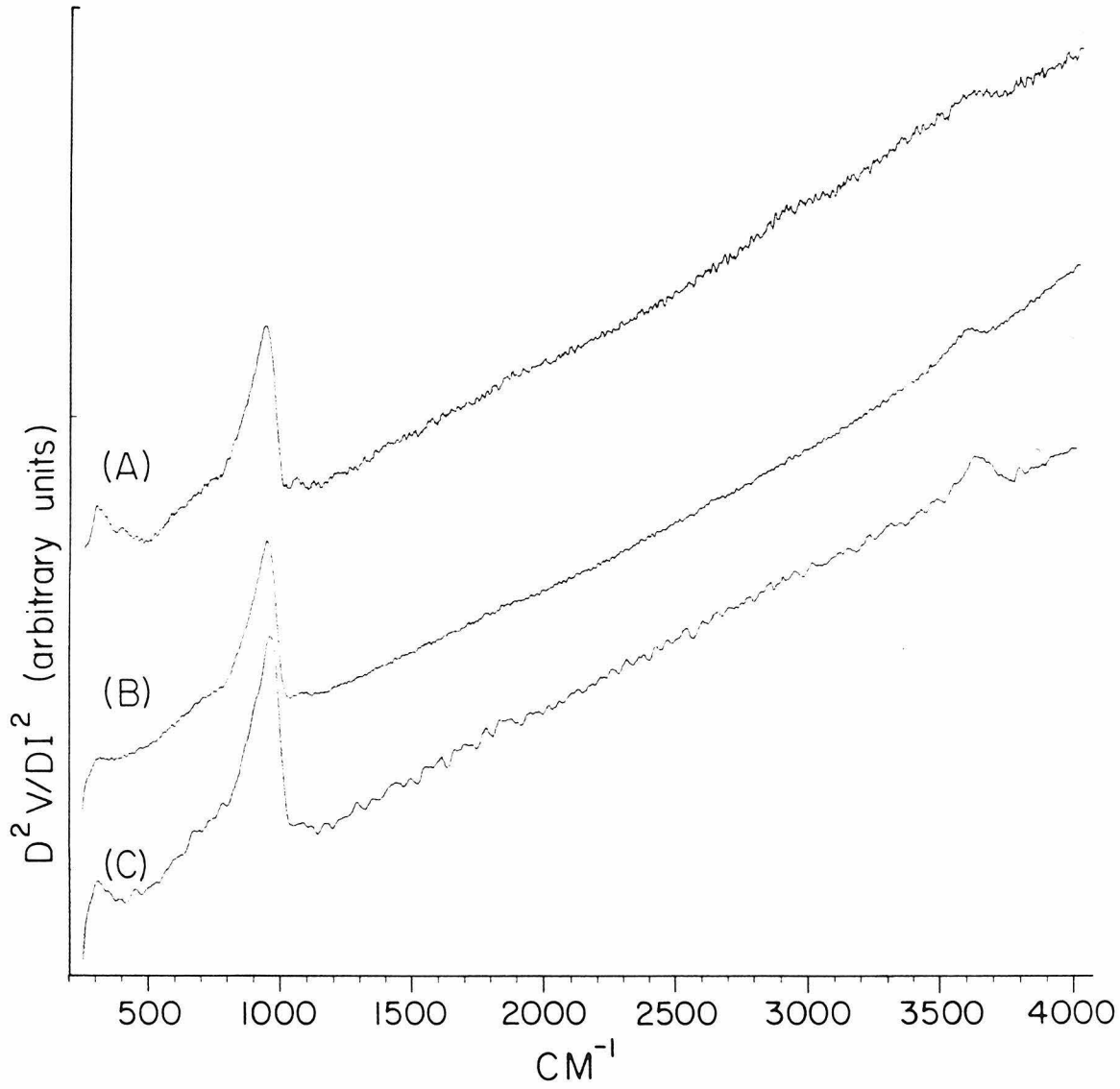
(A)
(B)
(C)
D^2V/DI^2 (arbitrary units)
500
1000
1500
2000
2500
3000
3500
4000
CM^{-1}

Fig. 6

Chapter Seven.

Inelastic Electron Tunneling Spectroscopic Studies of an Impure Molybdenum Hexacarbonyl and Reaction of Ethyl Aluminum Dichloride

I. Introduction

Inelastic electron tunneling spectroscopy has been used for the study of organometallic complexes adsorbed on an alumina surface. Systems that have been investigated include: $Ru_3(CO)_{12}$ **(1)**, $[Rh(CO)_2Cl]_2$ **(2)**, and $Zr(BH_4)_4$ **(3-7)**. Extensive reviews of this application of IETS have been published **(8-11)** as well as more general reviews of IETS theory and practice **(10-19)** and electron tunneling spectroscopy **(20)**.

The study of molybdenum carbonyl hydrides originated with Hieber's synthesis of $K_3[Mo_2(CO)_6(OH)_3]$ (I) **(21)**. Although this molybdenum compound proved too unstable, an X-ray crystal structure of the tungsten analog was obtained **(22)**. Infrared and NMR data indicate similar structures for the two compounds **(23)**. The probable structure of the molybdenum complex, based on the tungsten structure, is given in Fig. 1.

Addition of concentrated HCl to the anion produced a carbonyl hydride, formulated as $H_3Mo_2(CO)_6(OH)_3$ (II), which behaved as a moderately strong acid ($pk_A \sim 3$) **(21)**. Albano et al. later demonstrated that this complex was, in fact, tetrameric **(24)** and they were able to obtain a crystal structure of the tungsten analog **(25)**. The probable structure of the molybdenum complex $[Mo(H)(OH)(CO)_3]_4 \cdot 4H_2O$ (III) is shown in Fig. 1. Extensive characterization of the molybdenum complexes by IR and NMR was carried out by Sartorelli and coworkers **(23)** and selected results are presented in Table 1. Recent work on molybdenum carbonyl hydrides and other low oxidation state molybdenum hydrides has been reviewed by Kirtley **(26)**.

II. Experimental Procedures

Molybdenum hexacarbonyl was purified by sublimation *in vacuo*. The purified material was accidentally exposed to laboratory air (approximately 10 Torr

water vapor) by improper backfilling of the vac-line. In addition, the flask containing the contaminated material was exposed to ultraviolet and visible radiation from the fluorescent lights in the laboratory. These samples produced the tunneling spectra in Fig. 2. Properly prepared (and uncontaminated) samples of the sublimed hexacarbonyl produced the clean spectra of Fig. 3.

The spectra were obtained by forming a metal-insulator-adsorbate-metal tunnel junction as follows. A 900 Å thick lower metal electrode of aluminum was evaporated through a mask onto a glass substrate. The aluminum surface was oxidized in a glow discharge of 1000:1 oxygen:water vapor to produce an aluminum oxide layer approximately 20 Å thick. The molybdenum hexacarbonyl was then admitted to the fabrication chamber at its own vapor pressure at 22°C. After a 300 s exposure, the remaining vapor was pumped out and a 2500 Å thick lead upper electrode was evaporated. The procedure is described in greater detail elsewhere **(27)**.

The inelastic electron tunneling spectra were measured with a constant current spectrometer **(28)**, using a rapid scan technique to optimize the spectra. Typical measurement conditions are: 1000 scans, a 3 ms time constant, and a 1.2 mV rms modulation voltage. This provides an instrumental resolution of approximately 20 cm^{-1}. The spectra were processed to remove the background slope using the method of Gajda and Weinberg **(29)**

III. Results and Discussion: Impure Molybdenum Hexacarbonyl

Unlike the case of most IETS studies, we are faced with the problem of identifying an unknown starting material from the spectrum of its reaction product with aluminum oxide. Typically, the starting material is known (e.g. benzoic acid) and the product of the reaction is readily identified (e.g. benzoate ion **(30)**). However, several starting materials can lead to the same final product:

both benzoic acid and benzaldehyde react to form benzoate ion on alumina **(30)**. Thus we cannot insure the uniqueness of the starting material.

The spectrum that results from the pure molybdenum hexacarbonyl (Fig. 3A) is essentially that of a clean junction (Fig. 3B). This is in sharp contrast to the spectrum that results from exposure to the contaminated hexacarbonyl (Fig. 2A,B). The major modes from these spectra are summarized in Table 2.

One possible explanation for the synthesis of species compound II, and its possible surface reaction is given in Fig. 4. The photochemical reaction of molybdenum hexacarbonyl with water has been studied only in its initial steps. However, at low temperatures, $Mo(CO)_5(OH_2)$ forms, which is unstable above 230 K **(31)**. The decomposition products were not characterized, however.

If we hypothesize that compound II is, in fact, the volatile species, the surface reaction to produce the triply-bridged dimolybdenum carboxylate species represents primarily the reaction of a dibasic Bronsted acid with the hydroxylated alumina surface. The acidity of the molybdenum carbonyl hydride (III) is quite high (pk_a = 3.0), and reaction as a Bronsted acid would be expected.

The modes of the surface species produced by exposure to room temperature are listed in Table 2, along with possible assignments. In the absence of isotopic labeling studies, the assignments must be considered tentative. The presence of hydroxy stretching modes at $\sim$2900 cm^{-1} would be very unusual without the precedence of the known carbonyl hydride structures. The assignment of the 1470 cm^{-1} peak to a molybdenum hydride is also speculative since such low frequencies are unknown for terminal molybdenum hydrides. Thus, we proposed an oxygen-hydrogen-molybdenum bridging system. In view of the acidity of the hydride (the hydride protons are lost in the tri-anion), this is the Lewis acid equivalent of the usual Lewis base hydride bridge (i.e. donor-acceptor-donor vs.

acceptor-donor-acceptor). The observation of narrow, hydrogen-bonded vibrational modes is not unprecidented. For example, Sukarova et al. observe sharp (FWHM = 25-30 cm^{-1}) νOD modes in ice II (HDO) at 162 K and 280 MPa, even though the frequencies are downshifted by 300 cm^{-1} ($\sim$ 11%) indicating significant hydrogen bonding **(32)**.

The spectrum that results from post-heating the surface species to 100°C for 300 s is shown in Fig. 3(B). The vibrational modes are listed in Table 2. The modes of the basic molybdenum-oxide structure are present, but those assigned to the carboxylate are missing. This indicates desorption of the carboxylate, probably as carbon monoxide.

In the absence of additional spectroscopic information, or the availability of elemental composition information, further analysis of the identity of this impurity becomes increasingly speculative.

IV. Discussion: Ethyl Aluminum Dichloride

The original purpose of the system was to allow the use of aluminum alkyls and aluminum chloroalkyls to alter the nature of the aluminum oxide surface. This would allow the low-temperature removal of surface protons and the formation of aluminum chloride-like surfaces. In turn, this would greatly extend the variety of systems that could be studied by minimizing the unwanted decomposition of many organometallic species to their oxides or hydroxides. Unfortunately, aluminum chloroalkyls are prone to polymer formation in the presence of small amounts of water vapor or oxygen. Even the use of 'sacrificial' amounts of chloroalkyl on other substrates does not prevent the reaction. When prepared from solution, the compounds form a thin, opaque white film (for the ethyl aluminum dichloride, which is a solid at room temperature). The film is quickly coated with a thin layer of oxide and emits a small quantity of

'smoke' as the solvent evaporates. It pumps down poorly. When the junctions are exposed to air, a further quantity of 'smoke' is evolved and the film turns to a viscous liquid (hydrous aluminum oxide) and 'floats' the lead strips off the glass slide.

Attempts to prepare the surfaces with vapor phase reaction were similarly unsuccessful. There was no film formation but the junctions invariably had resistances greater than 20 MΩ. The small amount of hydroxyl is apparently sufficient to cause the formation of an aluminum chloroxy polymer which does not pump off. A similar problem is intrinsic to magnesium and lithium alkyls which are nonvolatile. Since these materials are nonvolatile, any excess applied in the liquid doping (to prevent reaction with residual water vapor) cannot be pumped off to leave only the first monolayer on the junction. Even limited polymer (oligomer) formation can render the junction resistance too large to measure.

The problem primarily results from the small area of the junction (about 1 cm^2 total or $\sim 10^{15}$ molecules/monolayer) versus the large amount of water vapor present in the system (~ 10 $ft^3 \times 10^{-7}$ atm partial pressure of $H_2O \sim 10^{18}$ molecules). At 0.1 ppm (10^{-7} atm), which is the limit of standard dehydration techniques, the amount of water is $\sim 10^{-6}$ moles. This is negligible for the usual organometallic work where solutions contain $\sim 10^{-3}$ moles of active component. In addition, the solvent limits the rate of reaction with the water by imposing a diffusion barrier. For the junctions, in contrast, we have about 10^{-9} moles of active sites and no diffusion barrier. This problem can be overcome in vapor-phase doping [e.g. $Zr(BH_4)_4$] since the partial pressure of water is $< 10^{-8}$ Torr (10^{-11} atm). To achieve this level in the glove box requires a four order of magnitude improvement in the current state-of-the-art.

As an alternative, volatile organometallic complexes can be employed, but few, if any, aluminum complexes appear suitable. The formation of polymers from the vapor phase reaction with the surface hydroxyls can severely limit the usefulness of otherwise sufficiently volatile compounds.

The glove box system can still be used for its inert atmosphere to guard against potential contamination from other laboratory activities and can be used with complexes that are oxygen-sensitive but only mildly water-sensitive. As better water and oxygen removal techniques become available, they can be used to increase the range of complexes that can be handled in the glove box system.

V. Conclusions

As these preliminary investigations demonstrate, IETS can provide evidence of surface reaction by small quantities of impurities in sample materials. Unfortunately, they also demonstrate some of the present limitations on the use of tunneling spectroscopy. The study of the reaction of molybdenum hexacarbonyl with water under matrix isolation conditions can clarify whether or not a species such as $H_3[Mo_2(CO)_6(OH)_3]$ forms and, if so, provides a source of well-defined material for further tunneling studies. The extremely slow time resolution of IETS prevents its use as an indicator of the extent of reaction. Techniques such as matrix-isolated FTIR or NMR are much better suited to these studies.

The use of extremely reactive compounds, such as $EtAlCl_2$, will require near UHV conditions in the fabrication system itself, and considerable reduction in the present level of water in the glove box to minimize contamination of the $EtAlCl_2$ by decomposition products. The present state-of-the-art in water removal from the glove box is inadequate, and the use of high vacuum techniques

(e.g. diffusion pumped systems and 100°C bakeout temperatures) may be necessary to extend the use of glove box techniques to the most reactive complexes.

References

1. W. M. Bowser and W. H. Weinberg, J. Am. Chem. Soc. **102**, 4720 (1980).
2. W. M. Bowser and W. H. Weinberg, J. Am. Chem. Soc. **103**, 1453 (1981).
3. H. E. Evans and W. H. Weinberg, J. Am. Chem. Soc. **102**, 872 (1980).
4. H. E. Evans and W. H. Weinberg, J. Vac. Sci. Technol. **17**, 47 (1980).
5. H. E. Evans and W. H. Weinberg, J. Am. Chem. Soc. **102**, 2548 (1980).
6. H. E. Evans and W. H. Weinberg, J. Am. Chem. Soc. **102**, 2554 (1980).
7. L. Forester and W. H. Weinberg, J. Vac. Sci. Technol. **18**, 600 (1981).
8. W. H. Weinberg, W. M. Bowser and H. E. Evans, Surface Sci. **106**, 489 (1981).
9. R. M. Kroecker and P. K. Hansma, Catal. Rev. Sci. Eng. **23**, 553 (1981).
10. *Tunneling Spectroscopy*, P. K. Hansma, Ed., Plenum, New York (1982).
11. W. H. Weinberg, Vibrational Spectra and Structure **11**, 1 (1982).
12. P. K. Hansma, Phys. Rep. C **30**, 146 (1977).
13. W. H. Weinberg, Ann. Rev. Phys. Chem. **29**, 115 (1978).
14. 'Inelastic Electron Tunneling Spectroscopy", T. Wolfram, Ed. Springer, Berlin (1978).
15. P. K. Hansma and J. R. Kirtley, Acc. Chem. Res. **11**, 440 (1978).
16. H. W. White and T. Wolfram, Methods Exp. Phys. A **16**, 149 (1980).
17. S. Ewert, Appl. Phys. A **26**, 63 (1981).
18. H. W. White, L. M. Godwin and R. Elliatioglu, J. Adhes. **13**, 177 (1981).
19. S. K. Khanna and J. Lambe, Science **220**, 1345 (1983).
20. E. L. Wolf, *Principles of Electron Tunneling Spectroscopy*, Oxford, New York

(1978).

21. W. Hieber, K. Englert and K. Rieger, Z. Anorg. Allg. Chem. **300**, 295 (1959).

22. V. G. Albano, G. Ciani and M. Manassero, J. Organomet. Chem. **25**, C55 (1970).

23. U. Sartorelli, L. Gariaschellli, G. Ciani and G. Bonora, Inorg. Chim. Acta. **5**, 191 (1971).

24. V. G. Albano, P. L. Bellon, G. Ciani and M. Manassero, Chem. Comm. 1242 (1969).

25. V. G. Albano, G. Ciani, M. Manassero and M. Sansoni, J. Organomet. Chem. **34**, 353 (1972).

26. S. W. Kirtley, in *Comprehensive Organometallic Chemistry*, G. Wilkinson, Ed., Pergamon, Oxford (1982).

27. G. J. Gajda and W. H. Weinberg, Rev. Sci. Instrum., submitted.

28. G. J. Gajda and W. H. Weinberg, Rev. Sci. Instrum. **56**, 700 (1985).

29. G. J. Gajda and W. H. Weinberg, J. Vacuum Sci. Technol. A **3**, 2208 (1985).

30. D. G. Walmsley, W. J. Nelson, N. M. D. Brown and R. B. Floyd, Appl. Surface Sci. **5**, 107 (1980).

31. M. J. Boylan, J. D. Black and P. S. Braterman, J. Chem. Soc. Dalton Trans., 1646 (1980).

32. B. M. Sukarova, W. F. Sherman and G. R. Wilkinson, Spectrochim. Acta. **14A**, 315 (1985).

Table 1. Infrared Modes (in cm^{-1} of Molybdenum Carbonyl Hydrides **(23)**.

Compound	νOH	νOH	δMOH
$K_3[Mo_2(CO)_6(OH)_3]\cdot 2H_2O$	2950	1855	1150
	2920	1680	
	2850		
$[(HO)Mo(CO)_3H]_4\cdot 4H_2O$	2950	2030	1050
	2920	2008	
	2850	1920	
		1880	
		1855	
$[(HO)Mo(CO)_3H]_4\cdot 4OPh_3$	2960	1995	
	2930	1910	
	2860	1895	

Table 2. Vibrational Modes from IETS Spectra and Possible Assignments (cm^{-1}).

Room Temperature Fig. 2(A)	Post-Heated Fig. 2(B)	Assignment
3650	3650	νOH
3295	~ 3300	$\nu M_2OH...H?$
2900vbr	2900vbr	$\nu M_3OH...H?$
~ 1800		$\nu C \equiv O?$
1667		$\nu C=O?$
1460	1460	νM-H?
1384		δC-O-H?
1273		νC-O?
1050	1050	$\delta M_3OH?$
945	945	νAl-O
715		δCOOH?
400		$\nu M-C \equiv O?$
269	303	metal-oxygen deformation modes

Figure Captions

Figure 1. Structures of the molybdenum carbonyl hydrides. Structures (I) and (III) are based on the X-ray crystal structures for the tungsten analogs. Structure (II) is hypothetical. (I) $[Mo_2(CO)_6(OH)_3]^{3-}$. (II) $H_3[Mo_2(CO)_6(OH)_3]$. (III) $[Mo(H)(CO)_3(OH)]_4$.

Figure 2. Tunneling spectra which result from exposure of an alumina surface to impure molybdenum hexacarbonyl. (A) Exposure at room temperature for 300 s. (B) As in (A), but then heated to 100°C for 300 s in vacuum.

Figure 3. Tunneling spectra which result from exposure of an alumina surface to pure molybdenum hexacarbonyl. (A) Exposure at room temperature for 300 s. (B) An unexposed junction.

Figure 4. Hypothetical reaction path from $[Mo(CO)_6 + H_2O$ to $H_3[Mo_2(CO)_6(OH)_3]$ (II), and possible reaction of (II) with an alumina surface to form a surface carboxylic acid.

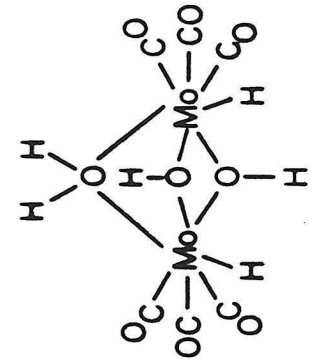

(II)

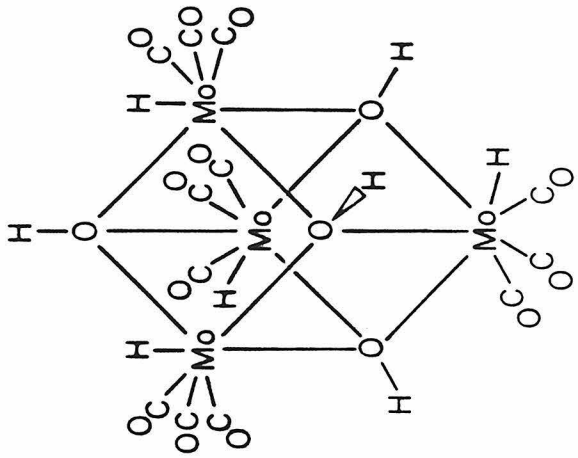

(III)

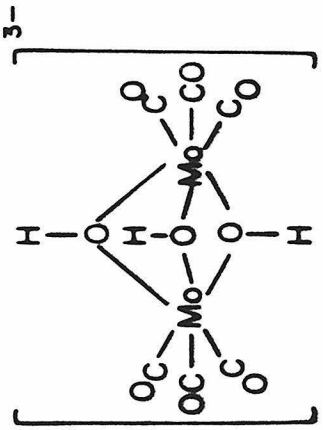

(I)

Fig. 1

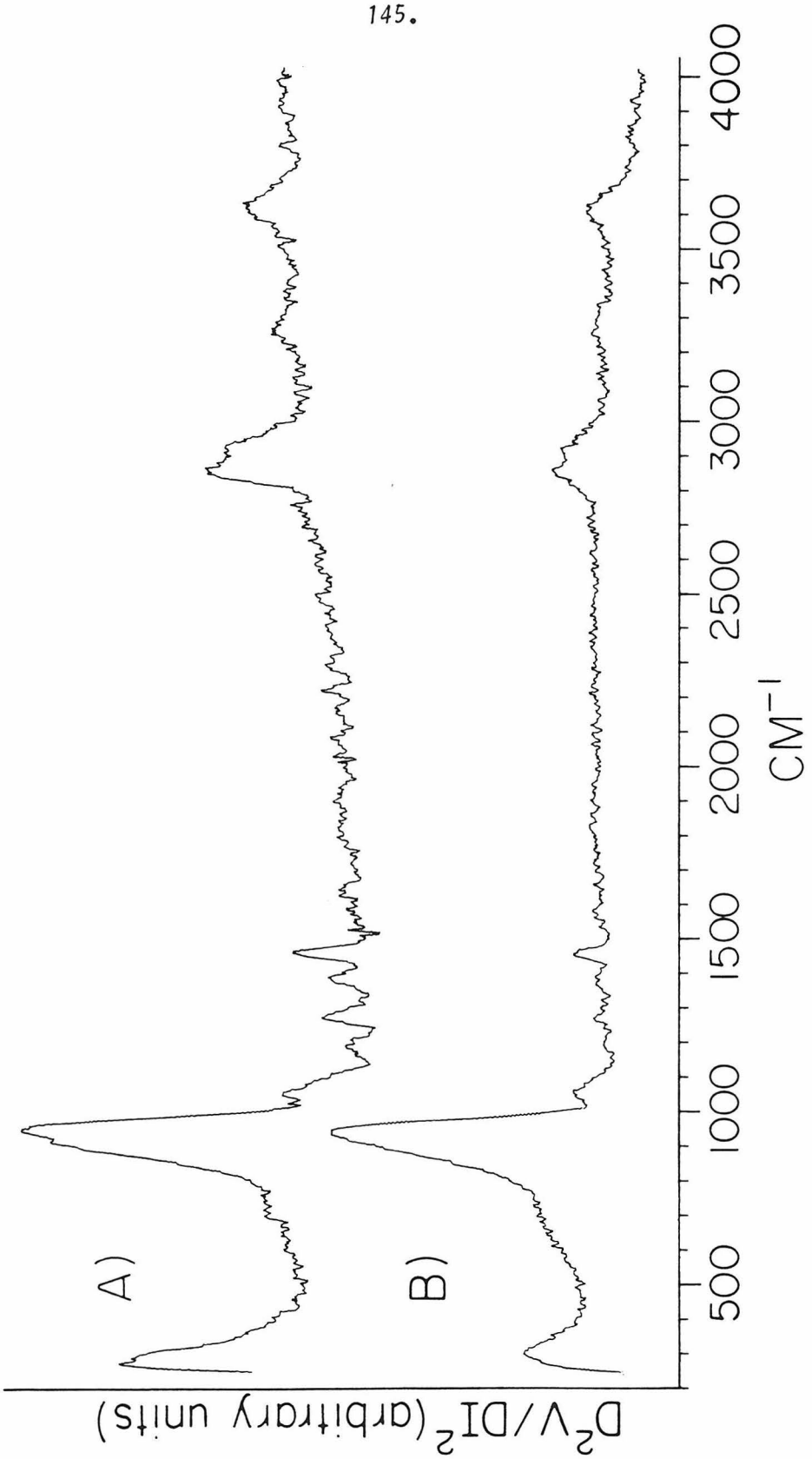
A)
B)
500
1000
1500
2000
2500
3000
3500
4000
CM⁻¹
D²V/DI² (arbitrary units)

Fig. 2

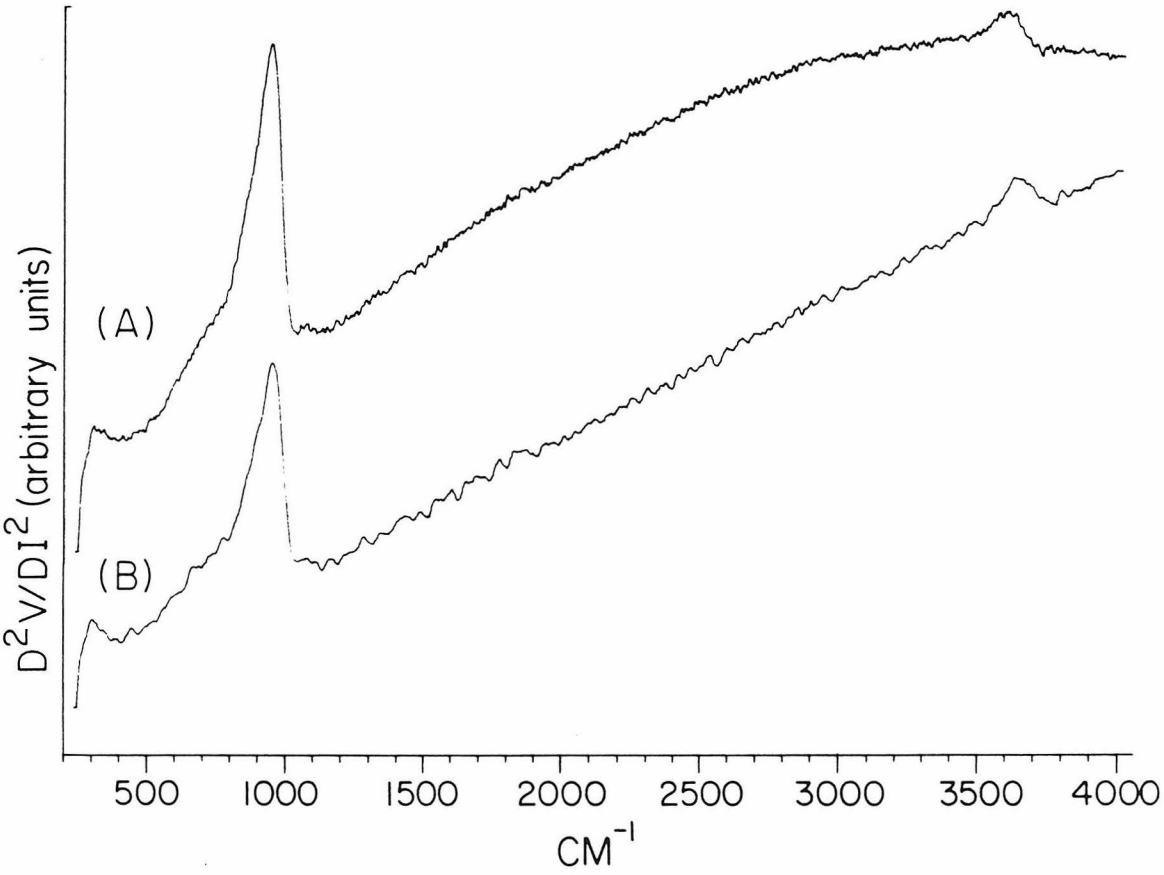
(A)
(B)
D^2V/DI^2 (arbitrary units)
500
1000
1500
2000
2500
3000
3500
4000
CM^{-1}

Fig. 3

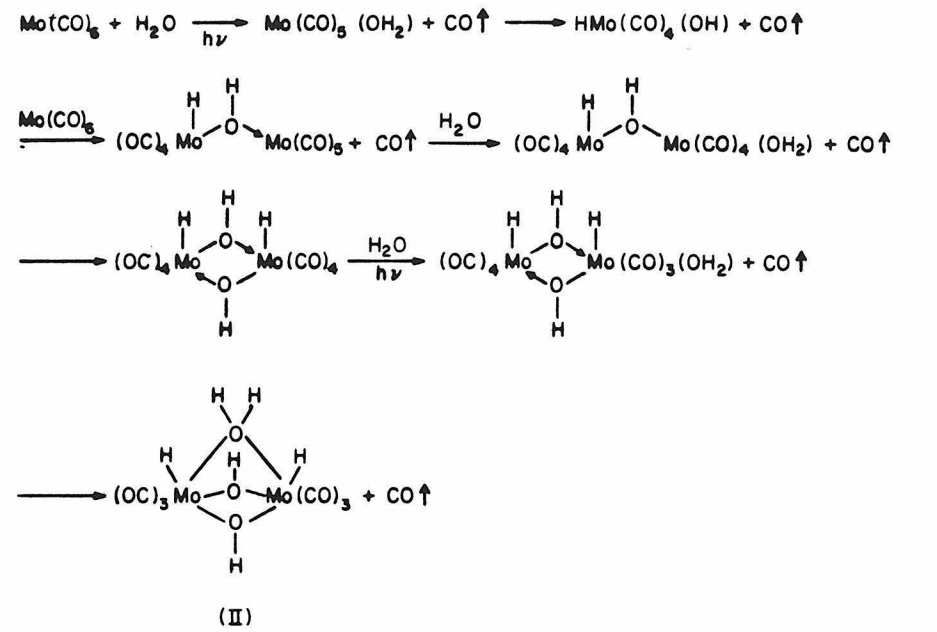

(II)

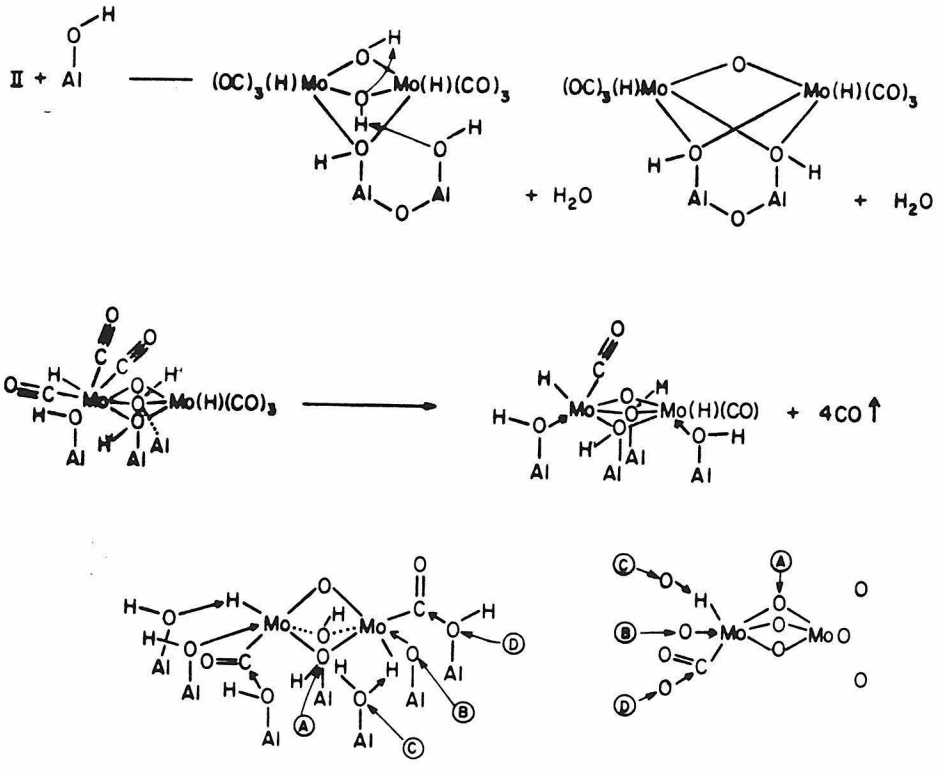

Fig. 4

Appendix A.

Program Listing: Data Collection Program for Tunneling Spectroscopy

[Supplemental Material for: G. J. Gajda and W. H. Weinberg,

Rev. Sci. Instrum. **56**, 700 (1985).]

```
CCCCCC
CCCCCC      PROGRAM IETS
C      DATA COLLECTION PROGRAM FOR INELASTIC ELECTRON TUNNELING
C      SPECTROSCOPY
C
C      A(2100) -> STORAGE ARRAY FOR LOCK-IN AMPLIFIER OUTPUT
C      (D2V/DI2)
C      INAME(6) -> FILENAME ARRAY
C      ILABEL(3,2) -> HEADER ARRAY FOR VLOW,VHIGH,VMOD,NP
C      VLOW -> STARTING BIAS VOLTAGE (MV*10)
C      VHIGH -> ENDING BIAS VOLTAGE (MV*10)
C      VMOD -> MODULATION VOLTAGE (RMS MV*100)
C      NP -> NUMBER OF POINTS PER SCAN
C      NS -> NUMBER OF SCANS PER SPECTRUM
C      IRES -> LOW/HIGH RESOLUTION FLAG
C      IDUM -> DUMMY VARIABLE FOR YES/NO QUESTIONS
C
C
C      DATACQ ->> FORTRAN SUBROUTINE TO COLLECT DATA
C      DELAY ->> FORTRAN SUBROUTINE TO CORRECT FOR LOCK-IN TIME CONSTANT
C      OSC ->> FORTRAN SUBROUTINE FOR QUICK SCAN SPECTRUM
C      PLOT ->> FORTRAN SUBROUTINE TO PLOT OUTPUT ON X-Y RECORDER
C      PLTOUT ->> FORTRAN SUBROUTINE THAT DRIVES DACS FOR PLOTTING
C      SCAN ->> FORTRAN SUBROUTINE TO STEP THROUGH SPECTRUM AND
C              PAUSE AT MAJOR PEAKS TO HELP GET THE ENTIRE
C              SPECTRUM ON SCALE
C      WROUT ->> FORTRAN SUBROUTINE TO OUTPUT DATA FILE ON DISK
C
C      INTPIO ->> MACRO ROUTINE TO INITIALIZE PARALLEL I/O
C      NDAC ->> MACRO ROUTINE TO SET NARROW DAC
C      READDC ->> MACRO ROUTINE TO READ THE ADC
C      RRLY ->> MACRO ROUTINE TO SET THE REED RELAYS
C      WDAC ->> MACRO ROUTINE TO SET THE WIDE DAC
C      XDAC ->> MACRO ROUTINE TO DRIVE THE X-AXIS PLOTTING DAC
C      YDAC ->> MACRO ROUTINE TO DRIVE THE Y-AXIS PLOTTING DAC
C
      PROGRAM IETS
C
C      USE VIRTUAL ARRAYS TO SAVE SPACE FOR THE MAIN PROGRAM
C      VIRTUAL ARRAYS USE SPACE ABOVE 64KBYTES THAT CAN'T BE
C      USED BY THE PROGRAM
C
      VIRTUAL A(2100)
C
C      SET UP REMAINING ARRAYS
C
      DIMENSION INAM(6),ILABEL(3,2)
C
C      SET FILE EXTENSION TO .DAT
C
      INAM(4)='.D'
      INAM(5)='AT'
      INAM(6)=0
```

```
C
C       INITIALIZE PARALLEL I/O, SET REED RELAY #2, SET WIDE DAC TO 0V
C       AND SET NARROW DAC TO 240CM-1 (119/2047*500MV)
C
      CALL INTPIO
      CALL RRLY(2)
      CALL WDAC(0)
      CALL NDAC(119)
C
C       GET THE NUMBER OF SCANS
C
   10 TYPE 900
      READ (5,901) NS
      IRES=2
C     RESOLUTION: IRES=1>HIGH RESOLUTION (2 CM-1)
C             IRES=2>LOW RESOLUTION (4 CM-1)
C
C       GET THE DESIRED RESOLUTION
C
      TYPE 916
      READ (5,903) IDUM
      IF (IDUM.EQ.'Y') IRES=1
C
C       GET THE FILE NAME
C
      TYPE 902
      READ (5,904) (INAM(IJ),IJ=1,3)
C
C       GET THE ACTUAL VLOW IN MV*10, STORED IN ILABEL(1,2)
C
      TYPE 910
      READ (5,901) ILABEL(1,2)
C
C       SET BIAS VOLTAGE TO 4000CM-1
C
      CALL NDAC(2047)
C
C       GET ACTUAL VHIGH IN MV*10, STORED IN ILABEL(2,1)
C
      TYPE 912
      READ (5,901) ILABEL(2,1)
C
C       SET BIAS VOLTAGE TO 2000CM-1 FOR MODULATION SETTING
C       AND INITIAL SPECTRAL PHASE ANGLE OPTIMIZATION
C
      CALL NDAC(1023)
C
C       GET MODULATION VOLTAGE MV*100, STORED IN ILABEL(2,2)
C
      TYPE 914
      READ (5,901) ILABEL(2,2)
C
C       SET DAC TO INITIAL VALUE (240CM-1) AND STEP THROUGH SPECTRUM
C       TO INSURE THAT IT IS ON SCALE ON THE LOCK-IN
```

```
C
    CALL NDAC(119)
 200  CALL SCAN
    CALL NDAC(119)
C
C       FIND OUT IF EVERYTHING IS OK
C
    TYPE 905
    READ (5,903) IDUM
C
C       YES -> START DATA COLLECTION
C
    IF (IDUM.EQ.'Y') GOTO 210
C
C       MAYBE -> TRY FURTHER OPTIMIZATION WITH QUICK SCANS
C
    IF (IDUM.EQ.'O') CALL OSC (A,1500)
C
C       REJECT -> THE JUNCTION IS BAD
C
    IF (IDUM.EQ.'R') GOTO 250
C
C       NO -> TRY TO GET THINGS ON SCALE
C
    GOTO 200
C
C       START DATA COLLECTION
C
 210  CALL DATACQ (A,2100,NS,NP,IRES)
C
C       SET BIAS TO 240CM-1 SO WE DON'T DESTROY THE JUNCTION
C
    CALL NDAC(119)
    ILABEL(1,1)=NP
C
C       WRITE OUT THE DATA FILE
C
    CALL WROUT (A,2100,INAM,NP,ILABEL)
C
C       PLOT OUT THE DATA ON THE X-Y RECORDER?
C
    TYPE 915
    READ (5,903) IDUM
C
C       GET A PLOT UNLESS SPECIFICALLY NOT REQUESTED
C
    IF (IDUM.NE.'N') CALL PLOT (A,2100,NP)
C
C       RUN ANOTHER JUNCTION?
C
 250  TYPE 908
    READ (5,903) IDUM
C
C       IF YES - START ALL OVER
```

```
C
    IF (IDUM.EQ.'Y') GOTO 10
C
C       IF NO - SUCCESSFUL RUN
C
    STOP 'SUCCESSFUL RUN'
 900  FORMAT(' ENTER THE NUMBER OF SCANS:',$)
 901  FORMAT(I7)
 902  FORMAT(' ENTER THE FILE NAME (AAAAAA):',$)
 903  FORMAT(A1)
 904  FORMAT(3A2)
 905  FORMAT(' START DATA COLLECTION?',$)
 908  FORMAT(' DO YOU WANT TO RUN ANOTHER JUNCTION (Y OR N)?', $)
 910  FORMAT(' ENTER IVMIN (MV*10):',$)
 912  FORMAT(' ENTER IVMAX (MV*10):',$)
 914  FORMAT(' SET MODULATION VOLTAGE AND ENTER VALUE(MV*10( )):',$)
 915  FORMAT(' DO YOU WANT A PLOT (Y OR N)?',$)
 916  FORMAT(' HIGH RESOLUTION?(Y OR N):',$)
    END
C
C-------------------<
C
C       SUBROUTINE PLOT(A,INDX1,NP)
C       FORTRAN SUBROUTINE TO PLOT DATA ON THE X-Y RECORDER
C
C       A => DATA STORAGE ARRAY
C       INDX1 => SIZE OF ARRAY A
C       NP => NUMBER OF POINTS IN A
C
    SUBROUTINE PLOT (A,INDX1,NP)
C
C       INITIALIZE PLOTTER TO (0,0)
C
    CALL YDAC (0)
    CALL XDAC (0)
C
C       SCALE X-AXIS SO EVERYTHING FITS ON THE PLOTTER
C
    AISIZE=NP
    XSCALE=4095./AISIZE
C
C       GIVE THE USER TIME TO SET UP THE PLOTTER
C
    PAUSE 'TYPE RETURN TO PLOT'
C
C       USE PLTOUT TO DO THE ACTUAL PLOTTING
C
    CALL PLTOUT (A,INDX1,NP,300,XSCALE)
    RETURN
    END
C
C-------------------<
C
C       SUBROUTINE PLTOUT(A,INDX1,NP,IDELAY,XSCALE)
```

```
C     FORTRAN SUBROUTINE TO OUTPUT DATA TO THE PLOTTER OR OSCILLOSCOPE
C
C      A => DATA STORAGE ARRAY
C      INDX1 => SIZE OF ARRAY A
C      NP => NUMBER OF POINTS IN ARRAY A
C      IDELAY => DELAY VALUE TO COMPENSATE FOR RECORDER PEN RESPONSE TIME
C          300 FOR X-Y, 10 FOR OSCILLOSCOPE
C      XSCALE => X-AXIS SCALE FACTOR TO COMPENSATE FOR DIFFERENT
C          AXIS LENGTHS FOR X-Y AND OSCILLOSCOPE
C
      SUBROUTINE PLTOUT(A,INDX1,NP,IDELAY,XSCALE)
C
C      SET UP ARRAYS
C
      VIRTUAL A(INDX1)
C
C      FIND MINIMUM AND MAXIMUM VALUES IN THE DATA
C
      AMIN=A(1)
      AMAX=A(1)
      DO 310 IJ=1,NP
      IF (A(IJ).GT.AMAX) AMAX=A(IJ)
      IF (A(IJ).LT.AMIN) AMIN=A(IJ)
  310 CONTINUE
C
C      USE THEM TO SET THE Y-AXIS SCALE (WHICH IS THE SAME SIZE FOR
C          THE X-Y AND OSCILLOSCOPE)
C
      ASCALE=4095./(AMAX-AMIN)
C
C      PLOT OUT EACH DATA POINT
C
      DO 330 IJ=1,NP
      IY=(A(IJ)-AMIN)*ASCALE
      AI=IJ
      IX=AI*XSCALE
      CALL YDAC(IY)
      CALL XDAC(IX)
C
C      WAIT FOR THE PLOTTER PEN TO CATCH UP, IF NEEDED.
C
      DO 330 JK=1,IDELAY
  330 AK=AK+JK
      RETURN
      END
C
C--------------------<
C
C      SUBROUTINE DATACQ(A,INDX1,NS,NP,IRES)
C      FORTRAN SUBROUTINE TO ACQUIRE DATA
C
C      A => VIRTUAL ARRAY FOR DATA STORAGE
C      INDX1 => SIZE OF ARRAY A
C      NS => NUMBER OF SCANS THROUGH SPECTRUM
```

```
C       NP => NUMBER OF POINTS IN EACH SCAN
C       ** => THIS VARIABLE IS SET IN DATACQ TO MINIMIZE THE
C             CHANCES FOR DESTRUCTION WHEN DATA COLLECTION
C             ROUTINES ARE CHANGED!
C       IRES => RESOLUTION FLAG
C
      SUBROUTINE DATACQ (A,INDX1,NS,NP,IRES)
      VIRTUAL A(INDX1)
C
C       SET THE NUMBER OF POINTS
C
      NP=965
C
C       FOR HIGH RESOLUTION (IRES=1), THE NUMBER OF POINTS DOUBLES
C
      IF (IRES.EQ.1) NP=965*2
C
C       CLEAR OUT ANY GARBAGE FROM A
C
      DO 10 J=1,INDX1
 10   A(J)=0.0
C
C       MAKE SURE REED RELAY #2 IS SET, AND WDAC IS AT 0V
C
      CALL RRLY(2)
      CALL WDAC(0)
C
C       MAIN DATA COLLECTION LOOP - REPEAT FOR EACH SCAN
C
      DO 100 I=1,NS
C
C       SET BIAS VOLTAGE TO START OF SCAN (240 CM-1)
C
      CALL NDAC(119)
C
C       WAIT FOR LOCK-IN TO RESPOND
C
      CALL DELAY
C
C       ACTUAL DATA COLLECTION LOOP - REPEAT FOR EACH POINT
C
      DO 100 J=1,NP
C
C       CALCULATE THE BIAS SETTING
C       SINCE NP=(IDAC_HIGH-IDAC_LOW)/IRES  +1,
C       IDAC=IPOINT*IRES +IDAC_LOW-2
C
      IDAC=IRES*J+117
C
C       SET BIAS VOLTAGE ACCORDINGLY
C
      CALL NDAC(IDAC)
C
C       SMALL DELAY LOOP (~1MS) TO ALLOW LOCK-IN TO RESPOND
```

```
C
    DO 60 JK=1,20
 60   AKL=AKL+JK
C
C       READ EACH POINT 12 TIMES (@1200HZ, THIS TAKES 10MS)
C
    DO 100 KL=1,12
C
C       COMMAND TO READ ADC CHANNEL ZERO WITH A GAIN OF ONE
C       IS JUST 1. SEE ADC OPERATING MANUAL FOR DETAILS.
C
    CALL READDC (1,IDAT)
C
C       CONVERT TO FLOATING POINT,
C
    AIDAT=IDAT
C
C       AND STORE IN ARRAY A
C
 100  A(J)=A(J)+AIDAT
    RETURN
    END
C--------------------<
C
C       SUBROUTINE OSC(A,INDX1)
C       FORTRAN SUBROUTINE TO TAKE A QUICK SCAN OF THE SPECTRUM
C      AND OUTPUT THE DATA ON THE OSCILLOSCOPE
C
C       A => DATA STORAGE ARRAY
C       INDX1 => SIZE OF ARRAY A
C
    SUBROUTINE OSC (A,INDX1)
C
C       USE DATACQ TO TAKE ON SCAN OF THE DATA
C
 100  CALL DATACQ (A,INDX1,1,NP,2)
C
C       SET BIAS VOLTAGE TO ITS LOWEST VALUE TO SAVE THE JUNCTION
C
    CALL NDAC(119)
C
C      SCALE X-AXIS SO ALL THE DATA FIT ON THE OSCILLOSCOPE
C
    AISIZE=NP
    XSCALE=3200./AISIZE
C
C      INITIALIZE OSCILLOSCOPE TO (0,0)
C
 400  CALL YDAC(0)
    CALL XDAC(0)
C
C      ALLOW TIME FOR USER TO SET UP OSCILLOSCOPE,ETC.
C
    PAUSE 'TYPE RETURN TO PLOT'
```

```
C
C       USE PLTOUT TO OUTPUT THE ACTUAL DATA
C
      CALL PLTOUT (A,INDX1,NP,10,XSCALE)
C
C       DO WE NEED ANOTHER PLOT?
C
      TYPE 902
      READ (5,903) IDUM
C
C       IF YES, PLOT THE DATA OUT AGAIN.
C
      IF (IDUM.EQ.'Y') GOTO 400
C
C       IF NO, DO WE NEED TO DO ANOTHER QUICK SCAN?
C       THIS IS FOR A NEW PHASE SETTING, ETC.
C
      TYPE 900
      READ (5,903) IDUM
C
C       IF YES, GO BACK AND SCAN AGAIN.
C
      IF (IDUM.EQ.'Y') GOTO 100
C
C       IF NO, RETURN
C
      RETURN
  900 FORMAT(' ANOTHER SCAN?(Y OR N):',$)
  902 FORMAT(' ANOTHER PLOT?(Y OR N):',$)
  903 FORMAT(A1)
      END
C-------------------<
C
C       SUBROUTINE SCAN
C       FORTRAN SUBROUTINE TO INDICATE MAJOR PEAKS
C       USED TO GET THE SPECTRUM ON SCALE ON THE LOCK-IN
C
      SUBROUTINE SCAN
C
C       SET BIAS TO STARTING VALUE
C
      CALL NDAC(119)
C
C       WAIT FOR THE LOCK-IN TO RESPOND
C
      DO 100 I=1,5
  100 CALL DELAY
C
C       SET BIAS TO VARIOUS MINIMA AND MAXIMA
C
      CALL NDAC(246)
      CALL DELAY
C
C       AL-O PEAK
```

```
C
      CALL NDAC(468)
      CALL DELAY
      CALL NDAC(560)
      CALL DELAY
C
C        C-H PEAK AREA
C
      CALL NDAC(1800)
      CALL DELAY
C
C        MAXIMUM BIAS VALUE
C
      CALL NDAC(2047)
      CALL DELAY
      RETURN
      END
C
C-------------------<
C
C        SUBROUTINE DELAY
C        FORTRAN SUBROUTINE TO DELAY MEASUREMENT
C        AND ALLOW THE LOCK-IN TIME TO RESPOND
C
      SUBROUTINE DELAY
C
C        STALLS FOR ABOUT 0.8S
C
      DO 100 IJ=1,5000
  100 AKL=AKL+IJ
      RETURN
      END
C
C-------------------<
C
C        SUBROUTINE WROUT(A,INDX1,INAM,NP,ILABEL)
C        FORTRAN SUBROUTINE TO WRITE OUT DATA FILES ON FLOPPY DISK
C
C        A => DATA STORAGE ARRAY
C        INDX1 => SIZE OF ARRAY A
C        INAM => DATA FILE NAME ARRAY
C        NP => NUMBER OF DATA POINTS IN THE FILE
C        ILABEL => FILE HEADER BLOCK ARRAY
C
      SUBROUTINE WROUT (A,INDX1,INAM,NP,ILABEL)
C
C        SET UP ARRAYS
C
      VIRTUAL A(INDX1)
      DIMENSION ILABEL(3,2),INAM(6)
      INTEGER*4 JDATA(2100)
C
C        OUTPUT LOGICAL UNIT = 2
C
```

```
      IOUT=2
C
C       OPEN AN OUTPUT FILE ON DISK
C
      OPEN (UNIT=IOUT,NAME=INAM,ACCESS='DIRECT',RECORDSIZE=1)
C
C       CONVERT FLOATING POINT DATA TO INTEGER*4 FORMAT FOR TRANSFER
C       TO THE VAX 11/780
C
      DO 10 I=1,NP
      ATEMP=-(A(I)*4096.)/32767.
 10   IERR=JAFIX(ATEMP,JDATA(I))
C
C       WRITE OUT HEADER BLOCK
C
      DO 50 I=1,3
      IREC=I
 50   WRITE (IOUT'IREC) (ILABEL(I,IJ),IJ=1,2)
C
C       WRITE OUT DATA POINTS
C
      DO 60 IJ=1,NP
      IREC=IJ+3
 60   WRITE (IOUT'IREC) JDATA(IJ)
C
C       CLOSE FILE
C
      CLOSE (UNIT=IOUT)
      RETURN
      END
C-------------------<
;
;       XDAC(IDAC) => MACRO ROUTINE FOR PLOTTER X-AXIS VALUE
;       SCALED FOR 0-4095 >> 0-10V
;
;       THROW AWAY NUMBER OF ARGUMENTS
;
XDAC::          MOV (R5)+, R0
;
;       MOVE X-DAC REGISTER TO R0
;
                MOV #170404, R0
;
;       MOVE X-VALUE TO DAC REGISTER -> SETS DAC TO IDAC
;
                MOV @(R5), (R0)
                RTS PC
;
;       YDAC(IDAC) => MACRO ROUTINE FOR PLOTTER Y-AXIS VALUE
;       SCALED AS FOR XDAC
;
YDAC::          MOV (R5)+, R0
;
;       MOVE Y-DAC REGISTER TO R0
```

```
;
                MOV #170406, R0
;
;       MOVE Y-VALUE TO DAC REGISTER AND THUS SET DAC
;
                MOV @(R5), (R0)
                RTS PC
                .END
C-------------------<
;
;
;       MACRO ROUTINES TO CONTROL PARALLEL I/O PORT
;
;       DEFINE LOCATIONS FOR CONTROL (C) AND DATA (D) REGISTERS
;       FOR PARALLEL PORTS A-D
;
        CSRA=164160
        DBRA=CSRA+2
        CSRB=CSRA+4
        DBRB=CSRA+6
        CSRC=CSRA+10
        DBRC=CSRA+12
        CSRD=CSRA+14
        DBRD=CSRA+16

;
;       INTPIO => MACRO ROUTINE TO INITIALIZE PARALLEL I/O PORTS
;
;       SET ALL CONTROL REGISTERS FOR OUTPUT OF DATA
;
INTPIO::MOV #400, @#CSRA
        MOV #400, @#CSRB
        MOV #400, @#CSRC
        MOV #400, @#CSRD
        RTS PC

;
;       WDAC(IDAC) => MACRO ROUTINE TO SET THE WIDE DAC
;
;       THROW AWAY THE NUMBER OF ARGUMENTS
WDAC::MOV @(R5)+, R0
;
;       GET THE INTEGER VALUE OF THE DAC SETTING
;
        MOV @(R5)+, R0
;
;       CONVERT IT TO OFFSET BINARY FOR THE DAC
;
        ADD #4000, R0
;
;       AND SEND IT OUT ON DATA LINE A
;
        MOV R0, @#DBRA
        RTS PC
```

```
;
;       NDAC(IDAC) => MACRO ROUTINE TO SET THE NARROW DAC
;       USE WDAC LOGIC, BUT OUTPUT DATA TO PORT B
;
NDAC:: MOV @(R5)+, R0
       MOV @(R5)+, R0
       ADD #4000, R0
       MOV R0, @#DBRB
       RTS PC

;
;       RRLY(IRLY) => MACRO ROUTINE TO SET ONE OF THE FOUR
;       REED RELAYS AS FOLLOWS:
;              IRLY=1 => REED RELAY 1
;              IRLY=2 => REED RELAY 2
;              IRLY=4 => REED RELAY 3
;              IRLY=8 => REED RELAY 4
;
;       RESULTS ARE UNPREDICTABLE IF MORE THAN ONE RELAY IS SET,
;       BUT THEY WILL PROBABLY BE BAD.
;
RRLY:: MOV @(R5)+, R0
       MOV @(R5)+, R0
;
;     COMPLeMENT THE VALUE SINCE THE OUTPUT IS ASSERTED LOW,
;       I.E. A ZERO OUTPUT SETS THE CORRESPONDING RELAY
;
       COM R0
;
;       SEND OUT THE APPROPRIATE SIGNAL ON THE C PORT
;
       MOV R0, @#DBRC
       RTS PC
;
;       READDC(ICMD,IDATA) => MACRO ROUTINE TO READ THE ADC
;       ICMD -> INTEGER VALUED COMMAND TO THE ADC,
;              SETS CHANNEL TO READ AND GAIN VALUE
;              THIS SHOULD BE SET IN THE FORTRAN PROGRAM!
;       IDATA -> INTEGER DATA VALUE RETURNED BY THE ADC
;
;       DISPOSE OF NUMBER OF ARGUMENTS
;
READDC::      MOV (R5)+, R0
;
;       MOVE LOCATION OF COMMAND REGISTER TO R0
;
              MOV #170400, R0
;
;       MOVE COMMAND TO COMMAND REGISTER
;
              MOV @(R5)+, (R0)
;
;       CHECK IF DATA READY
;
```

```
LP2:            TSTB (R0)
;
;       NO, GO BACK AND WAIT UNTIL DONE
;
                BPL LP2
;
;       YES - MOVE VALUE OF DATA REGISTER TO R0
;
                MOV #170402, R0
;
;       MOVE DATA FROM DATA REGISTER TO PROGRAM VARIABLE
;
                MOV (R0), @(R5)+
                RTS PC
                .END
C-------------------<
```

Appendix B.

Program Listing: Background Slope Removal Program for Tunneling Spectra

[Supplemental Material for: G. J. Gajda and W. H. Weinberg,

J. Vac. Sci. Technol., in press.]

```
CCCCCC
CCCCCC  PROGRAM DERIV2
C     BACKGROUND SLOPE REMOVAL PROGRAM FOR TUNNELING SPECTROSCOPY
C
C     A(2100),B(2100),C(2100) -> DATA STORAGE ARRAYS (VIRTUAL DATA)
C      <VIRTUAL DATA ARRAYS ARE USED TO MAXIMIZE DATA STORAGE
C       EFFICIENCY>
C      A -> SPECTRAL DATA
C      B -> NUMERICAL FIRST DERIVATIVE
C      C -> NUMERICAL SECOND DERIVATIVE AND PEAK LIST
C     INAME(6) -> FILENAME ARRAY
C     ILABEL(3,2) -> HEADER ARRAY FOR VLOW,VHIGH,VMOD,NP
C     VLOW -> STARTING BIAS VOLTAGE (MV*10)
C     VHIGH -> ENDING BIAS VOLTAGE (MV*10)
C     VMOD -> MODULATION VOLTAGE (RMS MV*100)
C     NP -> NUMBER OF POINTS IN THE SPECTRUM
C     IREC -> RECORD COUNTER IN THE DIRECT ACCESS FILE
C     JDATA -> INTEGER*4 DUMMY VARIABLE FOR READING DATA FROM FILE
C
C     DE11PT ->> FORTRAN SUBROUTINE TO CALCULATE NUMERICAL DERIVATIVES
C     FINDPK ->> FORTRAN SUBROUTINE TO LOCATE PEAKS IN THE SPECTRUM
C     PLOT ->> FORTRAN SUBROUTINE TO PLOT DATA ON THE X-Y RECORDER
C       <SEE PROGRAM IETS>
C     WROUT ->> FORTRAN SUBROUTINE TO OUTPUT DATA
C       <SEE PROGRAM IETS>
C
C     XDAC ->> MACRO ROUTINE TO DRIVE THE X-AXIS PLOTTING DAC
C       <SEE PROGRAM IETS>
C     YDAC ->> MACRO ROUTINE TO DRIVE THE Y-AXIS PLOTTING DAC
C       <SEE PROGRAM IETS>
C
      PROGRAM DERIV2
C
C       SET UP ARRAYS
C
      VIRTUAL A(2100),B(2100),C(2100)
      DIMENSION ILABEL(3,2),INAME(6)
C
C       DEFINE DATA TYPE
C
      INTEGER*4 JDATA
C
C       SET FILE EXTENSION TO .DAT
C
      INAME(4)='.D'
      INAME(5)='AT'
      INAME(6)=0
C
C       GET FILENAME
C
  100 TYPE 900
      READ (5,901) (INAME(IJ),IJ=1,3)
C
C       OPEN DIRECT ACCESS FILE
```

```
C
      OPEN (UNIT=2,NAME=INAME,ACCESS='DIRECT',RECORDSIZE=1,TYPE='OLD')
C
C     READ HEADER DATA
C
      DO 150 I=1,3
      IREC=I
  150 READ (2'IREC) (ILABEL(I,IJ),IJ=1,2)
C
C     SET NP=NUMBER OF POINTS
C
      NP=ILABEL(1,1)
C
C     AND MAKE IT AVAILABLE IN FLOATING POINT FORMAT
C
      ANP=NP
C
C     READ IN THE DATA POINTS IN INTEGER*4 MODE
C
      DO 160 IJ=1,NP
      IREC=IJ+3
      READ (2'IREC) JDATA
C
C     AND CONVERT TO FLOATING POINT MODE
C
  160 A(IJ)=-AJFLT(JDATA)
C
C     CLOSE THE INPUT FILE
C
      CLOSE (UNIT=2)
C
C     CALCULATE THE NUMERICAL DERIVATIVES
C
      CALL DE11PT(A,2100,B,C,NP)
C
C     AND FIND THE PEAKS
C
      CALL FINDPK(B,2100,C,NP,NPK)
C
C     CHECK TO SEE IF THE DATA START WITH A PEAK
C     I.E. IS THE STARTING POINT NO MORE THAN 10% ABOVE THE
C     MINIMUM VALUE IN THE SPECTRUM
C
      ISTART=1
C
C     FIND THE MAXIMUM AND MINIMUM VALUES
C
      AMAX=A(1)
      AMIN=A(1)
      IMINX=1.
      DO 304 I=1,NP
      IF (A(I).GT.AMAX) AMAX=A(I)
      IF (A(I).GE.AMIN) GOTO 304
C
```

```
C     WHEN WE FIND THE MINIMUM,MARK ITS LOCATION
C
      AMIN=A(I)
      IMINX=I
  304 CONTINUE
C
C     IF WE START WITH A PEAK, START THE CALCULATION AT THE
C      MINIMUM POINT
C
      IF (((A(1)-AMIN)/(AMAX-AMIN)).GT.0.1) ISTART=IMINX
C
C     RECALCULATE THE NUMBER OF POINTS IN THE SPECTRUM, IF NECESSARY
C
      ANP1=NP-ISTART+1
C
C     REMOVE THE BACKGROUND BY CALCULATING THE AVERAGE FIRST DERIVATIVE
C
      ATEMP=0.
      DO 305 I=ISTART,NP
  305 ATEMP=ATEMP+B(I)
      ATEMP=ATEMP/ANP1
C
C     AND SUBTRACTING THAT SLOPE FROM THE DATA
C
      DO 310 I=1,NP
      AI=I-1
  310 B(I)=A(I)-ATEMP*AI
C
C     GET THE STARTING AND ENDING BIAS VOLTAGES
C
      VLOW=ILABEL(1,2)
      VHIGH=ILABEL(2,1)
C
C     CALCULATE THE VOLTAGE STEP BETWEEN POINTS
C
      VINC=(VHIGH-VLOW)*.8065
      VINC=VINC/(ANP-1.)
C
C     AND THE CORRECTED VOLTAGE OFFSET
C
      VOFF=VLOW*.8065-1.13*8.065-VINC
C
C     PLOT OUT THE PROCESSED SPECTRUM
C
      CALL PLOT(B,2100,NP)
C
C     TELL THE OPERATOR TO LIFT THE PLOTTER PEN
C
      PAUSE 'RAISE PEN'
C
C     RESET THE PLOTTER POSITION TO THE LOWER LEFT CORNER
C
      CALL XDAC(0)
      CALL YDAC(0)
```

```
C
C     TELL THE OPERATOR TO LOWER THE PLOTTER PEN
C
      PAUSE 'LOWER PEN'
C
C     AND PREPARE TO PLOT THE PEAK POSITIONS. PEAKS ARE LOCATED
C      BY A SPIKE IN THE BASELINE OF THE OVERPLOT
C
C     SET UP THE PLOT SIZE BY SCALING THE DATA TO 0-10V
C
      XSCALE=4095./ANP
C
C     SET THE PEAK COUNTER TO THE FIRST PEAK
C
      ICNT=1
C
C     MAIN LOOP TO PLOT A BASELINE, WITH SPIKES AT THE PEAK LOCATIONS
C
      DO 510 I=1,NP
C
C     SET THE X-POSITION TO THE CURRENT POINT
C
      AI=I
C
C     DO WE HAVE A PEAK? IF NOT, INCREMENT THE X-AXIS POSITION
C
      IF (ICNT.GT.NPK) GOTO 500
      IF (AI.LT.C(ICNT)) GOTO 500
C
C     WE HAVE A PEAK! INCREMENT THE PEAK COUNTER
C
      ICNT=ICNT+1
C
C     PUT A HALF HEIGHT SPIKE ONTOP OF THE BASELINE
C
      CALL YDAC(4000)
C
C     GIVE THE PLOTTER PEN TIME TO RESPOND
C
      DO 390 IJK=1,1000
  390 AKL=AKL+IJK
C
C     RETURN TO THE BASELINE, AND DELAY FOR PEN RESPONSE
C
      CALL YDAC(0)
      DO 395 IJK=1,1000
  395 AKL=AKL+IJK
C
C     INCREMENT THE X-AXIS POSITION
C
  500 IX=AI*XSCALE
C
C     MOVE THE PEN ALONG THE X-AXIS,DELAY FOR THE PEN RESPONSE,
C      AND GO BACK FOR THE NEXT POINT
```

```
C
      CALL XDAC(IX)
      DO 510 IJK=1,500
  510  AKL=AKL+IJK
C
C     CALCULATE THE PEAK POSITIONS IN CM-1
C
      DO 520 IJK=1,NPK
  520  C(IJK)=C(IJK)*VINC+VOFF
C
C     AND TYPE OUT ON THE TERMINAL
C
      TYPE 902,(C(IJK),IJK=1,NPK)
C
C     CHANGE THE FILE EXTENSION TO .DTP
C
      INAME(5)='TP'
C
C     SHOULD WE OUTPUT THE PROCESSED FILE?
C
      TYPE 903
      READ (5,904) IDUM
C
C     IF YES, OUTPUT THE FILE, THEN QUIT. IF NO, JUST QUIT.
C
      IF (IDUM.EQ.'Y') CALL WROUT(B,2100,INAME,NP,ILABEL)
      STOP 'OK'
  900  FORMAT(' ENTER FILE NAME (AAAAAA):',$)
  901  FORMAT(3A2)
  902  FORMAT(20(5F12.2,/))
  903  FORMAT(' OUTPUT NEW DATA FILE?(Y OR N):',$)
  904  FORMAT(1A1)
      END
C-------------------<
C
C     SUBROUTINE DE11PT
C     FORTRAN SUBROUTINE TO CALCULATE 11-POINT FIRST AND
C      SECOND DERIVATIVES, USING THE NUMERICAL METHOD OF
C      A. SAVITSKY AND M.J.E. GOLAY,ANAL. CHEM.,36,1627 (1964)
C
C     A,B,C => VIRTUAL ARRAYS FOR DATA STORAGE
C      A => RAW SPECTRAL DATA
C      B => NUMERICAL FIRST DERIVATIVE
C      C => NUMERICAL SECOND DERIVATIVE
C     INDX1 => SIZE OF THE VIRTUAL ARRAYS
C     NP => NUMBER OF POINTS IN THE SPECTRUM
C
      SUBROUTINE DE11PT(A,INDX1,B,C,NP)
      VIRTUAL A(INDX1),B(INDX1),C(INDX1)
C
C     CALCULATE THE NUMERICAL DERIVATIVES AND STORE IN  THE
C      RESPECTIVE ARRAYS
C
      DO 100 I=1,NP-10
```

```
     B(I+5)=300.*(A(I)-A(I+10))-294.*(A(I+1)-A(I+9))-532.*
    &(A(I+2)-A(I+8))-503.*(A(I+3)-A(I+7))-296.*(A(I+4)-A(I+6))
     B(I+5)=B(I+5)/5148.
     C(I+5)=15.*(A(I)+A(I+10))+6.*(A(I+1)+A(I+9))-1.*(A(I+2)+A(I+8))
    &-6.*(A(I+3)+A(I+7))-9.*(A(I+4)+A(I+6))-10.*(A(I+5))
 100  C(I+5)=C(I+5)/429.
C
C     CORRECT FOR THE END EFFECTS OF AN 11-POINT CONVOLUTE
C      BY SETTING THE FIVE POINTS AT EACH END EQUAL TO THE
C      FIRST OR LAST CALCULATED POINT, RESPECTIVELY
C
     DO 200 I=1,5
     C(I)=C(6)
     C(NP+1-I)=C(NP-5)
     B(I)=B(6)
 200  B(NP+1-I)=B(NP-5)
     RETURN
     END
C-------------------<
C
C     SUBROUTINE FINDPK
C     FORTRAN SUBROUTINE TO FIND THE PEAKS IN THE SPECTRAL DATA
C
C     B,C => VIRTUAL DATA ARRAYS
C      B => FIRST DERIVATIVE DATA
C      C => SECOND DERIVATIVE DATA AND PEAK LOCATION ARRAY
C     INDX1 => SIZE OF THE VIRTUAL ARRAYS
C     NP => NUMBER OF POINTS IN THE SPECTRUM
C     NPK => NUMBER OF PEAKS FOUND
C
     SUBROUTINE FINDPK(B,INDX1,C,NP,NPK)
     VIRTUAL B(INDX1),C(INDX1)
C
C     INITIALIZE THE PEAK COUNTER
C
     NPK=0
C
C     FIND THE MINIMUM VALUE IN THE SECOND DERIVATIVE DATA
C
     AMIN=C(1)
     DO 100 I=1,NP
     IF(AMIN.GT.C(I)) AMIN=C(I)
 100  CONTINUE
C
C     SET THE SIGNIFICANCE LEVEL AT 17%. THE SIZE OF A PEAK IS
C      PROPORTIONAL TO -D2Y/DX2. THE 17% IS A COMPROMISE BETWEEN
C      FINDING SMALL PEAKS AND ELIMINATING INTERFERENCE FROM
C      NOISE.
C
     ASIG=AMIN*0.17
C
C     TO HAVE A PEAK, THE FIRST DERIVATIVE MUST GO THROUGH ZERO
C      FROM ABOVE, I.E. FROM POSITIVE TO NEGATIVE
C
```

```
      DO 200 I=3,NP-3
      IF (B(I).LE.0.) GOTO 200
      IF (B(I+1).GT.0.) GOTO 200
C
C     AND IT MUST BE SIGNIFICANT
C
      IF (C(I).GT.ASIG) GOTO 200
C
C     MARK THE CURRENT POSITION
C
      AI=I
C
C     INCREMENT THE PEAK COUNTER
C
      NPK=NPK+1
C
C     AND INTERPOLATE THE POSITION OF THE ZERO CROSSING
C
      C(NPK)=AI+(B(I)/(B(I)-B(I+1)))
C
C     GO BACK AND FIND THE NEXT PEAK
C
  200 CONTINUE
      RETURN
      END
C-------------------<
```